UNIVERSIDAD DE SEVILLA

FACULTAD DE QUÍMICA

DEPARTAMENTO DE QUÍMICA FÍSICA

Looking for synergies in solution chemistry between first-principles intermolecular potentials and EXAFS and XANES spectroscopies

Daniel Zein Caralampio Mínguez

Supervised by:

Enrique Sánchez Marcos

Jose Manuel Martínez Fernandez

DEPARTAMENTO DE QUÍMICA FÍSICA

Thesis submitted for the degree of Doctor of Theoretical Chemistry and Molecular Modellization by the Universidad de Sevilla.

Daniel Zein Caralampio Mínguez

Directores de la Tesis

Dr. Enrique Sánchez Marcos Dr. Jose Manuel Martínez Fernandez

Contents

List of Tables

List of Figures

Abstract

Physicochemical properties of aqueous solutions containing a broad spectrum of metal cations have been studied by means of Molecular Dynamic (MD) simulations employing classic ion-water intermolecular potentials based on ab initio potential energy surfaces. A polarizable ion and a flexible and polarizable water model, the MCDHO2,[1] were chosen. The aquaions were described by the Hydrated Ion Model, based on the idea of the concentric shells model of Frank and Evans.[2] This model was implemented in computer simulations in the mid 90's by this research group.[3–5]

The ions considered in this work have covered a wide range of the Periodic Table. Thus, the alkalines series, some alkaline-earths (Sr^{2+}, Ba^{2+} and Ra^{2+}), some d metals (Sc^{3+}, Cd^{2+} and Co^{2+}), some Lanthanoids (La^{3+}, Nd^{3+} and Tm^{3+}) and an actinoid (Th^{4+}) have been studied by means of MD simulations of systems formed by 1 cation and 1000 water molecules at 300K in the NVT ensemble using the DLPOLY code.[6]

The x-ray absorption spectroscopy (XAS) was used as the main method to asses the quality of the results derived from the developed intermolecular potentials. This was based on the comparison of the experimental EXAFS and XANES spectra with the simulated ones. Theoretical spectra computed using an ab-initio FEFF multiscattering formalism, as implemented in FEFF code,[7] employing an statistically significant number of structures provided by the MD simulations.

The obtained coordination numbers in aqueous solutions for Li^+, Na^+, K^+, Rb^+ and Cs^+ cations were 4.0, 5.8, 7.2, 7.9 and 9.9 with the metal-oxygen peak distances at 1.91, 2.34, 2.72, 2.87 and 3.12 Å, respectively. For the heavy alkaline cations, surface cluster structures are lower in energy than the inner ones. Then, the range of structures to be included in the fitting was extended to arrangements where the metal cation is not longer in the middle of a water cluster, but on the top. An specific method[8] was applied to the multi-electron excitation (MEE) of the experimental EXAFS spectra. The signal treactement, that removes multi-electron excitations, allows to analyze a larger k-range, improving the comparison between the theoretical and experimental data.

The solvation structure obtained for the Sr^{2+}, Ba^{2+} and Ra^{2+} is composed by 8.0, 9.4 and 9.8 water molecules with peak distances at 2.57, 2.81 and 2.93 Å, respectively. For Sc^{3+}, Co^{2+} and Cd^{2+} coordination numbers of 6.0, 6.0 and 6.6 with peak distances at 2.15, 2.29 and 2.09 Å were found. X-ray absorption measurements, EXAFS and XANES, were carried out at the SOLEIL synchrotron for the Co^{2+} aqueous solution. A very good agreement between the simulated and the experimental EXAFS spectra is obtained in all cases.

For the Lanthanoid cations studied: La^{3+}, Nd^{3+} and Tm^{3+}, coordination numbers of 9.0, 8.7 and 7.7 with a peak distance of 2.58, 2.50 and 2.33 Å, respectively, were found. In the case of the actinoid thorium cation coordination number of 9.0 and a peak distance of 2.47 Å was obtained.

Additional structural, energetical and dynamical properties have been calculated for the ions in solution. Thus, mean residence times and self-diffusion coefficient at 300 K, reorientational properties and hydrogen bond characterization. The comparison of the results obtained in this work with raw experimental data supports the generation of ab initio potentials combined with MD-XAS to study the ion hydration. This shows that the computational techniques can be used to provide accurate properties of the system when experimental data are not available.

0.1 Bibliography

[1] Villa, A.; Hess, B.; Saint-Martin, H. *J. Phys. Chem. B* **2009**, *113*, 7270–7281.

[2] Frank, H. S.; Evans, M. W. *J. Chem. Phys.* **1945**, *13*, 507–532.

[3] Pappalardo, R.; Sánchez-Marcos, E. *J. Phys. Chem.* **1993**, *97*, 4500–4504.

[4] Martínez, J. M.; Pappalardo, R. R.; Sánchez Marcos, E. *J. Chem. Phys.* **1998**, *109*, 1445–1455.

[5] Martínez, J.; Pappalardo, R.; Sánchez Marcos, E. *J. Am. Chem. Soc.* **1999**, *121*, 3175–3184.

[6] Smith, W.; Forester, T.; Todorov, I. T. The DL_POLY Classic. 2012; STFC Daresbury Laboratory, Daresbury (UK).

[7] Rehr, J. J.; Kas, J. J.; Vila, F. D.; Prange, M. P.; Jorissen, K. *Phys. Chem. Chem. Phys.* **2010**, *12*, 5503–5513.

[8] Ohta, A.; Kagi, H.; Tsuno, H.; Nomura, M.; Kawabe, I. *Am. Mineralogist* **2008**, *93*, 1384–1392.

Chapter 1

Introduction

The aqua ions are the common speciation of the charged ions in aqueous solutions at acidic and dilute conditions. They have long been studied due to their abundance and importance in many fields.[1]

A good starting point to describe the aqua ion structure is the concentric shell model of Frank and Evans,[2] where up to three solvation regionsmaybe defined around the ion. The first solvation region is composed by the nearest water molecules,that are the most affected by the cation charge. The second hydration shell water molecules are less affected by the ion and are forming hydrogen bonds with those of the first-shell. The third shell water molecules behaves like bulk water molecules, except for the cases of highly charged cations.

The water molecules in the first-shell are assigned to the aqua ion entity, $[M(H_2O)_m]^{n+}$, because some properties as diffusion are explained by the consideration of the hydrated ion as the most representative chemical species.[1] The first-shell water molecules of highly charged cations (+3 or +4) are strongly polarized by the ion and even a partial charge transfer takes place. The water molecules are affected structurally both intra and intermolecularly by modifying their O-H distances, H-O-H bond angle, as

well as arranged orientation towards the ion. But in the case of a low polarizing ion, such as large monovalent cations water molecules are not strongly polarized, and the ion-dipole orientation is lost, becoming a disordered aqua ion where the water structure is partially retained.

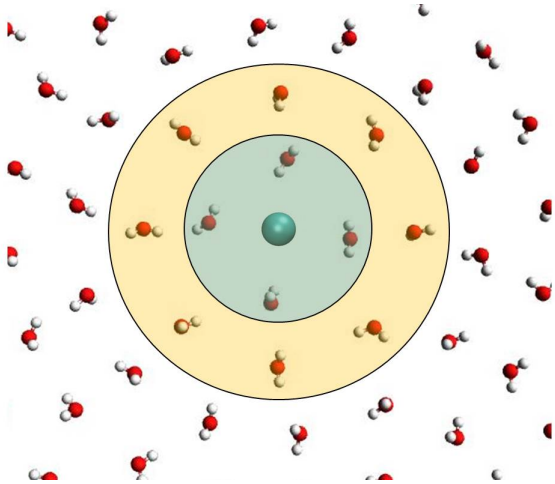

Figure 1.1: Scheme of the concentric shell model

The main parameters to define the structure of an aqua ion are the average number of water molecules in the first and second hydration shells, their orientation, the average distance between the ion and the hydration shells and the thermal disorder of the hydration shells. Other relevant properties of an aqua ion are its diffusion properties, mean residence time of the water molecules in the hydration shells, coordination geometry, water exchange mechanism, reorientational properties and its hydration enthalpy.

Based on the ion capability to order water molecules around it, ions are classified as structure maker or breaker.[3] A structure maker ion is able to create structure around it whereas a breaker one is unable to do it. For a structure maker ion the first-shell water molecules are polarized and ori-

entated by the ion interacting through a double hydrogen bond with the oxygen atoms of a second shell of water molecules.

Several theoretical approaches have been employed to study the ions in solution; from QM calculations to Monte-carlo simulations to know the most probable conformation or MD, QM/MM and AIMD simulations to get insight into dynamic processes and the disorder of the system.[1,4,5] Several experimental techniques as x-ray absorption spectroscopy, neutron diffraction, x-ray diffraction, nuclear magnetic resonance or raman spectroscopy are used to study the local structure of aqua ions.[1,3,5–8] In this thesis, we have employed ab initio intermolecular potentials in classical MD simulations. The statistical information produced is used to generate EXAFS and XANES spectra to compare with experimental spectra in order to validate the structural information coming from the simulation. The combination of MD simulations and XAS spectroscopy has been proved to be a robust methodology in determining structural properties of solvated ions.[9,10]

This thesis has explored the new exchangeable-HIW intermolecular potential strategy[11] on a wide set of metal cations covering the Periodic Table, from alkalines to heavy actinoid cations, including d-transition metal ones. The great difference among these ions is a demanding test to our methodology, an interesting source of new simulations to get a deeper insight into their physicochemical properties, as well as sources of challenges to improve the interaction potential building. In addition, the set of potentials presented in this thesis establishes a kind of database for future investigations involving aqueous solutions of salts. The group has previously worked on the development of interaction potentials for anions such halide.[12–15] Now, the option to include cations and anions in the simulation cell bring us closer to a wide range of salts that become accesible to the MD simulations with sophisticated models like the one here developed.

Diffraction techniques studies of the lighter alkalines, Li^+ and Na^+, provided consistently hydration numbers of 4[16–18] and above 5,[19,20] respectively. Some authors found higher coordination numbers for lithium[21,22]

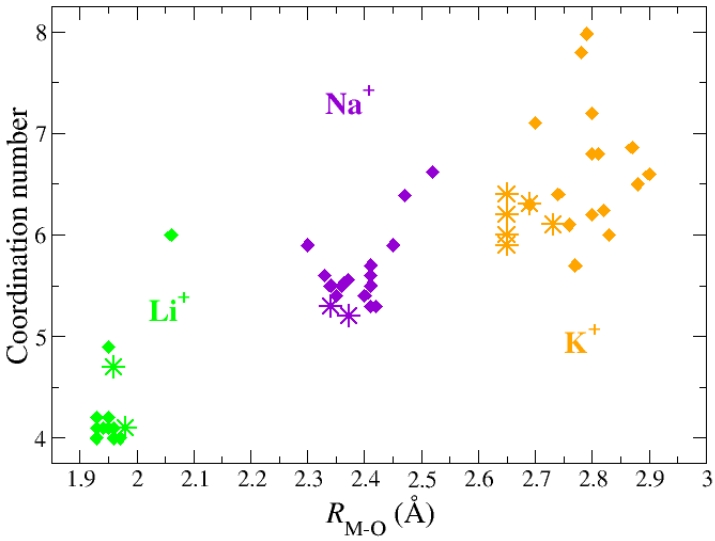

Figure 1.2: Coordination number vs M-O first-shell distance for Li^+, Na^+ and K^+.

and considered the existence of the hexahydrate in solution. Potassium, considered as the frontier between the alkaline structure makers and breakers, was studied by means of diffraction and spectroscopical techniques obtaining hydration numbers around 6.[19,23,24] Coordinations around 4, between 5 and 6 and between 6 and 7 for lithium,[25–30] sodium[25,31–37] and potassium[25,34,37,38] respectively have been obtained computationally, although some works found higher coordinations for sodium[38,39] and for potassium.[33,40] Figure 1 shows the experimental and theoretical estimations for the hydration number and first-shell metal-oxygen distances. Experimental distances of each cation show narrow ranges, and the agreement with theoretical values is fairly good except for the K^+ case where the ex-

perimental distances are consistently shorter.

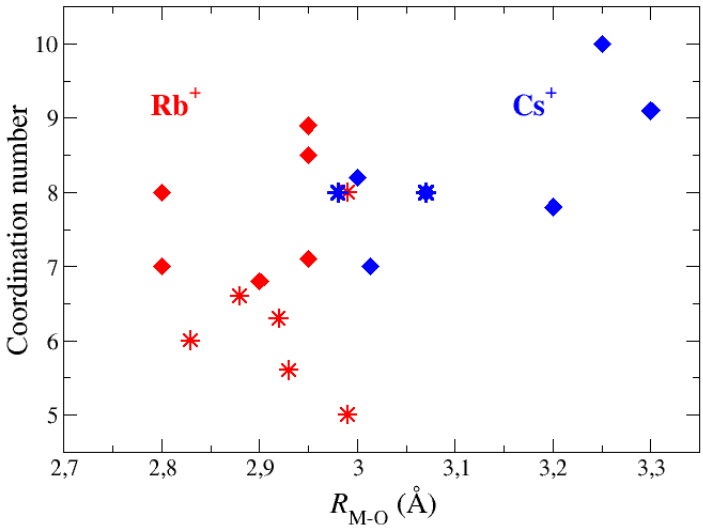

Figure 1.3: Coordination number vs M-O first-shell distance for Rb^+ and Cs^+.

In the case of the heavy alkalines (Rb^+ and Cs^+), the data dispersion of experimental results is much larger due to the difficulties associated to the low order of the aqua ion structure and the multi-electron excitations on the principal absorption edges. The rubidium studies find a wide range of hydration numbers, between 5.6 and 8.[41,42] The results about the caesium hydration is even more scarce than the rubidium case, and the hydration number has been fixed to 8.[43,44] Computationally, dispersion on the hydration number[45–47] for both cations is found. A distance range: 2.8-3.0 Å for Rb^+ and 3.0-3.1 Å for Cs^+ were found experimentally. Computational

works provide the same range of distances for rubidium but larger ones for caesium, 3.0-3.3 Å.

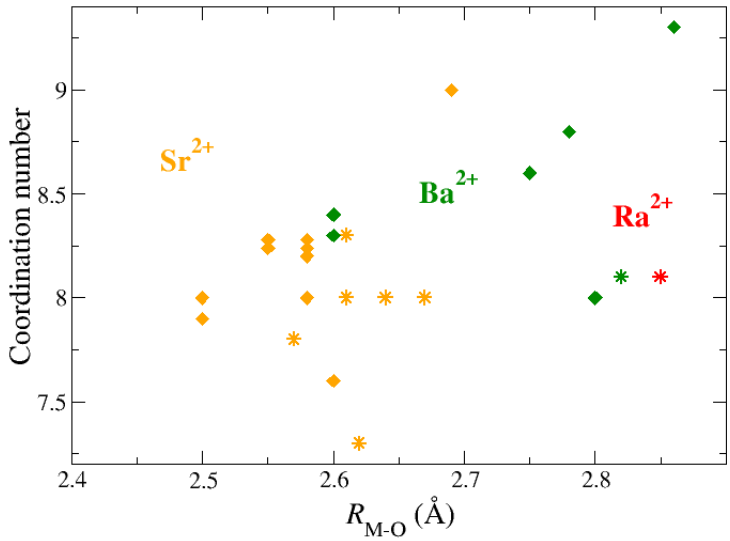

Figure 1.4: Coordination number vs M-O first-shell distance for Sr^{2+}, Ba^{2+} and Ra^{2+}

The heavy alkaline-earth Sr^{2+}, Ba^{2+} and Ra^{2+} cations have been mainly studied by means of spectroscopical techniques. The strontium hydration is supported by several experimental works that found hydration numbers near 8.[48–55] Computationally, coordination numbers between 7.3 and 8.3[49,50,56–60] were obtained. There is only one experimental work about the barium hydration that found a similar hydration to the strontium,[52] considering a coordination number of 8 for both cations. For the barium coordination numbers between 8 and 9.3[57,58,61] were found theoretically. The

first-shell metal-oxygen distance has been reported experimentally to be 2.6 Å for strontium[48,51–55] and 2.8 Å for barium.[52] Computationally the values reported are 2.5-2.6 Å for strontium[49,50,56–60] and 2.80 Å for barium.[57,58,61] There is only one theoretical work[62] about the radium hydration that found its hydration similar to that of barium and a coordination of 8 with a metal-oxygen distance of 2.85 Å.

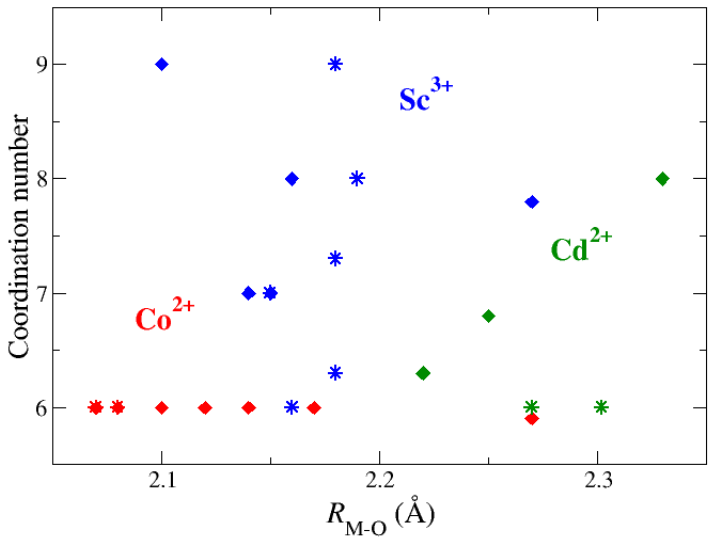

Figure 1.5: Coordination number vs M-O first-shell distance for Sc^{3+}, Co^{2+} and Cd^{2+}

The scandium hydration has been experimentally studied but without reaching a consensus on its hydration number that is thought to be between 6 and 8.[63–66] A hydration number of 7[67] was found by means of QM/MM simulations. The cadmium has been found to be a flexible aqua ion with a

hydration number between 6 and 7[68] while the cobalt is a well know hexahydrate.[69] Classical MD simulations predict coordination values for the cadmium between 6 and 8.[68] A tight range of experimental intermolecular distances have been found for those ions; $\sim$ 2.05 Å, 2.15-2.2 Å and 2.25-2.30 Å for the Co^{2+},[70,70,71] Sc^{3+}[63–65] and Cd^{2+},[68] respectively.

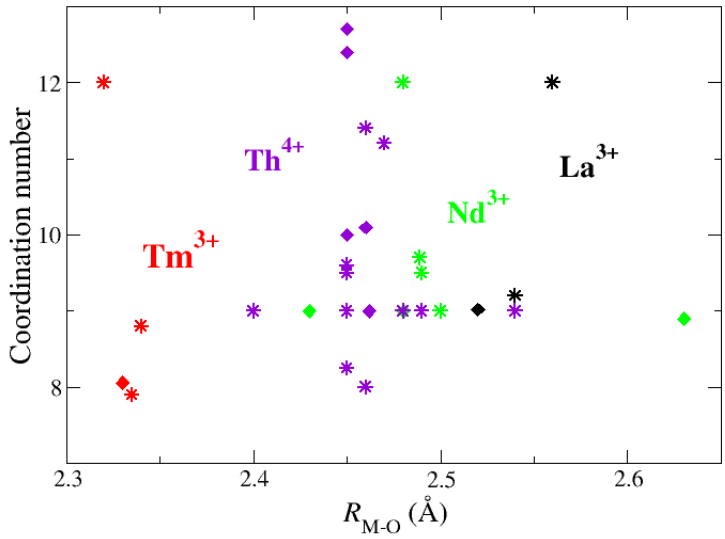

Figure 1.6: Coordination number vs M-O first-shell distance for La^{3+}, Nd^{3+}, Tm^{3+} and Th^{4+}

La^{+3}, Nd^{+3} and Tm^{+3} are representative ions of the lanthanoid series as are placed at the begining, the middle and the end of the series, respectively. The lanthanoid contraction along the series represents a shortening of the intermolecular distance and a decreasing of the hydration number, being around 9 for the light lanthanoids, 8 for the heavy ones and between 8 and

9 at the middle of the series.[72–74] The thorium ion has been studied experimentally by means of spectroscopical techniques obtaining a coordination number between 9[75] and 12.[76] Theoretical approaches provide hydration numbers between 8 and 10.[77–81]

Although there is a good agreement for some of the ion properties as the hydration number for the lithium or the cobalt or the metal-oxygen distances for the thorium or the lanthanides, there are other ions where the uncertainty is really high as in the case of rubidium, caesium or scandium, or simply the published resources are scarce as for barium, radium and cadmium. The main objective of this thesis has been to develop refined and specific metal-water interactions potentials along the Periodic Table, by the interaction modelling of metal-water systems under the Hydrated Ion concept. This has allowed us to improve our knowledge about the ion hydration using a polarizable and flexible water model and a polarizable ion to reproduce the water and ion properties. Summarizing, the main points undertaken in this thesis are:

- To test the MCDHO2 water model with cations of different charges (from charge 1+ to charge 4+).
- To shed light on the hydration of the rubidium and caesium, and revisit that of lighter alkaline cations.
- To study structural, dynamical and spectroscopical properties along the alkaline group.
- To contribute to the ongoing debate on the scandium hydration due to the uncertainty on its hydration number.
- To contribute to the study of the speciation of the cobalt in seawater building the cobalt-water potential and carrying out x-ray absorption measurements of highly diluted solutions containing this cation.
- To study the hydration properties of four poorly investigated cations, thorium, cadmium, barium and radium.

- To make a systematic characterization of the hydrogen bond network in the hydration structure around the whole set of metal cations studied, to stablish the similarities and differences of their hydration, finding, if possible a rational pattern.

1.1 Bibliography

[1] Richens, D. T. *The Chemistry of Aqua Ions*; John Wiley: Chichester, 1997.

[2] Frank, H. S.; Evans, M. W. *J. Chem. Phys.* **1945**, *13*, 507–532.

[3] Marcus, Y. *Ion properties*; Markel Dekker, Inc, 1997.

[4] Allen, M. P.; Tidesley, D. J. *Computer simulation of liquids*; Oxford University Press, 1989.

[5] Ohtaki, H.; Radnai, T. *Chem. rev.* **1993**, *83*, 1157–1204.

[6] Muñoz-Paez, A.; Marcos, E. S. En *Molecular structure of solvates and coordination complexes in solution as determined with EXAFS and XANES.*; Reedik, J., Poeppelmeier, K., Eds.; Comprehensive Inorganic Chemisry II, 2013; Vol. 9.

[7] Marx, D.; Hutter, J. *Ab initio molecular dynamics: Basic Theory and Advanced Methods.*; Cambridge: Cambridge University Press, 2009.

[8] Magini, M. *X-ray diffraction of ions in aqueous solutions: hydration and complex formation*; CRC Press., 1988.

[9] Merkling, P. J.; Muñoz-Páez, A.; Sánchez Marcos, E. *J. Am. Chem. Soc.* **2002**, *124*, 10911–10920.

[10] Galbis, E.; Hernández-Cobos, J.; den Auwer, C.; Naour, C. L.; Guillaumont, D.; Simoni, E.; Pappalardo, R. R.; Sánchez Marcos, E. *Angew. Chem. Int. Ed.* **2010**, *22*, 3811–3815.

[11] Galbis, E.; Hernández-Cobos, J.; Pappalardo, R. R.; Sánchez Marcos, E. *J. Chem. Phys.* **2014**, *140*, 214104.

[12] Ayala, R.; Martínez, J. M.; Pappalardo, R.; Marcos, E. S. *J. Chem. Phys.* **2004**, *15*, 7269–75.

[13] Ayala, R.; Martínez, J. M.; Pappalardo, R.; Marcos, E. S. *J Chem. Phys.* **2003**, *119*, 9538.

[14] Ayala, R.; Martínez, J. M.; Pappalardo, R.; Marcos, E. S. *J. Phys. Chem. A* **2000**, *104*, 2799–2807.

[15] Ayala, R.; Martínez, J. M.; Pappalardo, R. R. *J. Chem. Phys.* **2002**, *117*, 10512.

[16] Bouazizi, S.; Nasr, S. *J. Mol. Struct.* **2007**, *837*, 206–213.

[17] Rudolph, W.; Brooker, M. H.; Pye, C. C. *J. Phys. Chem.* **1995**, *99*, 3793–3797.

[18] Palinkas, G.; Radnai, T.; Hajdu, F. *Z. Naturforsch* **1979**, *35a*, 107–114.

[19] Mancinelli, R.; Boti, A.; Bruni, F.; Ricci, M. A.; Soper, A. K. *J. Phys. Chem. B* **2007**, *11*, 13570–13577.

[20] Galib, M.; Baer, M.; Skinner, L.; Mundy, C.; Huthwelker, T.; Schenter, G.; Benmore, C.; Govind, N.; Fulton, J. *J. Chem. Phys.* **2017**, *146*, 084504.

[21] Mason, E.; Anell, S.; Neilson, G.; Rempe, S. B. *J. Phys. Chem. B* **2015**, *119*, 2003–2009.

[22] Szasz, G.; Heinzinger, K.; Palinkas, G. *Chem. Phys. Lett.* **1981**, *78*, 194–196.

[23] Glezaku, V.; Chen, Y.; Fulton, J.; Schenter, G.; Dang, L. *Theor. Chem. Acc.* **2006**, *115*, 86–99.

[24] Vao-Soongnern, V.; Pipatpanukul, C.; Horpibulsuk, S. *J. Mater. Sci.* **2015**, *50*, 7126–7136.

[25] Lee, S. H.; Rasaiah, J. Y. *J. Phys. Chem.* **1996**, *100*, 1420–1425.

[26] San-Román, M. L.; Carrillo-Tripp, M.; Saint-Martin, H.; Cobos, J. H.; Ortega-Blake, I. *Theor. Chem. Acc.* **2006**, *115*, 177–189.

[27] Loeffler, H. H.; Rode, B. M. *J. Chem. Phys.* **2002**, *117*, 110–116.

[28] Lyubartsev, A. P.; Laasonen, K.; Laaksonen, A. *J. Chem. Phys.* **2001**, *114*, 3120–3126.

[29] Tongraar, A.; Liedl, K. R.; Rode, B. M. *Chem. Phys. Lett.* **1998**, *286*, 56–64.

[30] Sripa, P.; Tongraar, A.; Kerdcharoen, T. *J. Mol. Liq.* **2015**, *208*, 280–285.

[31] Sripa, P.; Tongraar, A.; Kerdcharoen, T. *J. Phys. Chem. A* **2013**, *117*, 1826–1833.

[32] Tongraar, A.; Liedl, K. R.; Rode, B. M. *J. Phys. Chem. A* **1998**, *102*, 10340–10346.

[33] Carrillo-Tripp, M.; Saint-Martin, H.; Ortega-Blake, I. *The J. Chem. Phys.* **2003**, *118*, 7062–7073.

[34] Ma, H. *Int. J. Quantum Chem.* **2014**, *114*, 1006–1011.

[35] Chandrasekhar, J.; Spellmeyer, D.; Jorgensen, W. *J. Am. Chem. Soc.* **1984**, *106*, 903–910.

[36] Gaiduk, A. P.; Zhang, C.; Gygi, F.; Galli, G. *Chem. Phys. Lett.* **2014**, *604*, 89–96.

[37] Bankura, A.; Carnevale, V.; Klein, M. L. *Molecular Physics* **2014**, *112*, 1448–1456.

[38] Faginas-Lago, N.; Lombardi, A.; Albertí, M.; Grossi, G. *J. Mol. Liq.* **2015**, *204*, 192–197.

[39] Spangberg, D.; Hermansson, K. *J. Phys. Chem.* **2004**, *120*, 4829–4842.

[40] Azam, S. S.; Hofer, T. S.; Randolf, B. R.; Rode, B. M. *J. Phys. Chem.* **2009**, *113*, 1827–1833.

[41] Pham, V.; Fulton, J. L. *J Chem. Phys.* **2013**, *138*, 044201.

[42] D'Angelo, P.; Persson, I. *Inorg. Chem* **2004**, *43*, 3543–3519.

[43] Fan, Q.; Tanaka, M.; Tanaka, K.; Sakaguchi,; Takahashi, Y. *Geochim. Cosmochim. Acta* **2014**, *135*, 49–65.

[44] Mähler, J.; Persson, I. *Inorg. Chem* **2011**, *51*, 425–438.

[45] Ikeda, T.; Boero, M. *J. Chem. Phys.* **2012**, *137*, 041101(1)–041101(4).

[46] Lee, S. H.; Rasaiah, J. C. *J. Chem. Phys.* **1994**, *101*, 6964–6974.

[47] San-Román, M. L.; Hernández-Cobos, J.; Saint-Martin, H.; Ortega-Blake, I. *Theor. Chem. Acc.* **2010**, *126*, 197–211.

[48] Pfund, D. M.; Darab, J. G.; Fulton, J. L.; M, Y. *J. Phys. Chem.* **1994**, *98*, 13102–13107.

[49] Deublein, S.; Reisser, S.; Vrabec, J.; Hasse, H. *J. Phys. Chem. B* **2012**, *116*, 5448–5457.

[50] Harris, D. J.; Brodholt, J. P.; Sherman, D. M. *J. Chem. Phys. B* **2003**, *107*, 9056–9058.

[51] Seward, T.; Henderson, C.; Charnock, J.; Driesner, T. *Geochim. Cosmochim. Acta* **1999**, *63*, 2409–2418.

[52] Persson, I.; Sandstrom, M.; Yokoyama, H.; Chaudhry, M. *Z. Naturforsch* **1995**, *50a*, 21–37.

[53] Caminiti, R.; Misinu, A.; Paschina, G.; Pinna, G. *J. Appl. Cryst.* **1982**, *15*, 482–487.

[54] Parkman, R. H.; Charnock, J. M.; Livens, F.; Vaughan, D. J. *Geochim. Cosmochim. Acta* **1998**, *62*, 1481–1492.

[55] Ramos, S.; Neilson, G.; Barnes, A.; Capitán, M. *J. Chem. Phys.* **2003**, *118*, 5542–5546.

[56] Hofer, T.; Randolf, B.; Rode, B. *J. Phys. Chem. B* **2006**, *110*, 20409–20417.

[57] Raieri, P.; Demichelis, R.; Gale, J. D. *J. Phys. Chem. C* **2015**, *119*, 24447–24458.

[58] Larentzos, J. P.; Crescenti, L. J. *J. Phys. Chem.* **2008**, *112*, 14243–14250.

[59] Tofteberg, T.; Öhrn, A.; Karlström, G. *Chem Phys. Lett.* **2006**, *429*, 436–439.

[60] Boda, A.; De, S.; Musharaf, S.; Tulishetti, S.; Khan, S.; Singh, J. *J. Mol. Liq.* **2012**, *172*, 110–118.

[61] Hofer, T. S.; Rode, B. M.; Randolf, B. R. *Chem. Phys.* **2004**, *312*, 81–88.

[62] Matsuda, A.; Mori, H. *J. Solution Chem.* **2014**, *43*, 1669–1675.

[63] Lindqvist-Reis, P.; Persson, I.; Sandström, M. *Dalton Trans.* **2006**, *28*, 3868–3878.

[64] Migliorati, V.; D'Angel, P. *Inorg. Chem.* **2016**, *55*, 6703–6711.

[65] Smirnov, P.; Wakita, H.; Yamaguchi, T. *J. Phys. Chem. B* **1998**, *102*, 4802–4808.

[66] Rudolph, W. W.; Pye, C. C. *J. Phys. Chem.* **2000**, *104*, 1627–1639.

[67] Vchirawongkwin, V.; Kritayakornupong, C.; Tongraar, A.; Rode, B. *Dalton Trans.* **2012**, *41*, 11889–11897.

[68] Chillemi, G.; Barone, V.; D'Angelo, P.; Mancini, G.; Persson, I.; Sanna, N. *J. Phys.Chem. B* **2005**, *109*, 9186–9193.

[69] Akesson, R.; Pettersson, L. G. M.; Sandström, M.; Wahlgreen, U. *J. Am. Chem. Soc* **1994**, *116*, 8691–8704.

[70] Inada, Y.; Hayashi, H.; Sugimoto, K.; Funahashi, S. *J. Phys. Chem. A* **1999**, *103*, 1401–1406.

[71] Spezia, R.; Duvail, M.; Vitorge, P.; Cartailler,; Tortajada, J.; Chillemi, G.; D'Angelo, P.; Gaigeot., M. *J. Phys. Chem. A* **2006**, *110*, 13081–13088.

[72] Angelo, P. D.; Spezia, R. *Chem. Eur. J* **2012**, *18*, 11162–11178.

[73] Duvail, M.; Spezia, R.; Vitorge, P. *ChemPhysChem* **2008**, *9*, 693–696.

[74] Villa, A.; Hess, B.; Saint-Martin, H. *J. Phys. Chem. B* **2009**, *113*, 7270–7281.

[75] Torapava, N.; Persson, I.; Eriksson, L.; Lundberg, D. *Inorg. Chem.* **2009**, *48*, 11712–11723.

[76] Rothe, J.; Denecke, M.; Neck, V.; Muller, R.; Kim, J. *Inorg. Chem.* **2002**, *41*, 249–258.

[77] Marjolin, A.; Gourlaouen, C.; Clavaguéra, C.; Ren, P.; Wu, J.; Gresh, N.; Dognon, J.; Piquemal, J. *Theor. Che, Acc.* **2012**, *131*, 1198.

[78] Carnaval, L.; Weiss, A.; Rode, B. *Comput. Chem.* **2013**, *1022*, 94–102.

[79] Spezia, R.; Beuchat, C.; Vuileumier, R.; D'Angelo, P.; Gagliardi, L. *J. Phys. Chem. B* **2012**, *116*, 6465–6475.

[80] Réal, F.; Trumm, M.; Vallet, V.; Schimmelpfenning, B.; Masella, M.; Flament., J. *J. Phys. Chem. B* **2010**, *114*, 15913–15924.

[81] Yang, T.; Tsushima, S.; Suzuki, A. *J. Phys. Chem. A* **2001**, *105*, 10439–10445.

Chapter 2

Methods

Several theoretical tools as quantum mechanical calculations, ab-initio intermolecular potentials, molecular dynamic simulations and x-ray absorption spectroscopy have been used in this work to study the ion hydration. In this section the main concepts of these techniques are briefly explained.

2.1 Quantum mechanics

Quantum mechanics (QM) is a theory applicable to interpret and predict the electronic structure and reactivity of chemical systems. This implies the resolution of the Schrödinger equation, $\hat{H}\psi = \mathrm{E}\psi$. The resolution of the equation for polyelectronic systems implies the use of approximations. The most used methods are the wavefunction based ab-initio methods and the density functional methods.

The simplest ab-initio method is the Hartree-Fock (HF) approach, which does not include any electron correlation except the Pauli exclusion principle, since it constructs a one–determinant electron wavefunction moving in the average field of the remaining electrons. In order to overcome this limitation the post–HF methods are used. These include different amounts of electron correlation. Among them, the MP2 method is used in this work.

Another way to include electron correlation is based on the DFT methods which, in general are less demanding computationally. DFT computes the electron correlation energy as an estimated functional of the electron density. Its main drawbacks are due to the fact that it is a single configuration methodology, and there is not a systematic way to improve its performance.

2.1.1 Moller-Plesset second order theory

The Moller Plesset perturbation theory is a post-HF method where correlation energy is included by means of the Rayleigh–Schrödinger perturbation theory. Møller-Plesset theory adds higher excitations to Hartree-Fock as non-iterative corrections. Moller-Plesset theory is based upon dividing the Hamiltonian into two parts, $\hat{H} = \hat{H}_o + \lambda \mathrm{V}$, being $\hat{H}_o$ the independent electron Hamiltonian or unperturbed Hamiltonian, V is a small perturbation and λ a dimensionless parameter. The one electron Hamiltonian is defined as the sum of one electron operator, $\hat{f}$:

$$\hat{H}_o = \sum \hat{f} \tag{2.1}$$

and the perturbation is defined as the energy difference between the true molecular electronic Hamiltonian and the unperturbed Hamiltonian:

$$V = \hat{H} - \hat{H}_o = \sum_i \sum_{j>i} \frac{1}{r_{ij}} - \sum_i \sum_j \left(\hat{J} - \hat{K} \right) \tag{2.2}$$

where $\hat{J}$, is the exchange operator and $\hat{K}$ is the exchange operator. When this approximation is included into the Schrödinger equation it implies the expansion of the energy and wavefunction of the perturbed system in powers of λ:

$$(\hat{H}_o + \lambda \mathrm{V})\psi = E_\lambda \psi \tag{2.3}$$

$$E = E^0 + \lambda E^1 + \lambda^2 E^2 + \lambda^3 E^3 + .. \tag{2.4}$$

Being E^2 the correlation energy calculated for a second order perturbation. The correlation energy is obtained from the second order expansion term:

$$E_{corr} = E^2 + E^3 + E^4 + .. \tag{2.5}$$

There are ways to minimize the cost of a Moller-Plesset calculation as the Frozen Core approximation (FC). On the FC approximation part of the occupied orbitals are constrained to remain double occupied while others are not, being included in the perturbative process.[1,2]

2.1.2 Density functional theory

DFT[3] is based on two theorems of Hohenberg-Kohn. The first theorem states that the electron density, ρ, is defined for a given external potential, V_{ext}, and hence the total energy, E, is a functional of the electron density:

$$E(\rho) = F[\rho] + \int \rho V_{ext}(\hat{r}) d\hat{r} \tag{2.6}$$

And the second theorem states that the exact electron density of a non–degenerate ground state can be calculated by determining the density that minimizes the energy of the ground state.

$$\left[\frac{\delta E(\rho)}{\delta \rho}\right] = 0 \tag{2.7}$$

As a practical consideration the electrons are considered as non interacting particles moving under the same external potential. Being the ground state energy defined by the minimum of the Kohn-Sham equations:

$$\hat{E}(\rho) = \hat{T} + \hat{V}_{ne} + \hat{V}_{ee} + E_{xc} \tag{2.8}$$

where $\hat{T}$ is the kinetic energy, $\hat{V}_{ne}$ is the nuclei-electron integration energy $\hat{V}_{ee}$ is the electron-electron interaction energy and E_{xc} is the exchange and correlation energy term. As the main DFT limitation, the exact correlation exchange functional E_{xc} is not know but there are some approximations as the LDA, LSDA, GGA and meta-GGA. In the LDA, Local Density Approximation, the exchange and correlation contributions are calculated separately, assuming a constant electron density using the electron gas of constant density model. In the LSDA approximation are included spin coordinates in the electron description. These approximations provide good results but they overestimate force constants and energies. The GGA, Generalized Gradient Approximation, includes the gradient density over the space in the calculations. The meta-GGA aproximation includes the second derivative of the electron density as well. Also there is an hybrid methodology to calculate the exchange correlation energy as a linear combination of the HF and the DFT results.[1,4–7] In this thesis B3LYP and M06 functionals have been employed. They are briefly described in the next two sections.

2.1.2.1 B3LYP functional

The B3LYP[8] is a hybrid-GGA functional that is one of the most used and cited DFT functionals. The exchange and correlation energy is calculated by the equation:

$$E_{\mathrm{xc}} = E_{\mathrm{xc}}^{\mathrm{LSDA}} + a_0(E_{\mathrm{x}}^{\mathrm{exact}} - E_{\mathrm{x}}^{\mathrm{LSDA}}) + a_{\mathrm{x}}\,\Delta E_{\mathrm{x}}^{\mathrm{B88}} + a_{\mathrm{c}}\,\Delta E_{\mathrm{c}}^{\mathrm{PW91}} \qquad (2.9)$$

where $a_0 = 0.20$, $a_{\mathrm{x}} = 0.72$ y $a_{\mathrm{c}} = 0.81$ are semiempirical coefficients which allow the reproduction of thermochemical data for a set of molecules, $\Delta E_{\mathrm{x}}^{\mathrm{B88}}$ is the gradient correction of Becke for the exchange and $\Delta E_{\mathrm{c}}^{\mathrm{PW91}}$ gradient correction for the correlation of Perdew and Wang.

2.1.2.2 M06 and M06-2X functionals

Functionals M06 and M06-2x[9–11] have been used in this work, that use a hybrid-meta GGA approximation to calculate the exchange and correlation energy. The exchange energy depends on the exchange density energy of the PBE functional, $F_{\mathrm{x}_\sigma}^{\mathrm{PBE}}$, an amplified factor of the kinetic density energy, $f\left(w_\sigma\right)$, on an approximation of the local spin density for the exchange, $\varepsilon_{\mathrm{x}_\sigma}^{\mathrm{LSDA}}$, and from a work function based on the VSXC functional, $h_{\mathrm{X}}(x_\sigma, z_\sigma)$, that has been parametrized with thermochemical, kinetic and non-covalent interactions data.

$$E_{\mathrm{x}} = \sum_{\sigma} \int \left[F_{\mathrm{x}_\sigma}^{\mathrm{PBE}}\left(\rho_\sigma, \nabla\rho_\sigma\right) f\left(w_\sigma\right) + \varepsilon_{\mathrm{x}_\sigma}^{\mathrm{LSDA}} h_{\mathrm{X}}(x_\sigma, z_\sigma) \right] d\hat{r} \tag{2.10}$$

The correlation energy depends on the alternate spin electron correlation energy, $E_{\mathrm{c}}^{\alpha\beta}$, and on parallel spin electrons, $E_{\mathrm{c}}^{\alpha\alpha}$ and $E_{\mathrm{c}}^{\beta\beta}$.

$$E_{\mathrm{c}} = E_{\mathrm{c}}^{\alpha\beta} + E_{\mathrm{c}}^{\alpha\alpha} + E_{\mathrm{c}}^{\beta\beta} \tag{2.11}$$

As hybrid functionals, in the M06 and M06-2X functionals the exchange and correlation energies are calculated as a linear combination of the HF exchange energy and the exchange and correlation energy calculated with the equations 2.10 and 2.11. The exchange-correlation energy for these functionals are calculated using equation (2.12) with X=27 for M06 and X=57 for M06-2X.

$$E_{\mathrm{xc}}^{\mathrm{hybr}} = \frac{X}{100} E_{\mathrm{x}}^{\mathrm{HF}} + \left(1 - \frac{X}{100}\right) E_{\mathrm{x}}^{\mathrm{DFT}} + E_{\mathrm{c}}^{\mathrm{DFT}} \tag{2.12}$$

As meta-GGA functionals the integrals are solved through numerical integrations which are depending of the grid used. In a previous work[12] convergence problems on molecular optimization were solved by increasing the grid density. In this work the same grid values have been used (250 and 974 points for the radial and angular components, respectively).

2.1.3 Basis sets

A basis set defines a set of one-electron functions to build molecular orbitals in the space. A molecular orbital, ϕ, is constructed as a lineal combination of atomic orbitals, χ, being $\phi = \sum_i C_i \chi_i$. In this work the aug-cc-pVTZ, def2-TZVPP and def2-TZVPPD basis sets have been used. The aug-cc-pVTZ[13] basis set consists of a triple zeta basis set augmented with diffuse and a polarization function. The def2-TZVPP[14] basis set consists of a triple zeta basis set with a double polarization function and the def2-TVPPD[15] includes diffuse functions.

2.1.4 Effective core potentials

The core electrons are not much affected by the environment being possible to substitute them by an Effective Core Potential (ECP). With this approximation the basis set and the number of electrons are reduced, therefore reducing the calculation effort while keeping accuracy. Relativistic effects can also be included in the ECP. These effects are important in heavy elements as some of the cases considered in this thesis.[16–18]

2.1.5 Quantum approaches to the ion solvation

Electronic and geometrical properties of a molecule change depending on its environment.

When a molecules is inmersed in a solvent there are several computational approaches to include solvent effects. In this work the Polarizable Continuum Model[19] (PCM) has been employed to include solvent effects in quantum calculations. When solvent molecules are included explicitly, the computational cost increases a lot, however, when the solvent is modeled by a dielectric polarizable continuum calculation, computation time is close to that of a conventional gas phase calculation.

The Hamiltonian of the PCM formulation, $\hat{H} = \hat{H}_{solute} + \hat{H}_{solute-solv}$, considers that the effective Hamiltonian correspond to a term for the isolated molecule, $\hat{H}_{solute}$ and a term of the molecule inside a cavity, $\hat{H}_{solute-solv}$ surronded by a polarizable continuum dielectric. In the PCM framework the hamiltonian part corresponding to the solute-sovent interaction has the status of free energy. The solvation free energy is defined as $\Delta G_{solv} = \Delta G_{cav} + \Delta G_{elec} + \Delta G_{rep} + \Delta G_{disp}$ where ΔG_{cav} is the energy related to the cavity generation inside the dielectric, ΔG_{elec} is the term related to the electrostatic interactions between the solute and the continuum, ΔG_{rep} is related to the exchange contribution and ΔG_{disp} is related to the dispersion contribution.[19]

2.2 Molecular dynamics

Molecular dynamics[20] (MD) is a computational technique which allows the atomistic simulation of a system evolving with time. When dealing with classical particles, MD is based on the integration of Newton‘s motion equation which uses the forces and their evolution over any of the particles of the system.

$$\vec{F}_{ij} = -\frac{\partial V(\vec{r}_{ij})}{\partial r_{ij}} \tag{2.13}$$

The system is described by the classical Hamiltonian defined by a kinetic and a potential energy term.

$$H = H(\vec{r}, \vec{p}) = \sum_i \frac{p_i^2}{2m_i} + V(\vec{r}) \tag{2.14}$$

The potential energy term is defined by the interaction potential among particles, commonly called force field. Interactions can be classified in bonded and non bonded types, i.e. intramolecular and intermolecular contributions to the total potential energy. The bonded interactions define the

molecule deformation energies, based on variations of angles and dihedral angles. The non-bonded interactions are commonly classified in electrostatic and van der Waals interactions. The van der Waals interactions are short range forces defined by force fields.

The velocity Verlet[21] integrator algorithm, employed in this work, performs the estimation of the position and velocity of the particles at time t+Δt from the the position and velocity at time t and t−Δt.

$$\vec{r}(t+\Delta t) = \vec{r}(t) + \vec{v}(t)\Delta t + \frac{1}{2}\vec{a}(t)\Delta t^2 \tag{2.15}$$

$$\vec{v}(t+\Delta t) = \vec{v}(t) + \frac{1}{2}\big[\vec{a}(t) + \vec{a}(t+\Delta t)\big]\Delta t \tag{2.16}$$

To keep average macroscopic properties constant along the simulation is needed to use an ensemble satisfying these conditions. The NVT ensemble has been used where the number of particles, *N*, the volume of the cell, *V*, and the average temperature, *T*, are constant. To control the temperature, the Noose-Hoover thermostat[22,23] has been used. The Noose-Hoover thermostat includes the thermostat friction parameter, χ_n, in the Newton's equations, which slows down or accelerates the velocities of the particles until the effective temperature matches the target one:

$$\frac{d\vec{v}_n}{dt} = \frac{\vec{F}_n}{m} - \chi_n \vec{v}_n \tag{2.17}$$

being χ_n defined as:

$$\frac{d\chi_n}{dt} = \frac{N_f k_B}{Q}(T_i - T_0) \tag{2.18}$$

where N_f is the number of freedom degrees, T_i and T_0 are the instant temperature and the target temperature, respectively, and Q is the thermostat mass.

2.3 X-ray absorption spectroscopy

X-ray absorption spectroscopy[24–26] (XAS) is an experimental technique based on the measurement of the absorption of X-rays photons as a function of energy. The absorption coefficient of a compound , $\mu(E)$, with thickness , d, is determined as the ratio between the incident photon beam, I_0, and the transmitted beam, I.

$$\mu(E)d = -ln\,(I/I_0) \tag{2.19}$$

A XAS spectrum is characterized by an abrupt increase of the absorption, called absorption edge, at the energy corresponding to the ionization potential of an inner occupied level. For molecules or embedded atoms there are some absorption oscillations above the absorption edge. The XAS spectra are analyzed in two separate regions. The EXAFS part is focussed on the oscillations after the absorption edge in a typical range of 1000 eV. In the XANES part the close region to the absorption edge, 50-100 eV, above this energyis analyzed.

When an atom is irradiated with photons of enough energy to allow its ionization a photoelectron is ejected, and propagates as a wave being backscattered by the neighbour atoms. Interacting in-phase or out-phase with the ongoing wave and creating specific oscillations. These oscillations define the so-called fine structure that brings information about the local atomic arrangement around the absorbing atom. The atomic absorption coefficient can be described by two contributions: one defined by the isolated absorber, $\mu_0(E)$, and the other containing the fine structure, $\chi(E)$, contribution defined by the absorber neigborhood:

$$\mu(E) = \mu_0(E)[1 + \chi(E)] \tag{2.20}$$

From the fine structure contributions to the local environment of the absorber atom it can be deduced a relation between the signal intensity and the number, N, of specific neighbor atoms, between the signal frequency and the distance, R_i, and between the Debye-Waller factor, σ^2, and the

statistical dynamical disorder. There are also other relevant parameters specific for the pair of atoms involved in the process, as the mean free path, λ, the amplitude reduction factor, S_0, the amplitude function of the backscattered path i, F_i, and the phase shift function, δ_i.

$$\chi(\mathrm{k}) = \Sigma \frac{\mathrm{NS_0^2 F}_i(\mathrm{k})}{\mathrm{kR}_i^2} \sin(2\mathrm{kR}_i + \delta_i) \mathrm{e}^{-2\sigma_i^2 \mathrm{k}^2} \mathrm{e}^{\frac{-2\mathrm{R_i}}{\lambda(\mathrm{k})}} \tag{2.21}$$

The XANES interpretation is complicated as there is not a simple analytic description. But it is known to be sensitive to the valence state of the absorber, the ligand type and the coordination geometry around the absorber atom.[26,27]

EXAFS and XANES spectra can be simulated using ab-initio codes, in this work the FEFF code[28] has being used. FEFF uses an ab-initio self-consistent real space multiple scattering (RSMS) approach, where core-hole effects are included, local field corrections and self-consistent spherical muffin-tin scattering potentials are also taken into account. EXAFS simulations in this work were carried out using the Hedin-Lundquist exchange-correlation potential for the fine structure and for the atomic background. To remove phase differences between simulated and experimental spectra Fermi level has been slightly shifted when generating the theoretical EXAFS function in order to get of phase between the simulated and experimental spectra. XANES simulations were run using the ground state potential model considering the full multiple scattering terms. In the XANES simulation the optical absorption and the edge position has been shifted a feweV to accommodate the simulated spectra to the experimental one. It must be pointed out that FEFF carries out ab-initio computations of the ionization potential of core levels, which are in the order of thousands of eV. All the XAS simulations were performed in two steps. In the first step the backscattering potential was calculated, considering all the atoms inside an 8 Å sphere centered on the absorber cation. For the rest of the calculation the hydrogen atoms were removed, because the backscattering capabilities of the hydrogen atoms are overestimated as found in previous works.[29–31]

2.4 Ab-initio intermolecular potentials

The ab-initio intermolecular potentials are parameterized equations that, using information from QM calculations, define the interactions among atoms and molecules. In this work the ion-water interactions have been modelled by effective pairwise site-site potentials.

The first requirement to build a site-site intermolecular potential is to define the equations that rule the interactions among the different particles, these equations together with the appropiate parameters, define the called force fields. In order to model an ab-initio potential an initial set of values for the force field parameters are nedeed together a minimization algorithm and a PES to drive the parametrization process. This process ends when the difference between the ab-initio interaction energies and the calculated by the interaction potential ones is below an user defined energy threshold, standard deviation.

There is not a "magic" recipe for the configurations to be included in a PES to build an intermolecular potential. However, but the inclusion of representative structures that may adopt the system we want to study is highly required. There is not a minimum or maximum number of structures to be included in the fitting procedure but it is safe to include a representative number of them. The intermolecular potential can be refined by including situations extracted from preliminary simulations in order to include relevant information previously not taken into account. Some flexibility can be introduced in the fitting procedure by including weights on the different structures. An increase of the weight for a given structure means to priorize it in the fitting. This process implies the location of a minimum in a multidimensional space that does not guarantee the absolute minima location. Then, the assessment of the energetic properties must be analyzed, together with the structural properties of the minimum energy structures. The underestimation or overestimation of these properties on the fitting will be reflected in the computer simulation results.

2.4.1 Hydrated ion model

The original implementation of the Hydrated Ion model[32–34] consists of the parametrization of two interaction potentials: the interaction between the ion with its first-shell water molecules (Ion-Water 1st shell) and the interaction of the aqua ion with the bulk water molecules (Hydrated Ion Water interaction):

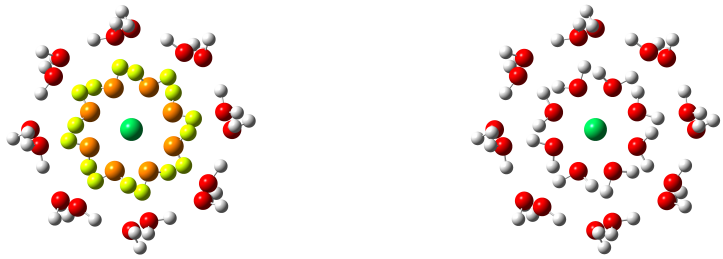

Figure 2.1: Scheme of the HIW model where the first-shell water molecules are defined differently to the bulk ones (left) and of the exchangeable HIW model where all the water molecules are defined by the same force field (right).

The HIW model allows the simulation of an aqua ion with a fixed number of first-shell water molecules that are structurally and electronically different from those bulk. In previous works[33,34] the first hydration shell water molecules have been defined with the water ab-initio geometry and incorporating the charge transfer state defined by the quantum mechanical minimum structure of the aqua ion. This Hydrated Ion approach generates a realistic model to be used in the determination of several properties of the first and second hydration shells. But it is no longer valid when the residence time of the first-shell water molecules are smaller than the simulation time, i.e when first-shell water molecule release appears.

In order to overcome this limitation the *exchangeable HIW* version of the model was proposed.[35,36] iithin this new model, first-shell water molecule exchange is permitted together with a flexible and polarizable water model that allows the solvent molecule properties to be modified by the environment. Additionally, in this model the polarizability of the ion is taken into account explicitly because its no consideration leads to an overestimation of the first hydration shell rigidity.

2.4.2 Water model

The MCDHO2[37] water model have been used throughout this work. The MCDHO2 water molecules are described as flexible and polarizable and the potential has been built parametrizing the single molecule dipole, quadrupole, polarizability, the monomer deformation energy and the theoretical limit of dimerization energy at the MP2/aug-cc-pVQZ' level. The MCDHO2 water model is a reparametrization of the MCDHO[38] water model where the water mobility has been improved. As can bee seen in the Table 2.1 both models give a good picture of the water molecule in gas phase and in solution.

Table 2.1: Water model properties

Phase	Properties	Experimental[38]	MCDHO[38]	MCDHO2
Gas	R_{OH} (Å)	0.9572	0.9590	0.9585*
	θ_{HOH} (°)	105.44	104.52	103.99*
	$\vec{\mu}$ (D)	1.870	1.8494	1.8671*
Liquid	R_{OH} (Å)	0.970	0.982	0.983[37]
	θ_{HOH} (°)	106.1	102.7	103.3[37]
	$\vec{\mu}$ (D)	2.9	2.94	2.89[37]
	D (10^{-5} cm^2/s)	2.4	1.16	1.8[37]

* this work

The water molecule is defined by its three positive charged nuclei (Z_O and Z_H) and a negative mobile charge density (q):

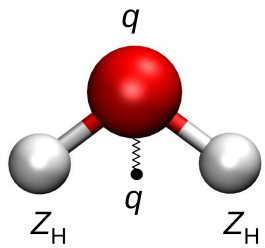

Figure 2.2: Schematic representation of a MCDHO/MCDHO2 water molecule

The polarizability of the water molecule is modeled by a harmonic function connecting the mobile charge density and the oxygen nucleus:

$$U_k = \frac{1}{2}k \cdot r^2 \tag{2.22}$$

The mobile charge is defined as a Gaussian charge distribution having a decaying constant λ:

$$\rho(r) = \frac{q}{\pi\lambda^3}\mathrm{e}^{-2\frac{r}{\lambda}} \tag{2.23}$$

The oxygen-hydrogen bond flexibility is defined by a Morse potential:

$$U_{d_{\mathrm{OH}}} = D_{\mathrm{OH}}\left(\mathrm{e}^{-2\gamma(R_\beta - r_\mathrm{e})} - 2\mathrm{e}^{-\gamma(R_\beta - r_\mathrm{e})}\right) \tag{2.24}$$

The water internal angle is defined by a quartic function:

$$U_{\Theta_{\mathrm{HOH}}} = \mathrm{a}_1(\Theta - \Theta_\mathrm{e}) + \mathrm{a}_2(\Theta - \Theta_\mathrm{e})^2 + \mathrm{a}_3(\Theta - \Theta_\mathrm{e})^3 + \mathrm{a}_4(\Theta - \Theta_\mathrm{e})^4 \tag{2.25}$$

The internal energy of a water molecule is then given by the addition of all the previous contributions:

$$U_{\text{internal}} = \frac{1}{2}kr_O^2 + \frac{Z_H^2}{R_{1,2}} + \frac{qZ_H}{r_\beta}\left[1 - \left(\frac{r_\beta}{\lambda} + 1\right)e^{-2r_\beta/\lambda}\right] + U_k + U_{d_{\text{OH}_1}} + U_{d_{\text{OH}_2}} + U_{\Theta_{\text{HOH}}} \tag{2.26}$$

The energy of a cluster of N water molecules is defined by a Lennard-Jones potential for the interactions among oxygen and hydrogen atoms and mobile charges of the different solvent molecules.

$$\begin{aligned} U_{\text{total}} = &\sum_{n=1}^{N}\sum_{m=1}^{n-1}\left(\frac{A}{r_{nm}}\right)^{12} - \left(\frac{B}{r_{nm}}\right)^{6} + \frac{q^2}{r_{nm}} + \frac{qZ_\beta}{r_{n\beta}}\left[1 - \left(\frac{r_{n\beta}}{\lambda} + 1\right)e^{-2r_{n\beta}/\lambda}\right] \\ &+ \sum_{\beta\in m}^{q}\left(\frac{A_{\alpha\beta}}{r_{\alpha\beta}}\right)^{12} - \left(\frac{B_{\alpha\beta}}{r_{\beta\alpha}}\right)^{6} + \frac{Z_\alpha\beta}{r_{\alpha\beta}} \end{aligned} \tag{2.27}$$

MCDHO2 force field parameters are given in section 3.12. In a previous Thesis[12] of the group an energetic gap between the MCDHO and the M062x/def2-TZVPP was found in scans of water dimers with particular orientations and distances (see Figure 2.3). A maximum energy discepancy of 2 kcal/mol was established. Aggregates with distances below this limit are excluded. The study for the MCDHO2 carried out in this work reveals minimum distances collected in Table 2.2. It can be seen that the MCDHO2 is less restrictive with respect the hydrogen-hydrogen distances.

An energy gap between the M062x/def2-TZVPP level and the MCDHO2 for first-shell ion-dipole configurations has been found. This gap depends on the QM level and on the distance between the water molecules. The energy error becomes higher for shorter water-water distances what introduces a bias in the coordination number. As a normal rule, for a given cation higher coordination numbers have slightly longer metal-ligand distances but the inter-ligand distance shortens, i.e. steric repulsion between

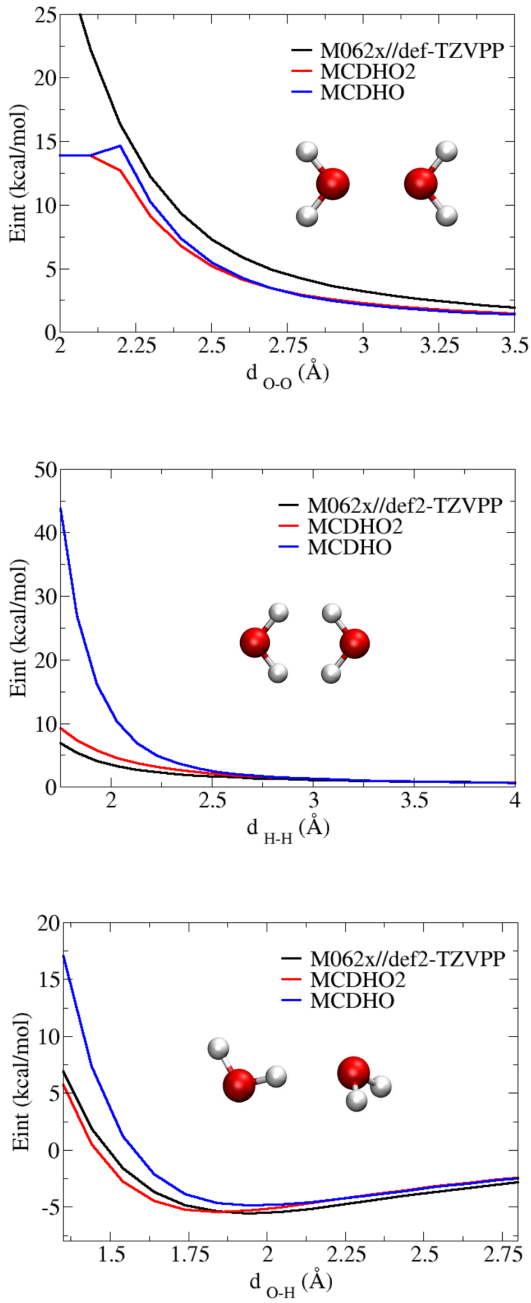

Figure 2.3: Water dimer scans employed in the filter criteria.

Table 2.2: MCDHO and MCDHO2 filter criteria

Properties	MCDHO criteria[12]	MCDHO2 criteria
R_{OO} (Å)	2.22	2.34
R_{OH} (Å)	1.64	1.42
R_{HH} (Å)	2.30	2.00

ligands increases with the coordination number.

As shown in Figure 2.4, when the cation is removed from an optimized hydrated ion cluster and a symmetric scan for all the water molecules approaching the centroid is carried out, i.e. the former position of the cation, the water model gives more repulsive energies, and this energy difference increases when water molecules approach each other.

This problem has been found to mainly affect trivalent and tetravalent hydrates. This energy difference is clearly detected when an aqua ion of a given coordination is fitted and the derived potential is used to check another coordination. Obviously it is possible to reduce the standard deviation of the fitting involving more than one coordination, but this leads to unnappropiate effects in the structural properties. As shown in the original MCDHO2 water model work[37] up to a 6 % larger metal-oxygen distance can be expected.

This energy error was very similar for all the QM levels used and the water model. Also it was found that when using the MP2 level the error decreases when increasing basis set size, being the gap smaller when is used the same quantum level employed in the water model parametrization (MP2/aug-cc-pVQZ'). Due to the high quantum-mechanical level used in the water model building, it was not possible to compute the hydrated ion clusters at the same level in order to reduce the energy gap.

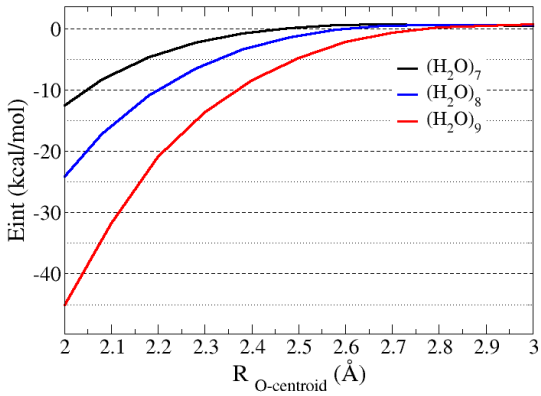

Figure 2.4: Interaction energy difference ($\Delta E = E_{QM}$-E_{Pot}) between the quantum-mechanical energy at the M062x/def2-TZVVP level and MCDHO2 potential energy function for water clusters in ion-dipole configuration corresponding to thullium optimized hydrates as a function of distance to the centroid position.

2.4.3 Ion-water model

The modelization of the ion-water interactions is based on the MCDHO2 scheme, which is composed by a water molecule formed by three sites (O, H and q) and the ion defined as a "core ion" (Z_M) and a mobile charge density (q_M). The charge values of Z_M and q_M guarantee the desired net charge. The constant associated to the harmonic function of the mobile charge of H_2O or the M^{n+} defines either their molecular solvent or cation polarizability (Equation 2.22). In the case of the ion the value was chosen to reproduce its experimental molar refractivity.[39] In Table 2.3 are shown the experimental values used of molar refractivity and the calculated "spring" constant.

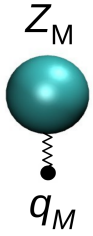

Figure 2.5: Schematic representation of the ion

Table 2.3: Spring constants based on experimental polarizability

Properties	q_{Ion}	q_{mobile}	R_∞ (10^{-6} m^2/mol)[39]	$k_r{}^{exp}$ (h/bohr)
Li^+	2	-1	0.08	4.67282
Na^+	2	-1	0.65	0.575250
K^+	3	-2	2.71	0.551890
Rb^+	3	-2	4.10	0.364708
Cs^+	3	-2	6.89	0.217025
Sr^{2+}	5	-3	2.65	1.269662
Ba^{2+}	5	-3	5.17	0.650790
Co^{2+}	5	-3	2.05	1.641271

The ion polarizability, α, can be defined by the experimental value of the molar refractivity, R_∞[39] :

$$\alpha = \frac{3}{\pi 4 N_A} R_\infty \tag{2.28}$$

The spring constant k_r is defined by the ion polarizability and the charge value q :

$$\alpha = \frac{q^2}{k_r} \tag{2.29}$$

In some cases the spring constant derived from experimental data suffered from electrostatic collapse during the simulations. This situation was found for low or highly polarizing ions. For these cases the spring constant was fixed at a working value. Table 2.4 displays the experimental based spring constant and the spring constant used. Although the fact of defining the polarizability from experimental values is a trial to model this property in a realistic way, no major differences have been found in the use of different values.

Table 2.4: Non experimental spring constant

Properties	q_{Ion}	q_{mobile}	R_∞ (10^{-6} m^2/mol) [39]	$k_r{}^{exp}$ (h/bohr)	$k_r{}^{used}$ (h/bohr)
La^{3+}	4	-1	2.74	0.136439756	1.011070
Nd^{3+}	4	-1	3.1	0.120595142	1.050000
Tm^{3+}	4	-1	2.1	0.178021401	1.120000
Ra^{2+}	3	-1	-	-	0.650790
Sc^{3+}	4	-1	1.6	0.233653098	1.6
Cd^{3+}	3	-1	22.5	0.016615329	1.0
Pu^{3+}	4	-1	1.71	0.218622759	1.295636
Th^{4+}	5	-1	6.8	0.054977197	1.050000

For the Li^+ case it was decided a non polarizable description of the cation because its low mass provide a high frequency vibration of the core ion-mobile charge spring. This forces a simulation with a very short timestep, making the simulation particularly expensive, when the intrinsic very hard character of Li^+ does not really need the inclusion of the polarizable character.

The ion-water interaction is modeled by considering all the electrostatic interactions between all the nuclei charges and by fitting the interaction between the mobile charge density of the ion and that of the oxygen atom, the interaction between the core ion and the hydrogen atoms and by fitting the electrostatic decayment of the mobile charge.

The interaction between the oxygen mobile charge, q_{O}, and the metal mobile charge, q_{M}, and the interaction between the core ion, Z_{M}, and the water molecule, $Z_i (i \equiv \mathrm{O}, \mathrm{H})$, is given by a two-exponential function:

$$U_{inter}(q_{\mathrm{O}}, q_{\mathrm{M}}) = A_{\mathrm{MO}} \cdot e^{-\alpha_{\mathrm{MO}} \cdot r_{\mathrm{MO}}} + B_{\mathrm{MO}} \cdot e^{-\beta_{\mathrm{MO}} \cdot r_{\mathrm{MO}}} \tag{2.30}$$

$$U_{inter}(Z_i, Z_{\mathrm{M}}) = C_{\mathrm{M}i} \cdot e^{-\gamma_{\mathrm{M}i} \cdot r_i} + D_{\mathrm{M}i} \cdot e^{-\delta_{\mathrm{M}i} \cdot r_i} \tag{2.31}$$

where r_{MO} is the metal-oxygen distance, r_i is the distance between the core ion and each i-th nucleus of the water molecule, and $\mathrm{A_{MO}}$, $\mathrm{B_{MO}}$, $C_{\mathrm{M}i}$, $\gamma_{\mathrm{M}i}$, $D_{\mathrm{M}i}$ and $\delta_{\mathrm{M}i}$ are fitting parameters. Electrostatic interaction between the water mobile charge density, q_{O} and the core ion, Z_{M}, is described by the following equation:

$$U_{inter}(q_{\mathrm{O}}, Z_{\mathrm{M}}) = \frac{q_{\mathrm{O}} Z_{\mathrm{M}}}{r'} \left[1 - \left(\frac{r'}{\lambda'} + 1 \right) e^{-2r'/\lambda'} \right] \tag{2.32}$$

where r' is the distance between the center of q_{O} and the nucleus M and λ' is the intermolecular screening described in the original MCDHO2 model.[37] The interaction energy for a cluster with N water molecules is computed by the expression:

$$\begin{aligned} U = \sum_{S=1}^{N} \Bigg(\sum_{i \in S} \sum_{j \in T} [& U_{inter}(Z_i, Z_j) + U_{inter}(q_i, q_j) \\ & + U_{inter}(q_i, Z_j) + U_{inter}(q_j, Z_i)] + \sum_{i \in S} \frac{1}{2} k_i \cdot r_{ii}^2 + \frac{1}{2} k_M \cdot r^2 \Bigg) \end{aligned} \tag{2.33}$$

where S runs over the water molecule/atoms.

2.4.4 Methodology

In this work the M06 and M062x, B3LYP and MP2 methods have been used. The M06 family is a relative new hybrid functional which was tested on water clusters obtaining good results compared to high level calculations.[40] Although they have not been extensively tested in the literature for solvated ions, they has been employed in previous studies obtaining good results.[12] In this work extensive test has been performed, checking the consistency of this functional family. The MP2 method was used as a benchmark for the M06 family calculations and was used to generate potentials when significant differences among different functionals were found. Although MP2 calculations could be considered more reliable than DFT methods, their computational cost may lead to choose DFT methods when similar results are found.

In this work effective pairwise potentials including hydrated clusters with a number of water molecules around the "expected coordination" in solution have been built. The fact of including several water molecules in the interaction energy calculation implies the implicit inclusion of many body interactions.

The main criteria to include in the fitting process a structure or not is its ability to represent useful arrangements of the system to study under the conditions we want to model. In addition, small set of repulsive structures must be considered to guarantee an appropriate shape of the effective potential energy surface defined by the force field. As an example, let us consider a trivalent ion in solution, (see figure 2.6). Its structure will be described by a well oriented first hydration shell that interacts by hydrogen bonds with the second shell, ideally each second shell water molecule forming one hydrogen bond with one of the first shell water molecules. A structure with a second hydration shell water molecules accepting more than one hydrogen bond (see Figure 2.6) is not a representative situation of what takes place in solution. This structure should be discarded but it could be used as a benchmark to check the potential ability to describe

arrangements which were not considered in the fitting procedure.

Figure 2.6: Representative (left) and non-representative structures (right) of water molecules around a trivalent ion.

The types of structures included in the intermolecular potential generation for this work are shown in Figures 2.7, 2.8 and 2.9: (a) energy optimized energy structures (minima), (b) structures obtained from the approaching of a water molecule to the ion in the optimized cluster (thereafter called "water extraction"), (c) structures from the approaching of a water molecule rotated by quaternions respect to the ion in the optimized cluster (thereafter called "rotated water extraction") (d) structures obtained from the normal modes of vibration, (e) structures with a partial second hydration shell obtained from the optimized hydrated aqua ion and (f) surface clusters for the less polarizing ions.

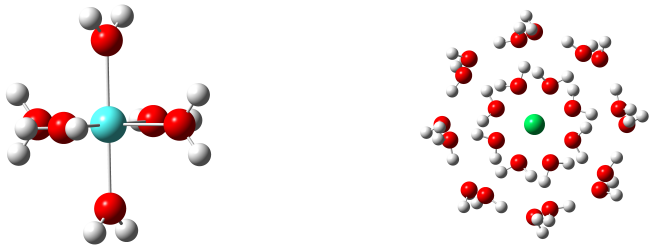

Figure 2.7: Optimized aqua ion (a) and optimized hydrated aqua ion (b).

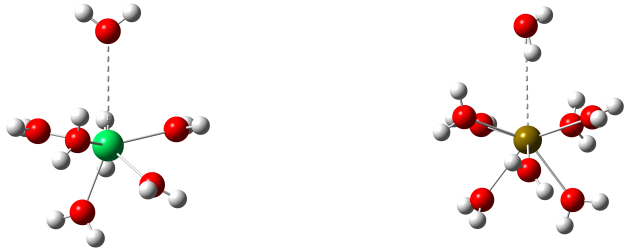

Figure 2.8: Water extraction (c) and rotated water extraction (d).

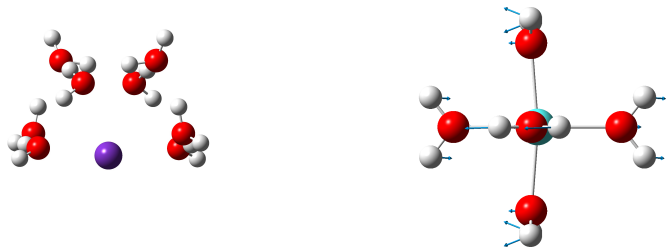

Figure 2.9: Surface cluster (e) and structure from a normal vibrational mode (f).

2.5 Bibliography

[1] Kohanoff, J. *Electronic structure calculations for solids and molecules. Theory and computational methods.*; Cambridge University Press, 2006.

[2] Levine, I. N. *Quantum Chemistry*; Pearson Prentice Hall: New York, 6ª ed., 2009.

[3] Parr, R. G.; Yang, W. *Density-Functional Theory of Atoms and Molecules*; New York: Oxford University Press, 1989.

[4] Becke, A. D. *J. Chem. Phys.* **1992**, *96*, 2155–2160.

[5] Becke, A. D. *J. Chem. Phys.* **1992**, *97*, 9173–9177.

[6] Hülsen, M.; Weigand, A.; Dolg, M. *Theoretical Chemistry Accounts: Theory, Computation, and Modeling (Theoretica Chimica Acta)* **2009**, *122*, 23–29.

[7] Leininger, T.; Nicklass, A.; Küchle, W.; Stoll, H.; Dolg, M.; Bergner, A. *Chem. Phys. Lett.* **1996**, *255*, 274–280.

[8] Becke, A. D. *J. Chem. Phys.* **1993**, *98*, 5648–5652.

[9] Zhao, Y.; Truhlar, D. G. *Theor. Chem. Acc.* **2008**, *120*, 215–241.

[10] Zhao, Y.; Truhlar, D. G. *Acc. Chem. Res.* **2008**, *41*, 157–167.

[11] Jacquemin, D.; Perpete, E. A.; Ciofini, I.; Adamo, C.; Valero, R.; Zhao, Y.; Truhlar, D. G. *J. Chem. Theory Comput.* **2010**, *6*, 2071–2085.

[12] Morales, N. Estudio teórico de propiedades fisicoquímicas de cationes metálicos en disolución: Evolución en el grupo de los alcalinos y en la serie de los lantánidos. bilio, Universidad de Sevilla, 2015.

[13] Dunning, T. *J. Chem. Phys.* **1989**, *90*, 1007.

[14] Weigend, F.; Ahlrichs, R. *Phys. Chem. Chem. Phys.* **2005**, *7*, 3297–3305.

[15] Rappoport, D.; Furche, F. *J. Chem. Phys.* **2010**, *133*, 134105(1)–134105(11).

[16] Fujiwara, T.; Mori, H.; Mochizuki, Y.; Osanai, Y.; Miyoshi, E. *Chem. Phys. Lett.* **2011**, *510*, 261–266.

[17] Fujiwara, T.; Mori, H.; Mochizuki, Y.; Takewaki, H.; Miyoshi, E. *J. Mol. Struct.* **2010**, *949*, 28–35.

[18] Yang, J.; Dolg, M. *Theor. Chem. Acc.* **2005**, *113*, 212–224.

[19] Tomasi, J.; Mennucci, B.; Camini, R. **2005**, *5*, 2999–3094.

[20] Alder, B.; Wainwright, T. *J Chem. Phys.* **1959**, *31*, 459.

[21] Swope, W.; Andersen, H.; Berens, P.; Wilson, K. *J. Chem. Phys.* **1982**, *76*, 637–649.

[22] Nosé, S. *J. Chem. Phys.* **1984**, *81*, 511–519.

[23] Hoover, W. G. *Phys. Rev. A* **1985**, *31*, 1695–1697.

[24] Muñoz-Páez, A.; Sánchez Marcos, E. En *Comprehensive Inorganic Chemistry {II} (Second Edition)*, second edition ed.; Poeppelmeier, J. R., Ed.; Elsevier: Amsterdam, 2013; págs. 133 – 159.

[25] Rehr, J.; Albers, R. *Rev. Mod. Phys.* **2000**, *72*.

[26] Koningsberg, D. C.; Prins, R. *X-ray absorption, principles, aapplication, techniques of EXAFS, SEXAFS and XANES.*; Wiley: New York, 1988.

[27] Bianconi, A.; Dell'Aricia, M.; Durham, P. J.; Pendry, J. B. *Phys. Rev. B* **1982**, *26*, 6502–6508.

[28] Rehr, J. J.; Kas, J. J.; Vila, F. D.; Prange, M. P.; Jorissen, K. *Phys. Chem. Chem. Phys.* **2010**, *12*, 5503–5513.

[29] Palmer, B.; Pfund, D.; Fulton, J. *J. Phys. Chem.* **1996**, *100*, 13393–13398.

[30] Campbell, L.; Rehr, J.; Schenter, G.; McCarthy, M.; Dixon, D. *J. Synchrotron Radiat.* **1999**, *6*.

[31] Merkling, P. J.; Muñoz-Páez, A.; Sánchez Marcos, E. *J. Am. Chem. Soc.* **2002**, *124*, 10911–10920.

[32] Pappalardo, R.; Sánchez-Marcos, E. *J. Phys. Chem.* **1993**, *97*, 4500–4504.

[33] Martínez, J. M.; Pappalardo, R. R.; Sánchez Marcos, E. *J. Chem. Phys.* **1998**, *109*, 1445–1455.

[34] Martínez, J.; Pappalardo, R.; Sánchez Marcos, E. *J. Am. Chem. Soc.* **1999**, *121*, 3175–3184.

[35] Galbis, E.; Hernández-Cobos, J.; den Auwer, C.; Naour, C. L.; Guillaumont, D.; Simoni, E.; Pappalardo, R. R.; Sánchez Marcos, E. *Angew. Chem. Int. Ed.* **2010**, *22*, 3811–3815.

[36] Galbis, E.; Hernández-Cobos, J.; Pappalardo, R. R.; Sánchez Marcos, E. *J. Chem. Phys.* **2014**, *140*, 214104.

[37] Villa, A.; Hess, B.; Saint-Martin, H. *J. Phys. Chem. B* **2009**, *113*, 7270–7281.

[38] Saint-Martin, H.; Hernández-Cobos, J.; Bernal-Uruchurtu, M. I.; Ortega-Blake, I.; Berendsen, H. J. C. *J. Chem. Phys.* **2000**, *113*, 10899–10912.

[39] Marcus, Y. *Ion properties*; Markel Dekker, Inc, 1997.

[40] Zhao, Y.; Truhlar, D. *Chem. Phys. Lett.* **2011**, *502*, 1–13.

Chapter 3

Intermolecular potentials

In this section the results of the potential fitting are shown. In order to assess the fitting quality, the interaction energy and the metal-oxygen average distance of the quantum mechanical structures and those given by the potential are compared. The interaction energy has been calculated as the energy difference between the hydrated cluster energy and the energy of its isolated components at its minimum energy geometry.

$$\mathrm{Eint} = \mathrm{E}_{[\mathrm{M(H_2O)}_n]^{m+}} - (\mathrm{E}_{\mathrm{M}^{m+}} + \mathrm{nE}_{\mathrm{H_2O}}) \tag{3.1}$$

The notation origin of the geometry used//quantum level employed in the calculation is used: if the structure is optimized at a quantum mechanical level the label is QM//QM, Pot//QM denotes single point calculations using the classical potentials over the QM structure, and Pot//Pot denotes optimized structures with the potential. Structures with water molecules in the first (i) and second shell (j) are defined as [i+j] structures. To describe the calculation level the notation Level/Basis set is used, that is refered to the quantum mechanical method and the basis set used for the ion, oxygen and hydrogen, respectively. If a pseudopotential is used for the metal it will be detailed in the corresponding section.

3.1 Alkaline group

The alkaline group from lithium to caesium has been studied. The intermolecular potential has been built at the M062x/def2-TZVPPD level using an already generated[1] Potential Energy Surface (PES) together with new sets of structures for K^+, Rb^+ and Cs^+. For Rb^+ and Cs^+ the ECP28MBW[2] and the ECP46MBW[2] effective core pseudopotentials (ECP) have been employed, respectively, together with the def2-TZVPPD basis set to describe the valence electrons (8 electrons that are filling the s and p orbitals of higher energy).

3.1.1 Light alkalines

Lithium-water and sodium-water intermolecular potentials were built using inner cluster structures with 3-5 water molecules in the first hydration shell and up to 5 water molecules in the second shell for lithium. For sodium, clusters including 4-6 water molecules in the first hydration shell and up to 4 water molecules in the second shell were used. In the case of lithium the ion was not considered polarizable. The hard character of this small cation justifies this option. Moreover, a polarizable Li^+ ion would force the use of a spring constant extremely high that would need an extremely short timestep for MD simulations.

The optimized lithium tetrahydrate has been calculated at the MP2/aug-cc-pVTZ level. An interaction energy of -102.4 kcal/mol and an average intermolecular ion-distance of 1.96 Å were obtained. Similar interaction energies were found in previous theoretical works, at the MP2/6-311++G(3d,3p)[3] level counterpoisse corrected -100.4 kcal/mol, at a MP2/6-311++G(2d,2p)//MP2/6-31+G(d,p)[4] calculation -99.9 kcal/mol and at the MP2/6-31G*//RHF/6-31+G*[5] a binding energy at 298 K of -98.6 kcal/mol. These values are similar to those obtained at the M062x/def2-TZVPPD, where the interaction energy is -107.4 kcal/mol and the interatomic distance is 1.92 Å.

Sodium hexahydrate at the MP2/aug-cc-pVTZ level has an interaction energy of -95.4 kcal/mol and an intermolecular distance of 2.50 Å. A larger interaction energy was found for the hydrate at the M062x/def2-TZVPPD level, -107.7 kcal/mol with a metal-oxygen distance equals to 2.38 Å. Gledening et al.[5] found a binding energy at 298 K of -91.2 kcal/mol for the sodium hexahydrate at the MP2/6-31+G*//HF/6-31+G* level.

As can be seen in Table 3.1, there is a good energetic and structural agreement of the most usual coordinations in solution, being the Lithium 4+1 structure more stable than the pentahydrate in the case of the potential. Also there is a good reproduction of the entire set of structures included in the fitting (see Figures 3.6 and 3.7) obtaining a mean error of 1.9 kcal/mol and 2.7 kcal/mol for lithium and sodium, respectively, with the obtained force field parameters (see Table 3.13).

Table 3.1: Energies (kcal/mol) and distances (Å) of Li^+ and Na^+ hydrates.

Structure	QM//QM	QM//Pot	Pot//Pot	R_{QM}	R_{Pot}
$Li(H_2O)_3^+$	-89.4	-91.7	-92.6	1.88	1.86
$Li(H_2O)_4^+$	-107.4	-107.6	-108.6	1.92	1.93
$Li(H_2O)_5^+$	-118.1	-114.0	-122.6*	2.02	4x1.93/1x3.63
$Na(H_2O)_4^+$	-80.1	-81.7	-82.3	2.28	2.28
$Na(H_2O)_5^+$	-93.5	-93.0	-94.5	2.36	2.35
$Na(H_2O)_6^+$	-107.5	-102.6	-105.4	2.38	2.38

*4+1 structure

3.1.2 Heavy alkalines

An initial intermolecular potential with inner cluster structures was built for the heavy alkalines potassium, rubidium and caesium. These potentials systematically overestimated the cation-oxygen distance in solution. When surface clusters were included in the set of structures to fit the new potentials represented much better the experimental properties of these ions in

water.

The surface clusters were generated running a gas phase MD simulation at 100 K of hydrates containing from 7 to 10 water molecules. From these simulations 50 equidistant structures were extracted, and optimized classically. The 5 structures having lower energies were optimized at the quantum mechanical level and added to the set of structures to be used in the fitting. In addition, the 10 lowest energy structures optimized classically are included in the training set.

Figure 3.1 and 3.2 show the Rb^+ clusters belonging to inner and surface clusters for coordination numbers 8 and 9.

Figure 3.1: Rb^+ octahydrate minimum structures, inner (left) and surface cluster (right).

In Table 3.2 the interaction energy values of the minimum energy structures of potassium, rubidium and caesium hydrates are displayed. In Figures 3.3, 3.4 and 3.5 shown a normalized histogram (normalized by the maximum amount of structures in a given range) of the interaction energy values of the structures included in the fitting. It can be seen that the interaction energy for potassium surface cluster structures with coordination 7 and 8 have similar energies to the lower energy of inner aggregates. However, this is not the case for Rb^+ and particularly for Cs^+. For these

Figure 3.2: Rb^+ enneahydrate minimum structures, inner (left) and surface cluster (right).

two cations surface clusters are more stable.

Table 3.2: QM interaction energy for surface and inner minimum energy structures (kcal/mol) of heavy alkalines.

Structure	inner structure	surface structure
$K(H_2O)_7{}^+$	-103.4	-102.9
$K(H_2O)_8{}^+$	-115.1	-116.9
$Rb(H_2O)_8{}^+$	-108.9	-113.3
$Rb(H_2O)_9{}^+$	-114.0	-126.1
$Cs(H_2O)_8{}^+$	-105.8	-107.1
$Cs(H_2O)_9{}^+$	-109.2	-118.3

The lowest energy structures for K^+, Rb^+ and Cs^+ with 7, 8 and 9 water molecules, respectively, have been optimized at the MP2/aug-cc-pVTZ level obtaining interaction energies of -93.2 kcal/mol, -99.3 kcal/mol and -127.7 kcal/mol (at MP2(full)/aug-cc-pVTZ), respectively are similar values to those obtained at the M062x/def2-TZVPPD level, -102.9 kcal/mol, -113.3 kcal/mol and -118.3 kcal/mol for the same type of structures.

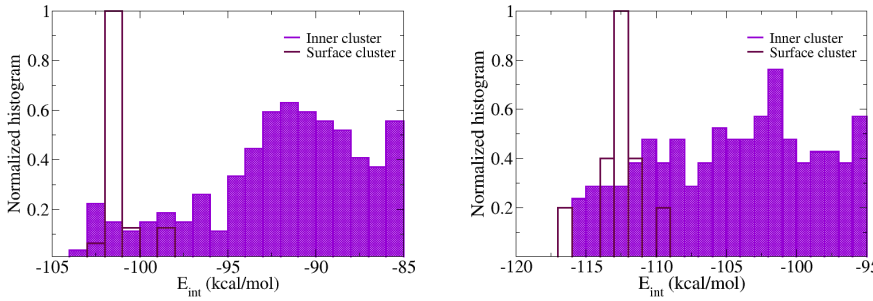

Figure 3.3: Energy distribution of K^+ heptahydrate (left) and octahydrate (right).

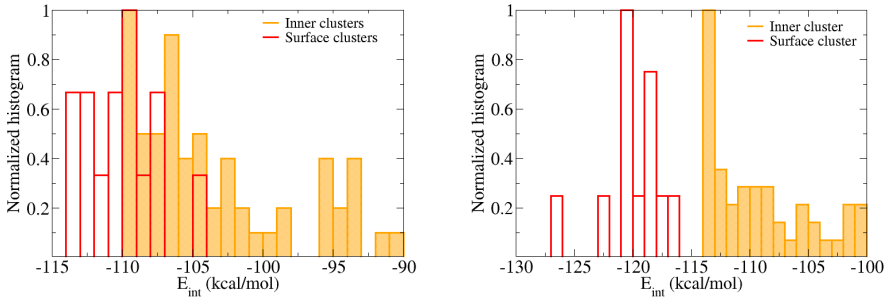

Figure 3.4: Energy distribution of Rb^+ octahydrate (left) and enneahydrate (right).

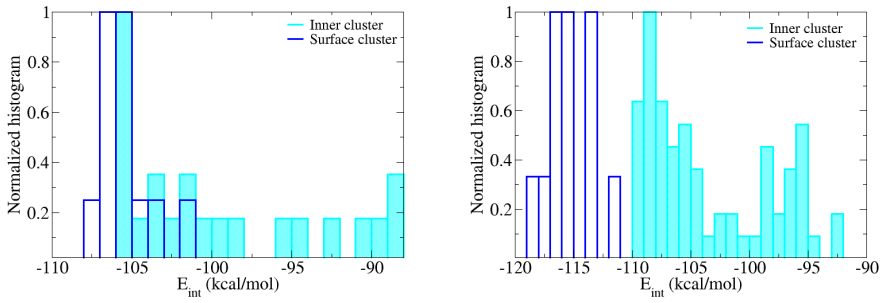

Figure 3.5: Energy distribution of Cs^+ octahydrate (left) and enneahydrate (right).

The rubidium and caesium fittings were performed using hydrated clusters from 6 to 10 water molecules in the first-shell, and up to 2 water molecules in the second shell for inner cluster structures. In the case of potassium structures with coordination number from 4 to 10 were employed, with up to 2 water molecules in the second shell for the inner cluster structures.

The new potentials were performed including the surface cluster structures and reparametrizing the previous potential without any constraint. The inclusion of surface cluster structures in the fitting provoqued a shortening of the intermolecular distances, as can be see in Table 3.3 and 3.4. On the fittings a good energetic reproduction has been found, having a fitting sigma error of 2.2 kcal/mol, 1.9 kcal/mol and 1.6 kcal/mol (see Figures 3.8, 3.9 and 3.10) for K^+, Rb^+ and Cs^+, respectively (see 3.13).

Table 3.3: Energies (kcal/mol) and distances (Å) of K^+, Rb^+ and Cs^+ inner cluster hydrates.

Structure	QM//QM	QM//Pot	Pot//Pot	R_{QM}	R_{Pot}
$K(H_2O)_6{}^+$	-89.7	-88.4	-91.1	2.77	2.72
$K(H_2O)_7{}^+$	-103.4	-103.4	-105.9	2.95	2.86
$Rb(H_2O)_8{}^+$	-109.9	-109.0	-111.5	3.02	2.95
$Rb(H_2O)_9{}^+$	-114.0	-110.1	-120.6	3.04	3.02
$Cs(H_2O)_8{}^+$	-105.81	-106.0	-108.6	3.20	3.14
$Cs(H_2O)_9{}^+$	-109.2	-107.4	-110.9	3.20	3.14

Table 3.4: Energies (kcal/mol) and distances (Å) of K^+, Rb^+ and Cs^+ surface cluster hydrates.

Structure	QM//QM	QM//Pot	Pot//Pot	R_{QM}	R_{Pot}
$K(H_2O)_6{}^+$	-86.9	-92.4	-92.7	2.78	2.74
$K(H_2O)_7{}^+$	-102.9	-104.0	-105.8	2.79	2.79
$Rb(H_2O)_8{}^+$	-109.5	-109.7	-112.5	3.24	3.12
$Rb(H_2O)_9{}^+$	-120.6	-119.6	-123.0	3.11	3.04
$Cs(H_2O)_8{}^+$	-107.1	-104.8	-108.0	3.31	3.20
$Cs(H_2O)_9{}^+$	-118.3	-115.6	-118.7	3.54	3.43

3.2 Alkaline-earth

The heavier alkaline-earth Sr^{2+}, Ba^{2+} and Ra^{2+} cations in solution have been studied. The intermolecular potentials have been built at the M062x/def2-TZVPP level using ECP of the Stuttgart's group: ECP28MDF[6] for strontium, ECP46MDF[6] for barium and ECP78MDF[6] for radium, including in the core 28, 46 and 78 electrons, respectively, and keeping 8 valence electrons in their higher energy s and p orbitals, that are described by the basis sets ECP28MDF, ECP46MDF and ECP78MDF.

At the MP2/aug-cc-pVTZ level, the strontium octahydrate has an in-

teraction energy of -234.5 kcal/mol with an intermolecular distance of 2.70 Å while the M062x/def2-TZVPP interaction energy is -272.5 kcal/mol and the interatomic distance of 2.59 Å. Kaltsoyannis et al.[7] found an interaction energy of -243.1 kcal/mol and an average distance of 2.65 Å for the octa-coordinated strontium at the TPSS/def-TZVPP level. The same bias can be found in other works,[8] where shorter distances are found when comparing DFT methods to the MP2 method.

For the barium enneahydrate minima the MP2/aug-cc-pVTZ level gives an interaction energy of -209.8 kcal/mol and an interatomic distance of 3.04 Å while the M062x/def2-TZVPP gives an interaction energy of -258.0 kcal/mol with an interatomic distance of 2.82 Å. Due to the energetic and structural differences among the methods this could be a good example of a case where is appropiate to built a potential for both methods. But the potentials where build at the M06 level to continue its testing.

The optimization of the radium enneahydrate at the MP2(full)/aug-cc-pVTZ gives an interaction energy of -238.1 kcal/mol and a average distance of 2.89 Å, which are similar values to those obtained at the M062x/def2-TZVPP level: interaction enegy of -236.6 kcal/mol and an average metal-oxygen distance of 2.93 Å. In a previous work[9] a binding energy ZPE corrected at the MP2/6-31G(d,p) level gave -84.6 kcal/mol and a M-O distance of 2.93 was found.

The strontium-water potential has been built using inner surface hydrates with 7, 8 and 9 water molecules with up to 2 water molecules in the second shell. The barium-water potential was built using structures with 8 and 9 water molecules and up to 2 water molecules in the second shell. The same process followed in the search of surface structures for the heavy alkalines was performed to find a deca-coordinated structure for barium and radium, obtaining a inner cluster structure with 8 water in the first-shell and 2 in the second shell accepting 2 hydrogen bonds each one. In these two cases, no surface clusters were found. The radium-water potential was built using structures with 8 and 9 water molecules in the first-shell and

structures with a water molecule in the second shell. The quality of the potentials built for the alkaline-earth cations is shown in Table 3.5.

As can be seen there is a good energetic and structural reproduction of the most plausible coordination numbers in solution. Also there is a good energetic reproduction of the entire set of structures included in the fitting (see Figure 3.8, 3.9 and 3.10) obtaining a mean error of 3.5 kcal/mol, 2.7 kcal/mol and 3.7 kcal/mol, for Sr^{2+}, Ba^{2+} and Ra^{2+}, respectively (force field parameters are in Table 3.14).

Table 3.5: Energies (kcal/mol) and distances (Å) of Sr^{2+}, Ba^{2+} and Ra^{2+} hydrates.

Structure	QM//QM	Pot//QM	Pot//Pot	R_{QM}	R_{Pot}
$Sr(H_2O)_7{}^{2+}$	-251.3	-254.6	-256.5	2.56	2.55
$Sr(H_2O)_8{}^{2+}$	-272.5	-272.4	-274.8	2.59	2.59
$Sr(H_2O)_8{}^{2+}(H_2O)$	-292.6	-288.8	-292.5	8x2.59/1x4.52	8x2.59/1x4.43
$Sr(H_2O)_9{}^{2+}$	-288.6	-284.1	-288.2	2.62	2.64
$Ba(H_2O)_8{}^{2+}$	-241.2	-241.1	-247.0	2.79	2.77
$Ba(H_2O)_8{}^{2+}(H_2O)$	-260.9	-258.9	-264.2	8x2.79/1x4.70	8x2.79/1x4.59
$Ba(H_2O)_9{}^{2+}$	-258.0	-257.0	-263.2	2.82	2.82
$Ra(H_2O)_8{}^{2+}$	-215.4	-214.2	-225.2	2.91	2.90
$Ra(H_2O)_9{}^{2+}$	-236.6	-235.1	-241.6	2.99	2.94
$Ra(H_2O)_{10}{}^{2+}$	-255.1	-253.0	-256.8	2.96	2.98

3.3 Transition metals cations

Different QM methods to build PES of the transition metal aqua ions have been employed.

The Co^{2+} PES was calculated at the B3LYP/aug-cc-pVTZ level using the ECP10MDF[10] for the cation, that includes the inner 10 electrons in the core and keeps 15 electrons explicitly, filling the high energy s and p orbitals, and includes 7 d electrons all of them described by the ECP10MDF basis set. In the cobalt case, which forms a well stablished hexahydrate

aqua ion in solution,[11] only structures with 6 water molecules has been used to build the potential corresponding to cobalt high spin electronic state (quartet multiplicity), that is sensible to the coordination number.

Akesson et al.[12] calculated the binding energy of the cobalt hexahydrate at the SCF level including CASSCF corrections and employing gaussian-like Huzinaga basis sets[13] obtaining -307.6 kcal/mol. A single point calculation at the NEVPT2/aug-cc-PVTZ quantum level with the ECP10MDF for cobalt over the optimized hexahydrate at the B3LYP/aug-cc-pVTZ level gave a binding energy of -354.6 kcal/mol. Similar value was found at the B3LYP/aug-cc-pVTZ, -342.7 kcal/mol.

The obtained potential (see Table 3.6) gives an accurate description of both energetic and structural properties of the mimimum energy hexahydrate as well as the entire set of structures included in the fitting (see Figure 3.18). A mean error of 1.5 kcal/mol for the parameter is found (see Table 3.16).

Table 3.6: Energies (kcal/mol) and distances (Å) of Co^{2+} hydrates.

Structure	QM//QM	Pot//QM	Pot//Pot	R_{QM}	R_{Pot}
$Co(H_2O)_6{}^{2+}$	-342.7	-342.7	-342.5	2.11	2.11

For the Cd^{2+} case the PES have been built at the M06/def2-TZVPP level using the ECP28MWB[14] pseudopotential, that includes 28 electrons and keeps 16 valence electrons filling the higher energy p and d orbitals, that are described by the basis set ECP28MWB. A previous work[12] at the HF level using Huzinaga basis set found a binding energy of -272.0 kcal/mol. At the MP2/aug-cc-pVTZ level was found an interaction energy of -302.8 kcal/mol, similar to the value found at the M06/def2-TZVPP, -299.2 kcal/mol. A good reproduction of the QM data is performed by the developed intermolecular potential, being the mean error 1.4 kcal/mol (see Figure 3.19).

Table 3.7: Energies (kcal/mol) and distances (Å) of Cd^{2+} hydrates.

Structure	QM//QM	Pot//QM	Pot//Pot	R_{QM}	R_{Pot}
$Cd(H_2O)_6{}^{2+}$	-299.2	-298.8	-301.8	2.294	2.294
$Cd(H_2O)_6{}^{2+}(H_2O)$	-319.3	-317.4	-320.7	6x2.293/1x4.317	6x2.289/1x4.504
$Cd(H_2O)_7{}^{2+}$	-315.2	-315.5	-319.0	2.361	2.352

The Sc^{3+} PES has been generated at the MP2/aug-cc-pVTZ level with the ECP10MDF[10] for the ion, that includes 10 electrons in the core and keeps 8 electrons in their higher energy s and p orbitals, described by the ECP10MDF basis set. Rudolph et al.[15] found a binding energy at the MP2/6-31+G* level of -560.5 kcal/mol for the hexahydrate. On a work[12] at the HF level using Huzinaga basis set a binding energy of -518.6 kcal/mol was found. Similar value to those previously published was found at the MP2/aug-cc-pVTZ, -539.3 kcal/mol.

In the case of Sc^{3+} 4 ion-water potentials have been generated. Hydrated clusters of a given coordination number for each potential due to the overestimation of the water-water interaction in repulsive geometries (see Figure 2.4). As the energy bias between the water model and the quantum method increases when water-water distances shorter, this results in a relevant energy bias coordination dependency.

For this reason, the potential fitting was performed for a single coordination, Pot4, Pot6, Pot7 and Pot8 using structures with 4, 6, 7 and 8 water molecules, respectively. These potentials have used a small amount of structures to be fitted: the optimized minimum structure, the extraction of a water molecule from the cluster, and structures extracted from the bending and stretching cluster deformations. In Table 3.9 are shown the interaction energy values for each potential at its optimized structures at a given coordination.

As can be seen in Table 3.9 Pot 6 is able to reproduce quite well the

information from coordination 6. But the interaction energy of $Sc(H_2O)_7{}^{3+}$ is underestimated. This can be explained by decomposing the interaction energy in an ion-water contribution and a water-water contribution:

$$E_{int} = E_{I-W} + E_{W-W} \tag{3.2}$$

If the water eskeletons of the minima are analyzed a more repulsive energy for the MCDHO2 than for the MP2/aug-cc-pVTZ is found (see Table 3.8), with a energy gap increasing with the coordination number.

Table 3.8: Energy (kcal/mol) comparison of water skeletons from optimized Sc^{3+} hydrates.

Structure	MP2//MP2	MCDHO2//MP2	Δ E
$(H_2O)_6$	16.0	20.9	-4.9
$(H_2O)_7$	25.8	33.3	-7.5
$(H_2O)_8$	33.1	43.4	-10.3

When the Pot6 is built as the water model gives a more repulsive energy than the QM computation, the E^{Pot}_{I-W} compensates it to match the E^{QM}_{int} obtained trough quantum mechanical calculations.

$$E^{Pot}_{I-W} = E^{Pot}_{W-W} - E^{QM}_{int} \tag{3.3}$$

When considering the case of the heptahydrate, the water molecules of the aqua ion shrinks, then the water-water energy repulsion increases with respect of the hexahydrate, thus the compensation in the E^{Pot}_{I-W} term of Pot6 fitting is not enough to match the heptahydrate interaction energy. When considering the Pot7 the opposite behaviour is observed if the hexahydrate is considered. Given that in the heptahydrate the compensation is higher, when Pot7 is used to describe the hexahydrate an overestimation appears (see Tablle 3.9, Pot7//QM gives an interaction energy of -554.1

kcal/mol, whereas the QM/QM energy is -539.3 kcal/mol). Pot4 and Pot8 are just two more extreme situations, in Pot4 the E_{I-W}^{Pot} compensation is the smallest one whereas in the Pot8 is the biggest. Thus, Table 3.9 collects for the $Sc(H_2O)_6{}^{3+}$ an interaction energy of -527.5 kcal/mol given Pot4//QM and -5606.5 kcal/mol given by Pot8//QM.

MCDHO2 model was built at the MP2/aug-cc-pVQZ' level with a correction of the 50% of the BSSE. When the calculation of the $(H_2O)_6$ is performed at the MP2/aug-cc-pVQZ' level the interaction energy turns to be 17.2 kcal/mol, and when is added a 50% correction of the BSSE the interaction energy is 17.7 kcal/mol. Thus, one factor responsible of the energy difference is related to the different calculation condition and other factor could be the parametrization of the ion-dipole configurations existing in the hydration shells of highly polarizing cations, as the Sc^{3+} case is.

The potential was performed for each coordination number because when the fitting of two coordinations was tried, simultaneously simultaneously forcing to reproduce the E_{int} of both coordinations the ion-water distance increases a 15%. In the way the scandium potentials have been built the fitted coordination has been well reproduced (see Figure 3.14, 3.15, 3.16 and 3.17) having a sigma error of 0.8 kcal/mol, 1.3 kcal/mol, 1.1 kcal/mol and 0.8 kcal/mol, for Pot6, Pot7, Pot4 and Pot8, repectively (see Table 3.15).

In spite of this water model limitation we were able to build a potential that describes quite well the coordination fitted. Being the main problem the energy understimation of higher coordinations. An illustrative way to quantify this problem, can be seen in the Pot6 section of Table 3.9. The interaction energy for $Sc(H_2O)_6{}^{3+}(H_2O)$ using the MP2/aug-cc-PVTZ level is 4 kcal/mol more stable than $Sc(H_2O)_7{}^{3+}$, but in Pot//Pot6 gives a difference of 16 kcal/mol.

Although the energy difference increases, this does not modify that the $Sc(H_2O)_6{}^{3+}(H_2O)$ is more stable than the $Sc(H_2O)_7{}^{3+}$. Although this comparison should not be taken as the way to evaluate the most probable coordination, because in $Sc(H_2O)_6{}^{3+}(H_2O)$ the second shell water molecule

Table 3.9: Energies (kcal/mol) and distances (Å) of Sc^{3+} hydrates.

Structure	QM//QM	Pot4//QM	Pot4//Pot4	R_{PotQM}	R_{Pot4}
$Sc(H_2O)_6^{3+}$	-539.3	-527.5	-531.4	2.18	2.18
$Sc(H_2O)_6^{3+}(H_2O)$	-574.2	-555.7	-564.7	6x2.24/1x4.181	6x2.18/1x4.32
$Sc(H_2O)_7^{3+}$	-570.5	-542.1	-547.4	2.23	2.26
$Sc(H_2O)_7^{3+}(H_2O)$	-606.2	-572.3	-594.6*	7x2.21/1x4.043	6x2.14/2x4.08
$Sc(H_2O)_8^{3+}$	-601.0	-560.4	-595.3*	2.28	6x2.17/2x3.91
Structure	QM//QM	Pot6//QM	Pot6//Pot6	R_{PotQM}	R_{Pot6}
$Sc(H_2O)_6^{3+}$	-539.3	-539.4	-543.1	2.18	2.18
$Sc(H_2O)_6^{3+}(H_2O)$	-574.2	-566.8	-576.5	6x2.24/1x4.18	6x2.18/1x4.32
$Sc(H_2O)_7^{3+}$	-570.5	-554.7	-559.7	2.23	2.25
$Sc(H_2O)_7^{3+}(H_2O)$	-606.2	-585.4	-606.5*	7x2.21/1x4.043	6x2.17/2x4.12
$Sc(H_2O)_8^{3+}$	-601.0	-573.9	-607.3*	2.28	6x2.17/2x3.90
Structure	QM//QM	Pot7//QM	Pot7//Pot7	R_{PotQM}	R_{Pot7}
$Sc(H_2O)_6^{3+}$	-539.3	-554.1	-557.8	2.18	2.17
$Sc(H_2O)_6^{3+}(H_2O)$	-574.2	-580.6	-591.3	6x2.24/1x4.18	6x2.17/1x4.31
$Sc(H_2O)_7^{3+}$	-570.5	-570.5	-607.2	2.23	2.25
$Sc(H_2O)_7^{3+}(H_2O)$	-606.2	-601.6	-621.5*	7x2.21/1x4.04	6x2.17/1x4.31
$Sc(H_2O)_8^{3+}$	-601.0	-590.6	-622.5*	2.28	6x2.16/2x3.90
Structure	QM//QM	Pot8//QM	Pot8//Pot8	R_{PotQM}	R_{Pot8}
$Sc(H_2O)_6^{3+}$	-539.3	-566.5	-570.8	2.18	2.15
$Sc(H_2O)_6^{3+}(H_2O)$	-574.2	-591.0	-604.6	6x2.24/1x4.18	6x2.15/1x4.30
$Sc(H_2O)_7^{3+}$	-570.5	-581.9	-586.4	2.23	2.23
$Sc(H_2O)_7^{3+}(H_2O)$	-606.2	-613.8	-634.9	7x2.21/1x4.04	6x2.15/1x4.10
$Sc(H_2O)_8^{3+}$	-601.0	-601.3	-635.8*	2.28	6x2.14/2x3.88

*[6+2] structure

forms two hydrogen bonds with first-shell water molecules, something that does not and this not happen in solution, then overestimating its interaction.

3.4 Lanthanides

The Lanthanide potentials has been built using M06 family functionals together with the def2-TZVPP basis set for oxygen and hydrogen. The Lanthanum PES was calculated during a previous work [1] at the M06/def2-TZVPP level using the ECP46MBW [16,17] pseudopotential and ECP46MBW-

I basis set for the ion. The neodymium and thullium PES were built at the M062x/def2-TZVPP level using the pseudopotentials ECP49MWB [16,17] and ECP58MWB, [16,17] respectively. In these pseudopotentials the f electrons are included in the core, with 8 valence electrons occuping the higher energy s and p orbitals, that are described by the ECP49MWB-I and ECP58MWB-I basis sets.

In a published work at the the MP2 level, [18] where the spMCP-dzp basis for Oxygen and the cc-pVDZ for hydrogen were used an interaction energy of -509.2 kcal/mol and an interatomic distance of 2.63 Å for the lanthanum enneahydrate were found. Similar values were provided by the M06/def2-TZVPP [1] description: interaction energy of -493.2 kcal/mol and interatomic distance of 2.631 Å.

Dolg and collegues [19] computed the binding energy taking into account the water cluster energy as monomer, and considering the ZPE correction and including the COSMO solvation model in the calculation, given a value of -406.6 kcal/mol, -426.7 kcal/mol and -461.8 kcal/mol and an average M-O distance of 2.591, 2.534 and 2.378 Å for the lanthanum and neodymium enneahydrates and thullium octahydrate.

For the thullium octahydrate at the MP2/aug-cc-pVTZ level, an interaction energy of -532.0 kcal/mol and an intermolecular distance 2.39 Å is found, which are similar values to those obtained at the M062x level: interaction energy of -556.6 kcal/mol and interatomic distance of 2.38 Å. For the Neodymium enneahydrate at the MP2/aug-cc-pVTZ level, the interaction energy is -509.8 kcal/mol and the interatomic distance 2.54 Å, similar to the interaction energy of -529.0 kcal/mol with interatomic distance of 2.55 Å found at the M062x/def2-TZVVP.

The fittings were performed using the minimum energy structure, a water extraction from the cluster, rotated scans, structures from normal modes of vibrations and structures with a first-shell and a partial second shell with first-shell coordinations between 7 and 8 for thullium and struc-

tures with coordination numbers of 8 and 9 for lanthanum and neodymium, and up to 2 water molecules in the second shell for all the cations. As in the scandium case there is a water model effect that limits the quality of the fittings when the first-shell water molecules have shorter distances among them and when there is more than one coordination to fit. Differently from the scandium case, for the lanthanoids there are more than one coordination number included in the fitting as this pathology has less impact on the fit. In this case the fitting has been performed in two steps. In the first step the most probable coordination, 8 for thulium and 9 for neodymium and lanthanum, have been fitted. At that point the force field exponentials terms $\mathrm{U}_{inter}(q_{\mathrm{O}}, q_{\mathrm{M}})$ and $\mathrm{U}_{inter}(Z_i, Z_{\mathrm{M}})$ were fixed, and the rest of the structures with other coordination numbers being added to get the final reparametrization.

As can be seen in Figures 3.20, 3.21 and 3.22 all the structures are not well reproduced. The main coordination fitted 8 in thullium and 9 in neodymium and lanthanum are well fitted. Meanwhile the lower coordinations 7 in thullium and 8 in neodymium and thullium are overestimated. The general sigma errors for the fitting are 4.3 kcal/mol, 2.8 kcal/mol and 4.4 kcal/mol for thullium, neodymium and thullium, respectively.

As can be seen in Table 3.10 there is a good agreement in the energy and structural properties for the main coordination numbers fitted, and the energetic bias explained in the previous section is observed. For higher coordinations is obtained an energy underestimation and for lower coordinations an overestimation. Anyway the structural properties are well reproduced for all coordinations.

Table 3.10: Energies (kcal/mol) and distances (Å) of La^{3+}, Nd^{3+} and Tm^{3+} hydrates.

Structure	QM//QM	Pot//QM	Pot//Pot	d_{QM}	d_{Pot}
$La(H_2O)_8{}^{3+}$	-464.4	-467.8	-472.1	2.59	2.59
$La(H_2O)_8{}^{2+}(H_2O)$	-494.3	-494.6	-499.2	8x2.59/1x4.41	8x2.59/1x4.40
$La(H_2O)_9{}^{3+}$	-493.2	-491.3	-495.5	2.62	2.63
$Nd(H_2O)_8{}^{3+}$	-498.7	-506.4	-509.7	2.52	2.52
$Nd(H_2O)_8{}^{2+}(H_2O)$	-529.8	-533.3	-537.3	8x2.51/1x4.35	8x2.51/1x4.34
$Nd(H_2O)_9{}^{3+}$	-529.0	-528.3	-532.0	2.55	2.56
$Tm(H_2O)_7{}^{3+}$	-518.2	-527.8	-532.0	2.35	2.34
$Tm(H_2O)_7{}^{3+}(H_2O)$	-553.8	-558.8	-563.5	7x2.35/1x4.14	7x2.34/1x4.15
$Tm(H_2O)_8{}^{3+}$	-556.3	-555.3	-559.0	2.38	2.38
$Tm(H_2O)_8{}^{3+}(H_2O)$	-588.1	-583.1	-583.1	8x2.38/1x4.24	8x2.38/1x4.23
$Tm(H_2O)_9{}^{3+}$	-583.2	-569.2	-585.9*	2.43	8x2.38/1x4.16

*[8+1] structure

3.5 Actinide

3.5.1 Thorium

The thorium potential was built at the M062x/def2-TZVPP level employing the ECP78MWB[20] and the basis set ECP78MWB-AVTZ on the cation. In this ECP 78 electrons are included in the core and the valence electrons are filling the higher energy s and p orbitals. In previous study at the B3LYP/6-31G*[21] level an interaction energy of -785.0 kcal/mol was found and in other at the MP2/cc-pVTZ[22] was found an interaction energy of -786.6 kcal/mol. This work found an interaction energy of -832.1 kcal/mol and an interatomic distance of 2.51 Å.

In the building of the thorium-water potential, as in the case of scandium and lanthanoids, limitations were experimented. The potential was built following the same process performed in the lanthanoid case, i.e. including coordination numbers from 9 to 10 in a fitting step-by-step process. First of all, the most probable coordination, 9, is included in the fitting, in a second step the coordination 10 is included keeping the exponencial param-

eters of the force field fixed. Structures with 9 and 10 water molecules in the first hydration shell, including the minimum structure, water extractions, structures from normal modes of vibration, rotated scans and structures with a first hydration shell and a partial second shell were employed.

As can be seen in Figure 3.23 there is not a well reproduction of the whole set of points, as we have a sigma error of 7.7 kcal/mol. In Figure 3.23 shows how decacoordinated and ennea-coordinated structures lie on either side of the perfect fitting line (red line), meaning a systematic underestimation on the decacoordinated structures and a systematic overestimation of the ennea-coordinated structures. Even though this uncertainty in the fitting can be seen in Table 3.11 that the interaction energy values obtained with the potential are similar to the quantum values and there is a good structural agreement with the obtained force field parameters (see Table 3.17).

Table 3.11: Energies (kcal/mol) and distances (Å) of Th^{4+} hydrates.

Structure	QM//QM	Pot//QM	Pot//Pot	d_{QM}	d_{Pot}
$Th(H_2O)_8{}^{4+}$	-786.7	-806.5	-811.7	2.47	2.47
$Th(H_2O)_9{}^{4+}$	-832.1	-840.6	-846.1	2.51	2.51
$Th(H_2O)_9{}^{4+}(H_2O)$	-874.9	-878.8	-884.9	9x2.51/1x4.29	9x2.51/1x4.31
$Th(H_2O)_{10}{}^{4+}$	-864.5	-857.6	-884.1*	2.55	9x2.51/1x4.29

*9+1 structure

3.6 Suplementary information

3.6.1 Water model force field coefficients

Harmonic constant, k_{M}, is in H/Bohr^2, electrostatic decaiment, λ_{O}, is in Bohr, distances are in Bohr and angles are in radians.

Table 3.12: MCDHO2 coefficients.

	MCDHO2
Z_{H}	0.62
Z_{O}	2.00
q_{O}	-3.24
k_{O}	1.00
λ_{O}	1.90
D_{OH}	0.42954802
r_{OH}	1.3440633
α_{OH}	1.1131102
θ_{HOH}	1.927
a_{HOH}	0.031621
b_{HOH}	0.043914
c_{HOH}	-0.012721
d_{HOH}	-0.00866

3.6.2 Ion-water force field coefficients

Harmonic constant, k_{M}, is in H/Bohr^2, ion electrostatic decaiment, $\lambda_{\mathrm{M}}^{'}$, is in Bohr, pre-exponential terms are in H and exponential terms are in Bohr^{-1}.

Table 3.13: Fitted parameters of the alkaline potentials.

	$\mathbf{Li}^+$	$\mathbf{Na}^+$	$\mathbf{K}^+$	$\mathbf{Rb}^+$	$\mathbf{Cs}^+$
k_{M}	4.672820	0.575250	0.551890	0.217025	0.364708
$\lambda_{\mathrm{M}}^{'}$	0.368792	0.261673	0.515188	0.621742	0.995166
A_{MO}	44.103664	134.158515	388.755193	539.102465	449.494649
α_{MO}	2.659083	2.198363	1.636593	1.357374	1.413723
B_{MO}	-0.048328	-1.147140	-249.062663	-383.448443	-362.094604
β_{MO}	0.485383	1.169133	1.548374	1.293485	1.371814
C_{MH}	0.032213	0.027106	1072.600533	1857.808870	1776.523448
γ_{MH}	0.635698	1.750888	1.547942	0.857618	0.834310
D_{MH}	-0.000702	-0.000009	-1076.366645	-1859.064561	-1776.616635
δ_{MH}	5.745071	0.045655	1.549057	0.857790	0.834339

Table 3.14: Fitted parameters of the alkaline-earth potentials.

	$\mathbf{Sr}^{2+}$	$\mathbf{Ba}^{2+}$	$\mathbf{Ra}^{2+}$
k_{M}	1.269662	0.650790	1.000000
$\lambda_{\mathrm{M}}^{'}$	0.414399	0.435619	0.554093
A_{MO}	277.432810	205.594587	248.886579
α_{MO}	1.560342	1.445294	1.474152
B_{MO}	-162.291509	-88.434493	-88.710280
β_{MO}	1.454231	1.289500	1.294386
C_{MH}	53.495873	79.272175	105.444582
γ_{MH}	2.603508	3.226664	2.628450
D_{MH}	0.000038	0.000048	0.000045
δ_{MH}	1.415779	1.574448	1.256433

Table 3.15: Fitted parameters of the scandium potentials.

	Sc^{3+} Pot 6	**Sc^{3+} Pot 7**	**Sc^{3+} Pot 4**	**Sc^{3+} Pot 8**
k_{M}	1.600000	1.600000	1.600000	1.600000
$\lambda_{\mathrm{M}}^{'}$	0.490671	0.531754	0.517506	0.500254
A_{MO}	100.036705	94.717791	101.098026	100.036705
α_{MO}	1.916500	1.880000	1.933011	1.916500
B_{MO}	-1.357411	-1.942813	-1.038266	-1.865932
β_{MO}	1.060138	1.060138	1.079167	1.060138
C_{MH}	66.066941	69.396867	65.840777	67.391159
γ_{MH}	5.714136	6.005367	5.694794	5.885833
D_{MH}	0.001121	0.001132	0.001118	0.001143
δ_{MH}	2.777914	2.919571	2.795934	2.833474

Table 3.16: Fitted parameters of the transition metal potentials.

	Co^{2+}	**Cd^{2+}**
k_{M}	1.000000	1.000000
$\lambda_{\mathrm{M}}^{'}$	0.501619	0.591948
A_{MO}	100.027184	110.325440
α_{MO}	1.407187	2.044628
B_{MO}	-75.696036	-0.097990
β_{MO}	1.335787	0.434356
C_{MH}	6.380953	69.896007
γ_{MH}	7.111711	8.171032
D_{MH}	0.001844	0.001516
δ_{MH}	3.720043	3.766755

Table 3.17: Fitted parameters of the Lanthanide and Actinide potentials.

	$\mathbf{La}^{3+}$	$\mathbf{Nd}^{3+}$	$\mathbf{Tm}^{3+}$	$\mathbf{Th}^{4+}$
k_{M}	1.011070	1.050000	1.120000	1.050000
$\lambda_{\mathrm{M}}^{'}$	0.506308	0.353208	0.362722	0.423617
A_{MO}	165.681078	322.805834	132.738900	354.010287
α_{MO}	1.422303	1.451632	1.800000	1.960000
B_{MO}	-76.695518	-219.290154	-6.782221	-0.938932
β_{MO}	1.280927	1.376586	1.196806	0.816922
C_{MH}	46.872467	49.845695	2.793025	40.492113
γ_{MH}	4.463182	2.804860	4.324097	3.680997
D_{MH}	0.001724	0.000034	0.001460	0.000036
δ_{MH}	3.362880	1.228342	2.849904	1.545206

3.6.3 Global energetic fitting comparison

Figure 3.6: Li^+ fitting.

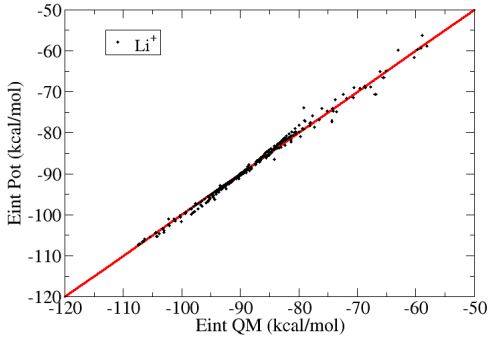

Figure 3.7: Na^+ fitting.

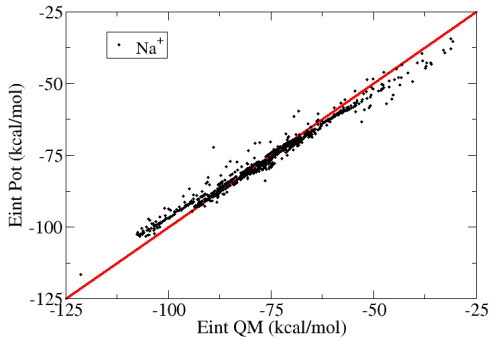

Figure 3.8: K^+ fitting.

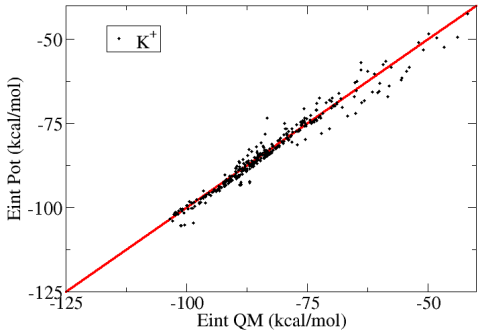

Figure 3.9: Rb^+ fitting.

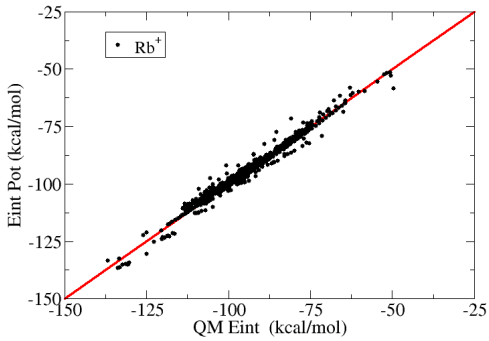

Figure 3.10: Cs^+ fitting.

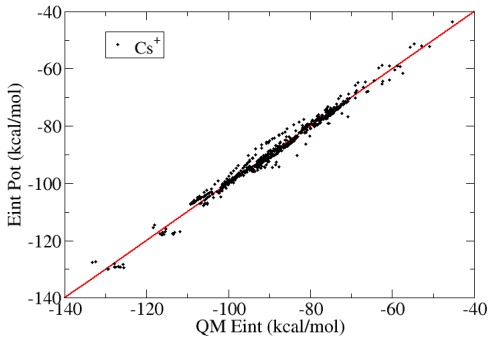

Figure 3.11: Sr^{2+} fitting.

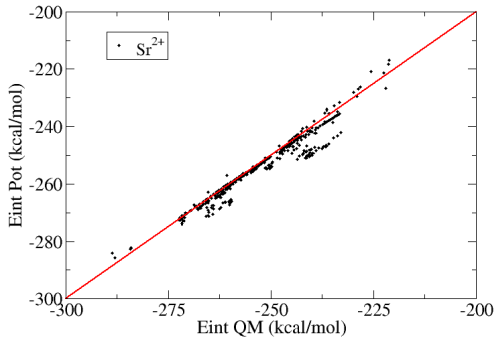

Figure 3.12: Ba^{2+} fitting.

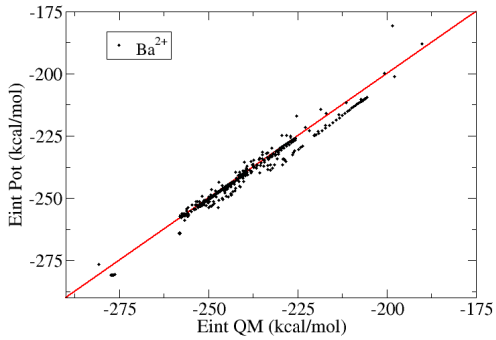

Figure 3.13: Ra^{2+} fitting.

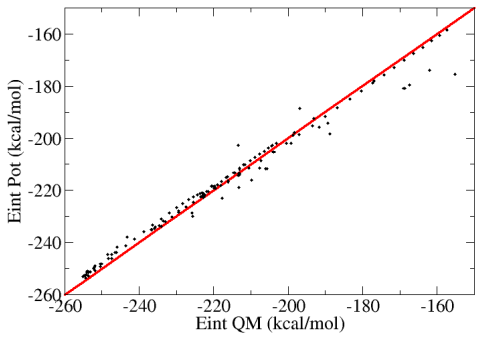

Figure 3.14: Sc^{3+} Pot 6 fitting.

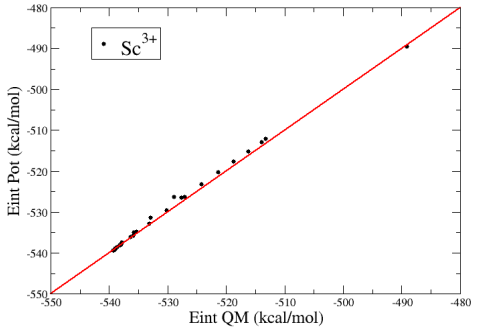

Figure 3.15: Sc^{3+} Pot 7 fitting.

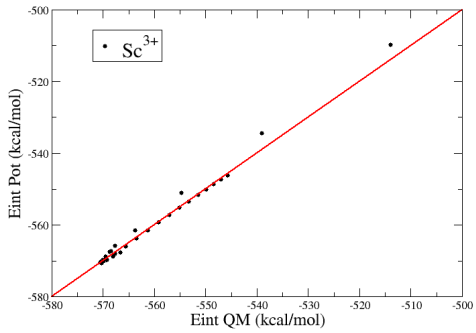

Figure 3.16: Sc^{3+} Pot 4 fitting.

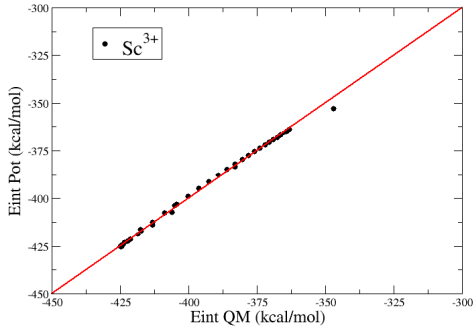

Figure 3.17: Sc^{3+} Pot 8 fitting.

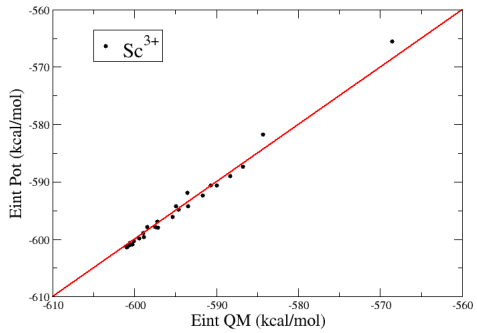

Figure 3.18: Co^{2+} fitting.

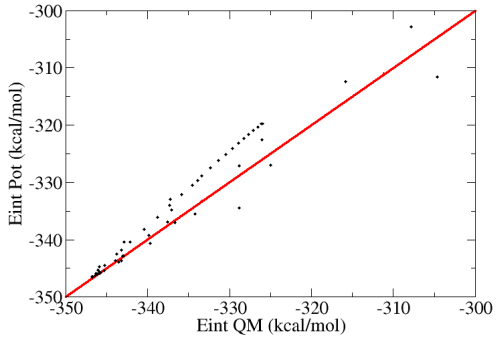

Figure 3.19: Cd^{2+} fitting.

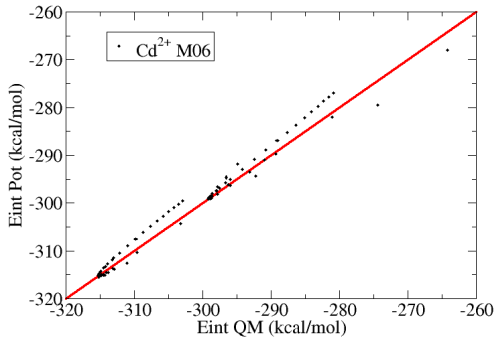

Figure 3.20: La^{3+} fitting.

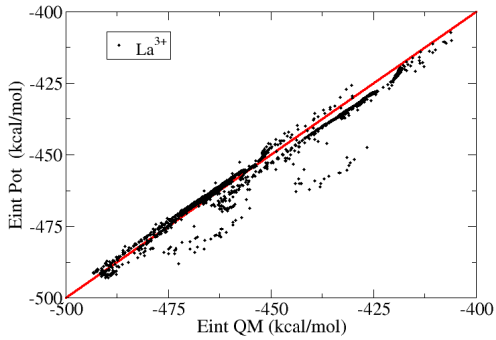

Figure 3.21: Nd^{3+} fitting.

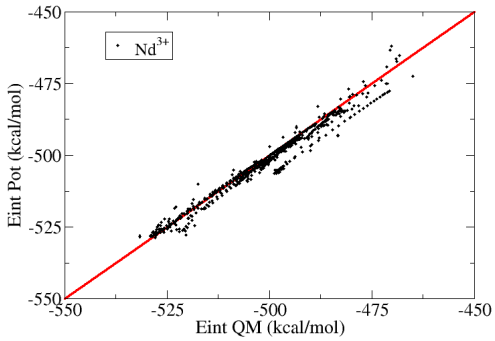

Figure 3.22: Tm^{3+} fitting.

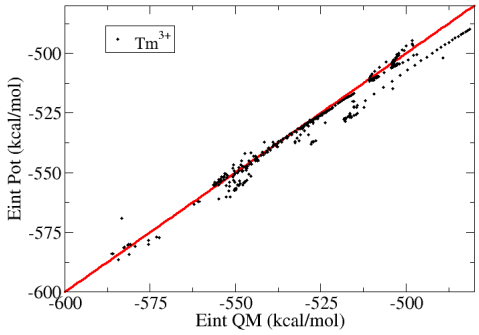

Table 3.18: Fitting error

Ion	σ error
Li^+	1.9
Na^+	2.7
K^+	2.2
Rb^+	1.9
Cs^+	1.6
Sr^{2+}	3.5
Ba^{2+}	2.7
Ra^{2+}	3.7
Sc^{3+} /Pot 6/	0.8
Sc^{3+} /Pot 7/	1.3
Sc^{3+} /Pot 4/	1.1
Sc^{3+} /Pot 8/	0.8
Co^{2+}	3.2
Cd^{2+}	1.7
La^{3+}	4.4
Nd^{3+}	2.8
Tm^{3+}	4.2
Th^{3+}	7.7

3.7 Bibliography

[1] Morales, N. Estudio teórico de propiedades fisicoquímicas de cationes metálicos en disolución: Evolución en el grupo de los alcalinos y en la serie de los lantánidos. bilio, Universidad de Sevilla, 2015.

[2] Leininger, T.; Nicklass, A.; Kuchle, W.; Stoll, H.; Dolg, M.; Bergner, A. *Chem. Phys. Lett.* **1996**, *255*, 274–280.

[3] San-Román, M. L.; Carrillo-Tripp, M.; Saint-Martin, H.; Cobos, J. H.; Ortega-Blake, I. *Theor. Chem. Acc.* **2006**, *115*, 177–189.

[4] Li, X.; Yang, Z. *J. Phys. Chem. A* **2005**, *109*, 4102–4111.

Figure 3.23: Th^{4+} fitting.

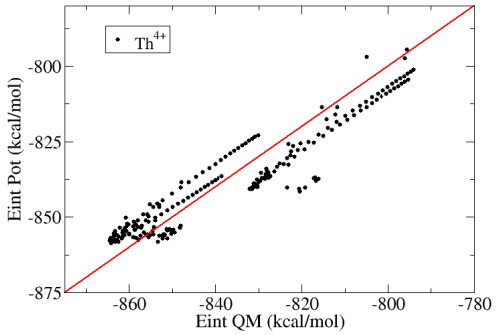

[5] Glendening, E.; Feller, D. *J. Phys. Chem.* **1995**, *99*, 3060–3067.

[6] Lim, I.; Stoll, H.; Schwerdtfeger, P. *J. Chem. Phys.* **2006**, *124*, 034107.

[7] Kerridge, A.; Kaltsoyannis, N. *Chem. Eur. J* **2011**,

[8] Boda, A.; De, S.; Musharaf, S.; Tulishetti, S.; Khan, S.; Singh, J. *J. Mol. Liq.* **2012**, *172*, 110–118.

[9] Matsuda, A.; Mori, H. *J. Comput. Chem. Jpn.* **2014**, *13*, 105–113.

[10] Dolg, M.; Weding, U.; Stoll, H.; H.Preuss, *J.Chem. Phys.* **1987**, *86*, 866–872.

[11] Furukawa, K.; Ohashi, K.; Koga, N.; Imamura, T.; Judai, K.; Nishi, N.; Sekiya, H. *Chem. Phys. Lett.* **2011**, *508*, 202–206.

[12] Akesson, R.; Pettersson, L. G. M.; Sandström, M.; Wahlgreen, U. *J. Am. Chem. Soc* **1994**, *116*, 8691–8704.

[13] Huzinaga, S. **1965**, *42*, 1293.

[14] Andrae, D.; Haeussermann, U.; Dolg, M.; Stoll, H.; Preuss, H. *Theor. Chim. Acta* **1990**, *77*, 123–141.

[15] Rudolph, W. W.; Pye, C. C. *J. Phys. Chem.* **2000**, *104*, 1627–1639.

[16] Dolg, M.; Stoll, H.; Savin, A.; Preuss, H. *Theor. Chim. Acta* **1989**, *75*, 173–194.

[17] Dolg, M.; Stoll, H.; Preuss, H. *Theor. Chim. Acta* **1993**, *6*, 441–450.

[18] Fujiwara, T.; Mori, H.; Mochizuki, Y.; Takewaki, H.; Miyoshi, E. *J. Mol. Struct.* **2010**, *949*, 28–35.

[19] Ciupka, J.; Cao-Dolg, X.; Wiebke, J.; Dolg, M. *Phys. Chem. Chem. Phys.* **2010**, *12*, 13215–13223.

[20] Moritz, A.; Cao, X.; Dolg, M. *Theor. Chem. Acc.* **2007**, *118*, 845–854.

[21] Yang, T.; Tsushima, S.; Suzuki, A. *J. Phys. Chem. A* **2001**, *105*, 10439–10445.

[22] Marjolin, A.; Gourlaouen, C.; Clavaguéra, C.; Ren, P.; Wu, J.; Gresh, N.; Dognon, J.; Piquemal, J. *Theor. Che, Acc.* **2012**, *131*, 1198.

Chapter 4

System definition and analyzed properties

In the following chapters the main results from the Molecular Dynamics simulations are shown. Simulated systems are defined by one cation and 1000 water molecules. Simulations were run using the DLPOLY[1] code in the NVT ensemble and with a boxlength which reproduces the water experimental density at 300K, 0.997 g/cm^3. The dynamical shell model to account for the polarization,[2] the Ewald summation to calculate the electrostatic interactions[3] and periodic boundary conditions (PBC)[4] to approximate to bulk conditions were employed. The results are obtained from 1 ns simulation production period wich was previously equilibrated during 200-300 ps. Initial configurations come from a previous simulation of the same cation or from a similar one. The results are shown for each cation individually. At the end of the sections the evolution of some properties along the group or series are discussed.

First-shell coordination number is calculated as the running integral of the first M-O peak in the RDF up to the first minimum. The coordination number of the second shell is calculated as the integration of the M-O RDF between the first and the second minima of the distribution. 1st and 2nd

shell distances are taken from M-O RDF maxima. The Debye-Waller factor (DW), an index employed in EXAFS analysis that reflects geometrical fluctuations, is considered as the second cumulant of the first-shell distances. The tilt angle, ϕ, is calculated as the angle between the ion-oxygen vector and the vector of the bisector of the water molecule plane.

The molecular eccentricity, ϵ, was calculated by means of the equation 4.1, i.e. the distance between the metal cation position and the center of mass of the first hydration shell. This structural parameter accounts for the assymetry of the hydrated ion, i.e. the displacement of the metal ion from the mass center of the hydrate.

$$\epsilon = |\vec{r}_{M^{n+}} - \vec{r}_{CM}| \tag{4.1}$$

The hydrogen bonds are calculated using the geometrical Chandra criteria:[5] R(O···H) $\leq$ 2.45 Å, R(O···O) $\leq$ 3.5 Å and $\angle$ O···H-O $\leq 30^{\circ}$.

The hydration enthalpy, ΔH_{hyd}, is calculated as the energy difference between a box with the ion plus a given number of water molecules, U_{dis}, and a box with the same number of water molecules under the same simulation conditions, U_{water}, plus the ion energy in gas phase.

$$\Delta H_{hyd} = H_{dis} - H_{water} - H_{ion} \simeq U_{dis} - U_{water} - 0.6 kcal/mol \tag{4.2}$$

The interaction energy per hydrogen bond, E_{HB}, has been computed by the formula:

$$E_{HB} = E_{AB} - (E_A + E_B) \tag{4.3}$$

This calculation has been performed extracting all the dimers forming hydrogen bonds and computing a single point calculation of the dimer and monomers keeping the polarization formed in the simulation. Then, E_{HB} is averaged for each type of hydrogen bond analyzed.

Mean residence times (MRT) are calculated by the Impey method,[6] defined by equation 4.4. MRTs larger than 50 ps has been calculated from the entire simulation, and MRTs smaller than 50 ps has been calculated employing blocks of 200 ps from the full simulation time.

$$\tau = \frac{1}{N_t} \sum {N_t}^{n=1} \sum P_j(t_n, t; t*) \tag{4.4}$$

In Equation 4.4 N_t is the number of configurations, P_j is a function that takes the value 1 when the water molecule j is inside a given region at time t_n and $t+t_n$ without leaving the region for a time longer than t^*, otherwise the function takes the value 0.

Ion self-diffusion coefficient, D_i, a measure of the ion mobility, is calculated by the mean square displacement (MSD) equation:

$$D_i = \frac{< |\vec{r}_i(t)\vec{r}_i(0)| >}{6t}. \tag{4.5}$$

Self-diffussion coefficients has been corrected of the effect of periodic boundary conditions using the Yeh and Hummer equation:[7]

$$D_{corr} = D_i + \frac{K_B T \zeta}{6\pi\eta L} \tag{4.6}$$

where D_i and D_{corr}, are the self-diffusion coefficients before and after the correction,K_B is the Boltzmann constant, T the temperature, ζ is the self-term which for a cubic lattice at room temperature is 2.83773, η is the viscosity and L is the boxlength.

Reorientational times for the first and second order correlations functions associated to the reorientional motion of the dipole moment vector μ, the hydrogen-hydrogen vector HH, the normal vector to the molecular plane $\perp$ and the oxygen-hydrogen axis OH (see Figure 4.1) has been computed. Reorientational times (τ_1 and τ_2) have been calculated from the correlation function defined in equations 4.7 and 4.8 (see the evaluated coordinates in Figure 4.1). Also, the time correlation of the eccentricity has

been evaluated.

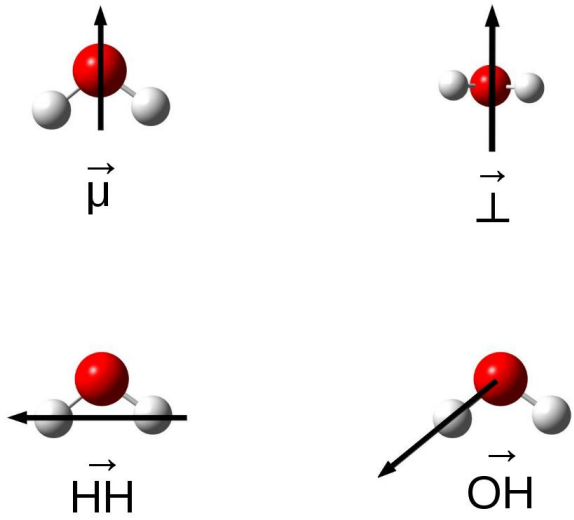

Figure 4.1: Reorientational time coordinates.

$$C_{1,i}(t) = \left\langle (\vec{u}_i(0)\vec{u}_i(t)) \right\rangle \tag{4.7}$$

$$C_{2,i}(t) = \frac{1}{2}\left\langle 3(\vec{u}_i(0)\vec{u}_i(t))^2 - 1 \right\rangle \tag{4.8}$$

The reorientational correlation functions were calculated from a 1 ns simulation time with a distance between consecutive structures of 0.01 fs.

The correlation dynamics of the eccentricity vector (Equation 4.9) has been calculated using Equation 4.10.

$$\vec{\epsilon} = \vec{r}_{M^{n+}} - \vec{r}_{CM} \tag{4.9}$$

$$C(t) = \frac{<\epsilon(\vec{t})\epsilon(\vec{0})>}{<\vec{\epsilon}(0)^2>} \tag{4.10}$$

The EXAFS and XANES functions were simulated with FEFF 9.6 code[8] using 500 snapshots evenly taken from the production period including first and second shells coordinates, except for the EXAFS simulations of the alkalines where the inclusion of the second shell added noise to the spectra. The models used in the XAS calculations are explained in section 2.3 and examples of inputs files are included in the Appendix (section 10.2). Experimental EXAFS spectra of K^+,[9] Cs^+,[10] Co^{2+}, Sc^{3+},[11] Cd^{2+},[12,13] Tm^{3+} and Nd^{3+} dilute aqueous solution have been extracted using the autobk code[14] considering the maximum derivative of the edge as E_0. Some spectra were digitalized as Ba^{2+}[15] and Th^{4+},[16] and other spectra were provided by the authors of the original experiments as Na^+[17] and Rb^+.[18]

4.1 Bibliography

[1] Smith, W.; Forester, T.; Todorov, I. T. The DL_POLY Classic. 2012; STFC Daresbury Laboratory, Daresbury (UK).

[2] Mitchell, P.; Fincham, D. *Condensed Matter Physics* **1993**, *5*, 1031–1038.

[3] Ewald, P. P. *Ann. Phys.* **1921**, *369*, 253–287.

[4] Allen, M.; Tildesley, D. *Computer Simulation of Liquids*; Clarendon Press, 1983; Capítulo 3.

[5] Chandra, A. *Phys. Rev. Lett.* **2000**, *85*.

[6] Impey, R.; Madden, P.; McDonald, I. *J. Phys. Chem.* **1983**, *87*, 5071–5083.

[7] Yeh, I.; Hummer, G. *J. Phys. Chem. B* **2004**, *108*, 15873–15879.

[8] Rehr, J. J.; Kas, J. J.; Vila, F. D.; Prange, M. P.; Jorissen, K. *Phys. Chem. Chem. Phys.* **2010**, *12*, 5503–5513.

[9] Glezaku, V.; Chen, Y.; Fulton, J.; Schenter, G.; Dang, L. *Theor. Chem. Acc.* **2006**, *115*, 86–99.

[10] Rossetti, I.; Sordelli, L.; Ghigna, P.; Pin, S.; Scavini, M.; Forni, L. *Inorg. Chem* **2011**, *50*, 3757–3765.

[11] Lindqvist-Reis, P.; Persson, I.; Sandström, M. *Dalton Trans.* **2006**, *28*, 3868–3878.

[12] D'Angelo, P.; Chillemi, G.; Barone, V.; Mancini, G.; Sanna, N.; Persson, I. *J. Phys. Chem. B* **2005**, *109*, 9178–9185.

[13] Chillemi, G.; Barone, V.; D'Angelo, P.; Mancini, G.; Persson, I.; Sanna, N. *J. Phys.Chem. B* **2005**, *109*, 9186–9193.

[14] Newville, M. Automated background removal for XAFS data. 1997; `https://bruceravel.github.io/demeter/documents/Athena/bkg/rbkg.html`.

[15] Persson, I.; Sandstrom, M.; Yokoyama, H.; Chaudhry, M. *Z. Naturforsch* **1995**, *50a*, 21–37.

[16] Rothe, J.; Denecke, M.; Neck, V.; Muller, R.; Kim, J. *Inorg. Chem.* **2002**, *41*, 249–258.

[17] Galib, M.; Baer, M.; Skinner, L.; Mundy, C.; Huthwelker, T.; Schenter, G.; Benmore, C.; Govind, N.; Fulton, J. *J. Chem. Phys.* **2017**, *146*, 084504.

[18] Pham, V.; Fulton, J. L. *J Chem. Phys.* **2013**, *138*, 044201.

Chapter 5

Alkalines

The alkaline group, from lithium to caesium, has been studied. The lithium has industry applications principally on the ion batteries field[1] and the sodium and potassium cations are involved in important biological processes.[2] There are several studies[3–6,6,6–15,15–18,18,19] involving lithium and sodium aqueous solutions, their hydration being well established. But for the heavy alkalines the situation is different as the range of structural published results reflects.[6,6,20–30,30–32] This fact is also correlated with the techniques and methodologies used.

5.1 Lithium

The lithium ion is the smallest and most polarizing single-charge cation. Four water molecules in the first-shell has been observed by means of Neutron Diffraction and Raman spectroscopy[33,34] for aqueous solutions with a maximum salt concentration of 1 M. A Neutron Diffraction study obtained a higher coordination, 4.7,[35] when considering the existence in solution of the hexahydrate together with the tetrahydrate. For these studies, the metal-oxygen interatomic distance is just below 2.0 Å. For higher concentrations a coordination number of 4 is obtained, but longer interatomic distances ranging between 1.95 and 2.25 Å[36,37] are found. Most compu-

tational studies found 4 as coordination number[6–11,16,38] but one study proposed a higher value of 6.1.[39] Distances between 1.93 and 1.97 Å were found. Only for the simulation that obtained a coordination of 6.1 a longer interatomic distance, 2.17 Å, is reported. All these values are collected in Table 5.1.

In this work the lithium cation was considered as a non polarizable ion due to its hard character. There is a technical reason connected to the shell-model employed for the description of the atomic polarizability. The high hardness character of the cation forces to use a very high resort force constant. The low mass of the core leads to a very high resort frequency of the core ion-mobile charge bond, which conversely forces to a really short timestep to properly describe the mobile charge dynamics. Due to the low polarizability of the cation the non-polarizable model seems to be realistic and more efficient computationally.

In this work coordination numbers of 4.0 and 14.6 with peak distances at 1.91 Å and 4.05 Å for first and second shell, respectively, have been found (see RDF's in Figures 5.20 and 5.21). Main properties of lithium hydration are shown in Table 5.1 together with previous published results. Along the simulation, coordination number changes were observed, increasing or decreasing during very short intervals, being 4, by far, the most probable coordination and 4.0 the average coordination number (see Figure 5.1).

The lithium ion polarizes the first-shell water molecules increasing their dipole in 0.3 D with respect to the bulk value ($\Delta\mu$=μ(shell)-μ(bulk)). This small cation also favors a preferential orientation of its hydration shell, the average tilt angle being 141°. The mean residence time found in this work is smaller than the experimental in two orders of magnitude, a fact systematically found in this work. It seems to be a common gap in computer simulations.[40,41] Although the lithium, due its small ionic radius is considered a highly polarizing ion it has been found that the first-shell water molecules not only donates hydrogen bonds, but also can accept them (see Table 5.10). This finding was previously observed in quantum mechanical

optimizations with a second hydration shell.[42]

Table 5.1: Properties of Li^+ aqueous solution. Standard deviation in parenthesis.

Property	this work	Literature
$R_{\text{M-O}_\text{I}}$ (Å)	1.91	1.96,[35] 1.98,[33] 1.99[43] 1.93-1.95,[8] 1.95[6,16] 1.97,[7] 2.0,[32] 2.05[38] 1.96,[9] 1.94-2.06,[10] 1.93[38] 1.93-1.96,[11] 2.25,[36] 2.13,[39] 2.17[37]
CN_I	4.0	4.0,[7,9,32,34,36–38,43] 4.1[6,10,33] 4.7,[35] 5.7,[38] 4.1-4.2[8,11] 4.9,[16] 6.1[39]
DW (Å^2)	0.015	
tilt angle$_\text{I}$ (°)	137(26)	159.6,[38] 140,[7] 141[43]
$R_{\text{M-O}_\text{II}}$ (Å)	4.05	3.71-3.95,[11] 4.1-4.2,[10] 4.1[6]
CN_II	14.6	13,[10] 16.1[6]
tilt angle$_\text{II}$ (°)	104(39)	
$\Delta\mu_\text{I}$ (D)	0.3(0.3)	0.2,[7] 0.06[43]
$\Delta\mu_\text{II}$ (D)	0.0(0.3)	0.0[7]
MRT(t*=0) (ps)	74	$\sim$ 100,[44] 400,[6] 2.13-4.43[11]
MRT(t*=2) (ps)	96	
ΔH_hyd (kcal/mol)	−133(11)	−127.0,[45] −114[38]
D (10^{-5} cm^2/s)	0.7(0.1)	0.2,[43] 0.92,[32] 1.03[45] 0.89,[38] 1.18[6]

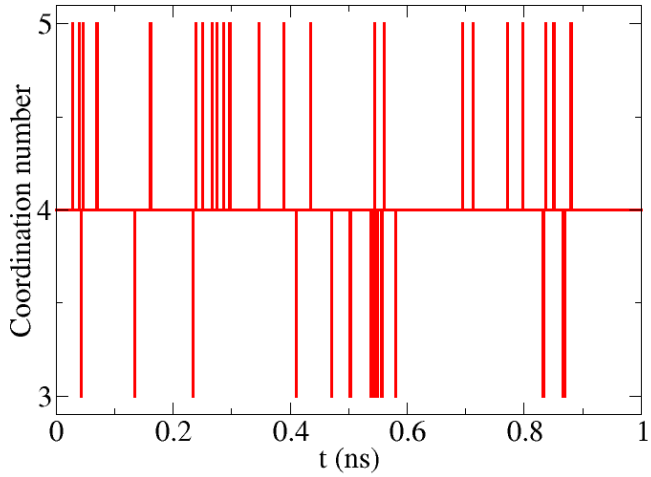

Figure 5.1: Time evolution of Li^+ coordination number in aqueous solution.

5.2 Sodium

The Na^+ coordination number covers from 5 to $\sim$ 6.6 (see Table 5.2). Neutron Diffraction[5] provides a coordination number of 5.3 with a peak distance of 2.34 Å, although a concentration effect was evaluated finding that water coordination decreased while the first-shell peak distance remained at 2.34 Å when salt concentration increased. Recently, for the first time, an EXAFS analysis[46] of the hydrated sodium was performed. A hydration number of 5.4 water molecules for the first-shell was obtained with the peak distance at 2.37 Å. This work[46] was combined with XRD measurements obtaining a coordination number of 5.9 with a peak distance at 2.38 Å. Additional DFT-MD simulations gave coordination number between 4.9 and 6.1 and first-shell distances between 2.39 and 2.56 Å, depending on the level theory used.

Several computational studies have been performed to study the sodium hydration. By means of classical MD,[6,16,19,38] using rigid water models, coordinations between 5.9 and 6.6 with first-shell peak distances between 2.33 and 2.52 Å were obtained. Likewise, coordinations between 13 and 17.5 with peak distance between 4.35 and 4.60 Å for the second shell were reported. Using a flexible and polarizable[14] model a coordination number of 5.5 with peak distance at 2.45 Å was obtained. Hybrid QM/MM studies[13,15] obtained hydrates with coordination numbers between 5.6 and 6.5 with peak distances between 2.33 and 2.36 Å and QM and CPMD simulations obtained[12,17,18,43] coordination numbers between 5.2 and 5.4 and peak distances between 2.35 and 2.41 Å. Experimental and theoretical results are collected in Table 5.2.

This work obtained an aqua ion with a coordination number of 5.8 with first-shell peak distance at 2.34 Å. The second shell is formed by 17 water molecules with the peak distance at 4.40 Å (see RDF's in Figures 5.20 and 5.21). The first-shell coordination number changes dynamically between 4 and 7 (see Figure 5.3), being 6 the most probable coordination (see Figure 5.4). Although sodium is one of the smallest alkalines, it doesn't have the capability to increase the first-shell water molecule polarization, even more, a depolarization of 0.1 D was found as already reported in previous theoretical studies.[14,43] The depolarization happens when the cation electric field is not strong enough to orient the water dipole moment, the tilt angle reflecting this fact.

First-shell water molecules are not strongly coordinated by the single Na^+ ion, so the competition whith the surrounding water molecule leads to an intermediate structural and electronic polarization. This does not fit either the ion-water or water-water interactions, resulting in an asymmetric structural and electronic polarization which explains a smaller water molecule dipole than in bulk (See Figure 5.2).

The small tilt angle found on Na^+, 131°, is similar to those found for

potassium, rubidium and caesium, 126°, 125° and 122°. This is also reflected in the HB energy between first and second shell molecules, that is 0.3 kcal/mol less energetic than bulk in water (see Figure 5.25 and Table 5.9).

Table 5.2: Properties of Na^+ aqueous solution. Standard deviation in parenthesis.

Property	this work	Literature
$R_{\text{M-O}_\text{I}}$ (Å)	2.34	2.3,[15] 2.33,[16] 2.33-2.36[13] 2.34,[5] 2.35,[12] 2.37,[14] 2,4[32,43] 2.372,[46] 2.41,[17] 2.41-2.42[18] 2.45,[6] 2.47,[19] 2.42-2.52[38]
CN_I	5.8	5.13,[32] 5.2,[43] 5.4[12,46] , 5.3[5,17,18] 5.9,[6,15] 6.39,[19] 5.5-5.6[13] 5.56,[14] 6.0,[16] 5.68-6.62[38]
DW	0.034	0.0061-0.02[46]
tilt angle$_\text{I}$ (°)	131(22)	128-147,[38] 134,[43] 132[14]
$R_{\text{M-O}_\text{II}}$ (Å)	4.40	4.35-4.60,[38] 4.50[6]
CN_II	16.9	13.9-15.5,[38] 17.5[6]
tilt angle$_\text{II}$ (°)	102(40)	
$\Delta\mu_\text{I}$ (D)	-0.1(0.3)	-0.08,[14] -0.09[43]
$\Delta\mu_\text{II}$ (D)	0.0(0.3)	
MRT(t*=0) (ps)	15(2)	$\sim$ 26.4,[6] 4.1-9.7[13]
MRT(t*=2) (ps)	23(4)	
ΔH_hyd (kcal/mol)	-94(12)	-99.4,[45] -98,[14] -89–135[38]
D (10^{-5} cm^2/s)	1.1(0.1)	0.3,[43] 0.73,[32] 1.33[45] 1.22,[6] 1.48-2.03[38]

Recently, XAS spectra of the sodium ion in aqueous solution has been recorded.[46] The sodium XAS measurement is an experimental challenge due to the low absorption energy at its K-edge ($\sim$ 1071 eV). Sodium atom

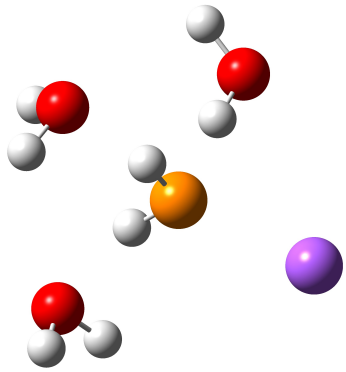

Figure 5.2: Enviromment of a Na^+ first-shell water molecule (orange).

has a low X-ray absorption coefficient as this depends on the atomic number ($\mu \sim Z^4/E^3$, being Z the absorber atomic number and E the radiation energy). Comparison between our result and the experimental EXAFS spectrum is shown in Figure 5.5. The experimental spectra contains two intense multi-electron excitations at 4 A^{-1} and 5 A^{-1} ($KL_{2,3}$ transitions,[46] respectively). There is a good agreement in the frequency, meaning a good description of the first-shell distance, but there is a relevant difference in the signal intensity. It should be pointed out the high uncertainty in the intensity due to the importance of the self-absorption correction, which is important for low Z elements,[46] together with the multi-electron excitation (MEE) effect, hinders the intensity comparison beyond 4 $Å^{-1}$. In the simulated spectrum, MEE effects have not been taken into account. Figure 5.6 shows the simulated XANES spectra using the FEFF code together with the experimental one.[46] The agreement is acceptable except in the edge neighbourhood due to the multi-electron excitations which are not

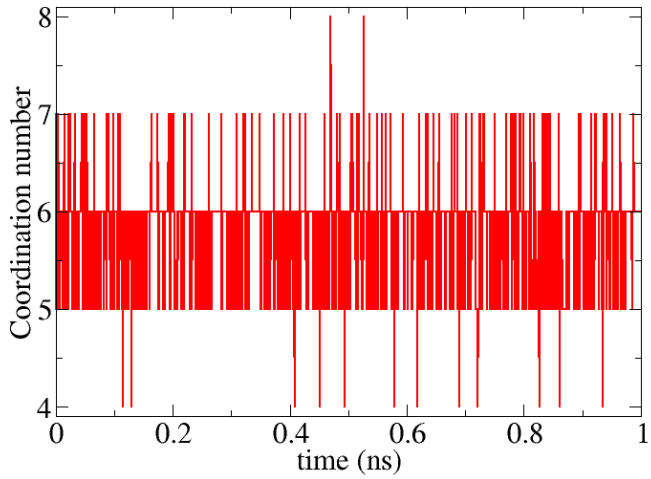

Figure 5.3: Time evolution of Na^+ coordination number in aqueous solution.

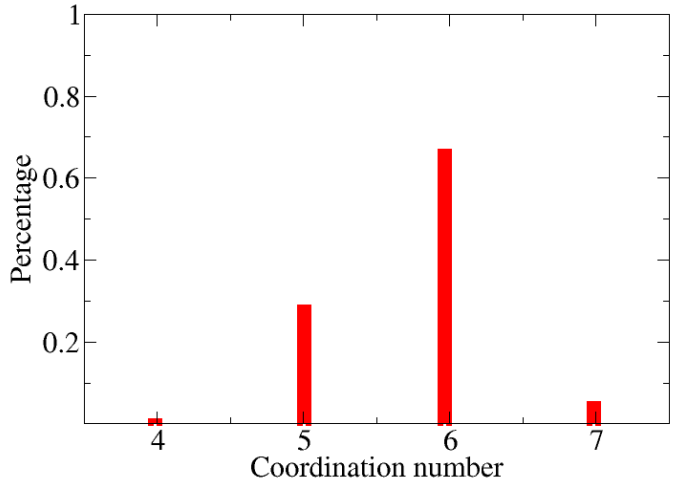

Figure 5.4: Coordination number histogram of Na^+ in aqueous solution.

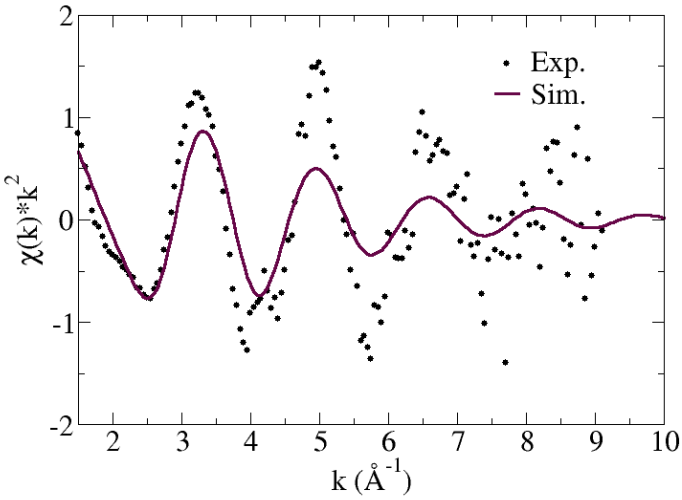

Figure 5.5: k^2-weighted Na^+ K-edge EXAFS.

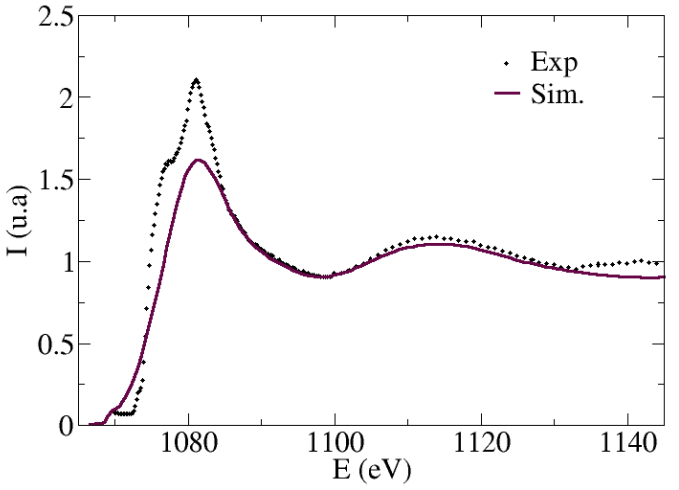

Figure 5.6: Na^+ K-edge XANES.

considered by the computations.

5.3 Potassium

XAS spectroscopy studies of potassium aqueous solutions provide coordination numbers between 6.1 and 6.3 with interatomic distances between 2.73 and 2.69 Å.[3,4] Neutron diffraction studies on potassium halides solutions gave coordination numbers between 6 and 6.4 and a first coordination shell distance of 2.65 Å.[5] Classical MD[6,14,19] obtained coordination numbers between 6.9 and 8.0 with first-shell peak distances between 2.79 and 2.87 Å. A series of QM/MM studies yielded a coordination number range between 6.2 and 8.3 and a peak distance between 2.70 and 2.81.[13,15,47] A set of AIMD simulations[18] using different theory levels obtained coordination numbers between 6.1 and 6.8 and peak distances between 2.74 and 2.9 Å. Data are collected in Table 5.3.

This work obtained a coordination number of 7.2 with peak distance at 2.72 Å. There is a well defined second hydration shell formed by 18 water molecules at 4.80 Å (see RDF's in Figures 5.20 and 5.21). The first-shell is labile, allowing the coordination number to change between 5 and 10 along the simulation. The most common NC is 7, although there is an important percentage of 6 and 8 (see Figure 5.8). As already observed the case of sodium, the ion electric field is not enough to arrange the water molecules following an ion-dipole orientation.

The simulated EXAFS function is compared with an experimental spectrum[3] in Figure 5.9. The experimental signal oscillations are observable up to 7 Å $^{-1}$. In the 2-7 Å^{-1} range there is a good frequency agreement, as well as discrepancy in the intensity. Figure 5.10 shows the comparison between the experimental[3] and the simulated XANES. Again the agreement is very satisfactory except for the fact that the intensity of the main ressonance is not as well reproduced.

Table 5.3: Properties of K^+ aqueous solution. Standard deviation in parenthesis.

Property	this work	Literature
$R_{\text{M-O}_\text{I}}$ (Å)	2.72	2.73-2.77,[3] 2.69-2.73,[4] 2.65[5] 2.7,[15] 2.8,[32] 2.82,[48] 2.85[43] 2.74-2.88,[18] 2.79,[14] 2.8[6,47] 2.87,[19] 2.78-2.81[13]
CN_I	7.2	6.55,[32] 7.1,[43] 6.1[3] 6.3-6.8,[4] 6-6.4,[19] 7.1[15] 6-6.8,[18] 7.2,[6] 6.86[19] 7.8-8.3,[13] 6.2,[47] 7.98[14] 6.1-6.8,[18] 6.2-6.8[47]
DW	0.049	0.0293,[3] 0.029[4]
tilt angle$_\text{I}$ (°)	126(25)	124,[43] 128[14]
$R_{\text{M-O}_\text{II}}$ (Å)	4.80	4.75[6]
CN_II	18.4	21.2[6]
tilt angle$_\text{II}$ (°)	101(39)	
$\Delta\mu_\text{I}$ (D)	-0.1(0.3)	-0.13[43]
$\Delta\mu_\text{II}$ (D)	0.0(0.3)	
MRT(t*=0) (ps)	6(1)	$\sim$ 100[44]
MRT(t*=2) (ps)	10(1)	
ΔH_hyd (kcal/mol)	-83(10)	-79.8,[45] -71,[4] -88[14]
D (10^{-5} cm^2/s)	1.5(0.3)	1.96,[45] 2.02[6]

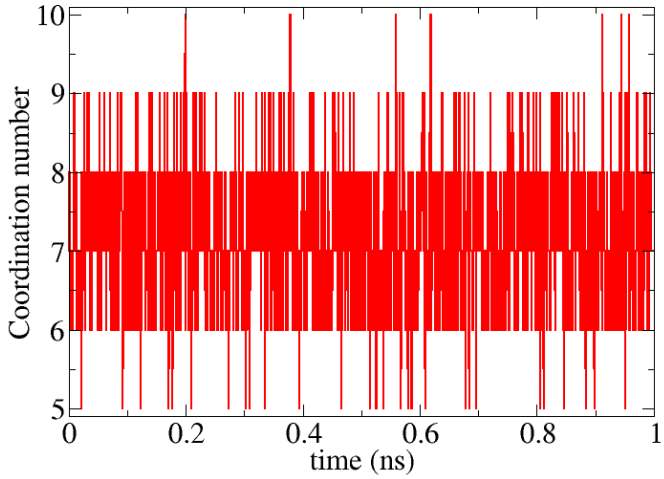

Figure 5.7: Time evolution of K^+ coordination number in aqueous solution.

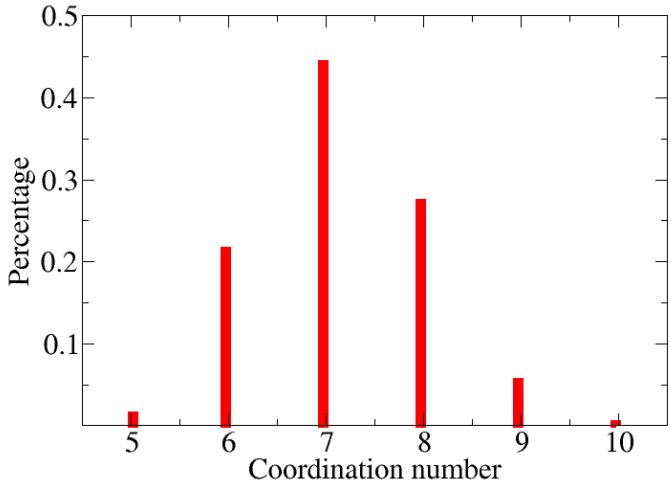

Figure 5.8: Coordination number histogram of K^+ in aqueous solution.

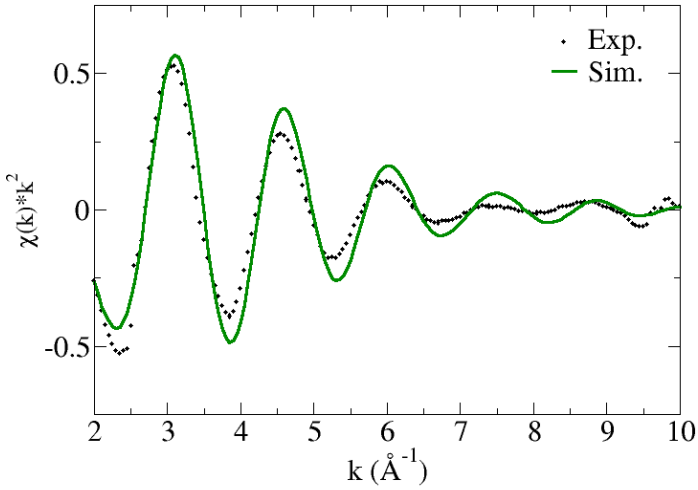

Figure 5.9: k^2-weighted K^+ *K*-edge EXAFS.

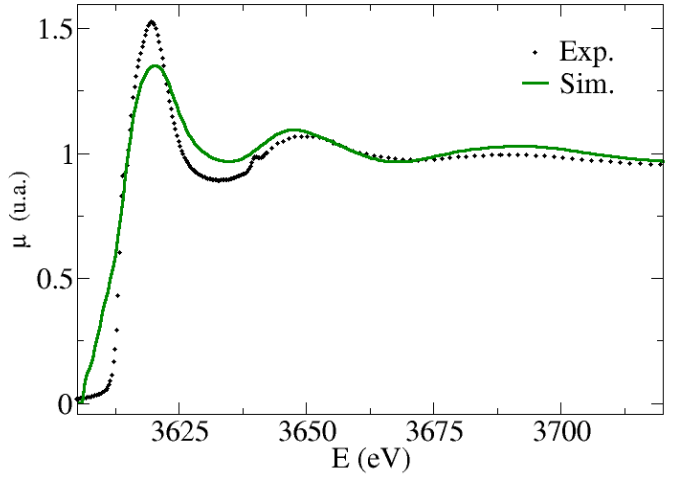

Figure 5.10: K^+ *K*-edge XANES.

5.4 Rubidium

The hydration structure of the Rb^+ is an experimental challenge due to the weak ion-water interactions. In addition, its XAS spectra are affected by multi-electron excitations that makes much more difficult to extract the hydration structure from the EXAFS signal. There is a remarkable dispersion of coordination numbers in previous studies, values between 5.6 and 8 being found experimentally. Studies combining experimental techniques, such XAS-XRD and XAS-LAXS, obtained different results for the coordination numbers, 5.6[25] and 8.[21] R(Rb^+-O) has been found by means of EXAFS spectroscopy between 2.83 and 2.99 Å.[21–25] The computational methods didn't solve the coordination number dispersion, results between 6.8 and 8.9 and interatomic distances between 2.8 and 3.0 Å[6,20,26,27] being found. For the sake of comparison data are collected in Table 5.4.

The structural analysis of our MD simulation shows a weak hydrate with an average coordination number of 8 with peak distance at 2.87 Å (see RDF's in Figure 5.20 and 5.21). During the simulation, the first-shell contains between 6 and 10 water molecules, but mainly between 7 and 9, as shown in Figure 5.11. The second shell is slightly defined between 3.66 and 5.77 Å and contains over ∼19 water molecules (see Figure 5.20). The water molecules in the first-shell are not ion-dipole orientated towards the cation, tilt angle is 125°. This arrangement between the water dipole and ion electric field produces a depolarization of the water molecules around 0.1 D, with respect to bulk water molecules.

The rubidium EXAFS spectrum contains a multi-electron excitation at 6 $Å^{-1}$ ($KM_{4,5}$ transition[50]) making not visible the EXAFS oscillations for higher k values. To increase the EXAFS range, a methodology to remove the MEE from the function has been used. This methodology was employed successfully in the analysis of lanthanoid aqua ions.[51] The method is based on the parametrization of equation 5.1 with the k^3-weighted EXAFS function. Because rubidium EXAFS spectrum doesn't present clear oscillations above 6 $Å^{-1}$ the method was adapted using only the previous

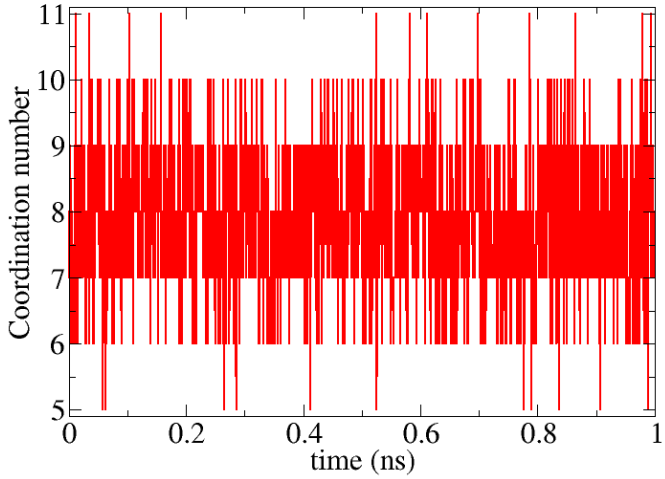

Figure 5.11: Time evolution of Rb^+ coordination number in aqueous solution.

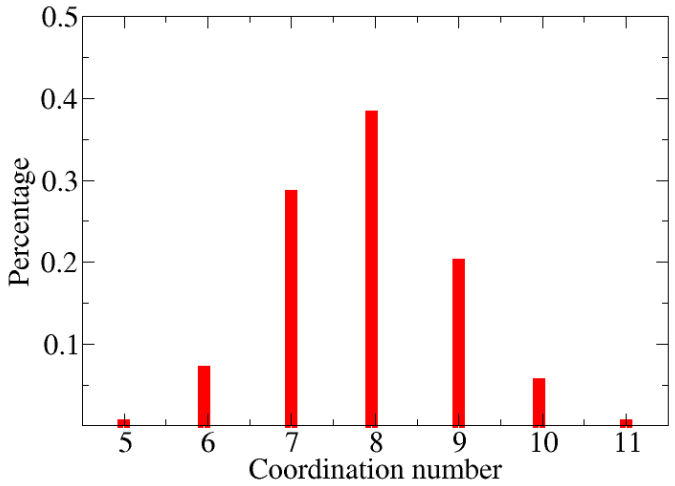

Figure 5.12: Coordination number evolution of Rb^+ in aqueous solution.

Table 5.4: Properties of Rb^+ aqueous solution. Standard deviation in parenthesis.

Property	this work	Literature
$R_{\text{M-O}_\text{I}}$ (Å)	2.87	2.83,[20] 2.93,[25] 2.98-2.99[21] 2.93,[22] 2.9,[27] 2.83[24] 2.95,[26] 2.88-2.92,[23] 3.0[6]
CN_I	7.9	5.6,[25] 7-8,[20] 6.95[6] 6.8,[27] 7.1-8.5,[28] 8[21] 8.9,[26] 6,[24] 6.3-6.6[23]
DW (Å^2)	0.060	0.0120[21] , 0.034,[25] 0.0341,[22] 0.035[23]
tilt angle$_\text{I}$ (°)	125(27)	130,[28] 126,[27] 121[20]
$R_{\text{M-O}_\text{II}}$ (Å)	4.97	
CN_II	18.6	21.0[6]
tilt angle$_\text{II}$ (°)	79(39)	
$\Delta\mu_\text{I}$ (D)	-0.1(0.3)	-0.1[27]
$\Delta\mu_\text{II}$ (D)	0.0(0.3)	0.0[27]
MRT(t*=0) (ps)	5(1)	$\sim$ 1000,[49] 0.5,[28] 11.4[26]
MRT(t*=2) (ps)	10(1)	
ΔH_hyd (kcal/mol)	$-63(17)$	-73.6,[45] -61.0[27]
D (10^{-5} cm^2/s)	1.5(0.2)	2.1,[45] 1.1,[32] 1.06[6]

range. Equation 5.1 is the last version of equations used to overcome the multi-electron excitation contribution in the EXAFS analysis.[52] There is a good agreement between the damped sine function, resulting from the ME removal, and the experimental spectrum (see Figure 5.13). Figure 5.14 shows the experimental EXAFS,[25] the damped sine and the simulated spectra. As can be seen there is a good agreement between the damped sine and the simulated spectra. The agreement in the XANES function is also satisfactory (see Figure 5.15).

$$f(x) = (\mathrm{Ak}^2 + \mathrm{B})\exp(-\mathrm{Ck}^2)\sin(\mathrm{Dk}^2 + \mathrm{Ek} + \mathrm{F}) + \mathrm{G} + \mathrm{Hk} \qquad (5.1)$$

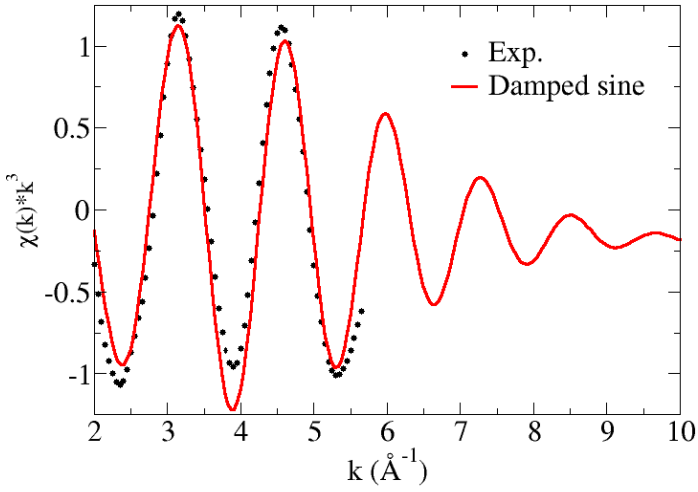

Figure 5.13: k^3-weighted damped sine function fitting.

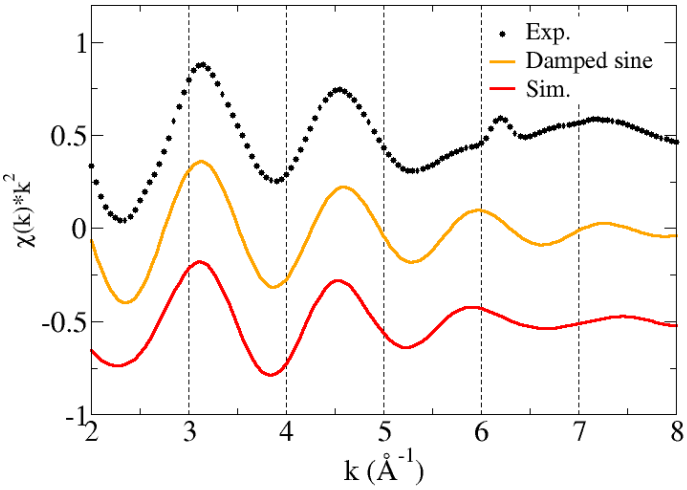

Figure 5.14: k^2-weighted Rb^+ K-edge EXAFS.

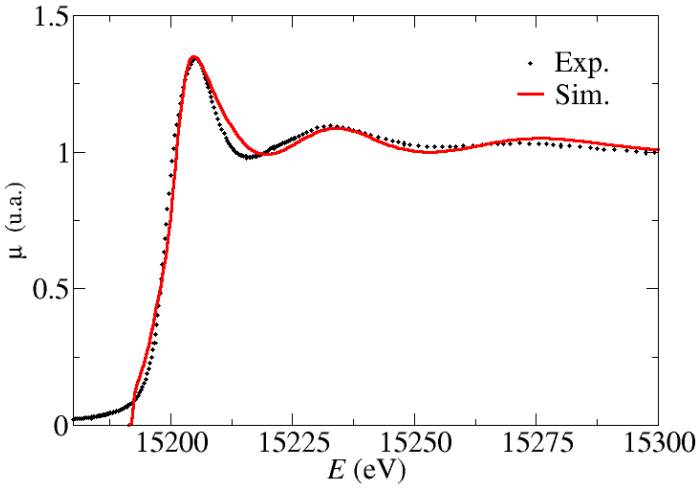

Figure 5.15: Rb^+ K-edge XANES.

5.5 Caesium

As in the rubidium case, the study of the caesium hydration is challenging. In this case the ion-water interaction is even smaller, leading to a weaker hydration. Likewise, the Cs^+ XAS spectra contains multi-electron excitations. There are few experimental studies about the caesium hydration. By means of EXAFS spectroscopy[21] and LAXS,[31] Cs-O distances are found to be 2.98 and 3.07 Å, respectively. These values have been obtained assuming a coordination number of 8. An EXAFS work which did not fix the coordination number obtained an unphysical value, 2.8.[53] Computationally, coordination numbers between 10 and 7.8 and interatomic distances between 3.0 and 3.25 Å[6,29,31,32] have been found. Data are collected in Table 5.5.

The structural analysis of our Cs^+ aqueous solution MD simulation shows a weak aqua ion with an average coordination number of 9.9 with peak distance at 3.12 Å (see Figure 5.6). The coordination number changes between 8 and 12 (see Figure 5.16). There is not a well defined second minimum in the Cs-O RDF, so that the second shell can be considered as bulk (see RDFs in Figure 5.20 and 5.21).

The multi-electron excitation removal procedure[54] used for the Rb^+ was applied to the Cs^+ EXAFS spectrum[55] as there is a MEE at 5 Å associated to the channel $LN_{4,5}$.[56] Its application obtained a clean EXAFS function to compare with the simulated spectrum. Good agreement was found, supporting a good structural description of the caesium hydration (see Figure 5.18). A good agreement in the XANES function (see Figure 5.19) was also found. The main difference is located in the second resonance where an intense multi-electron excitation, which was not simulated, is present in the experimental data.

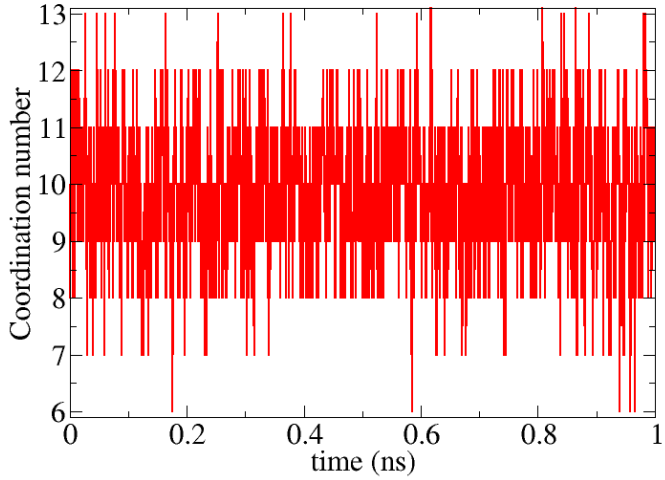

Figure 5.16: Time evolution of Cs^+ coordination number in aqueous solution.

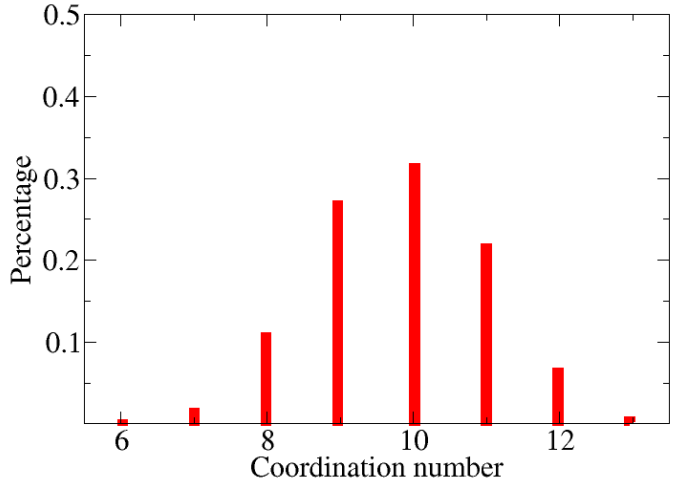

Figure 5.17: Coordination number histogram of Cs^+ in aqueous solution.

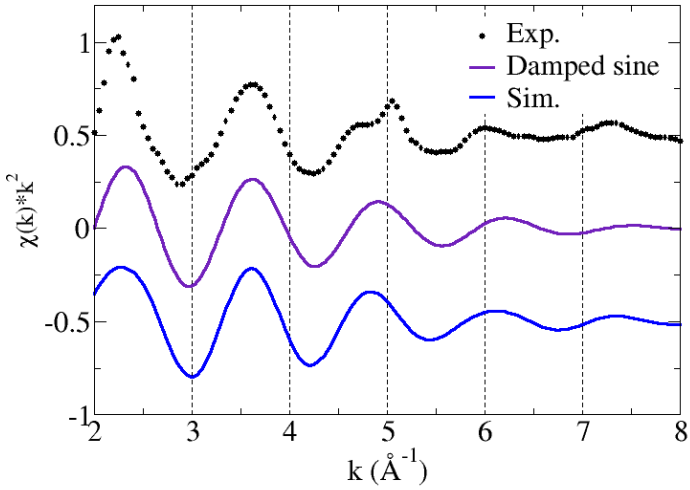

Figure 5.18: k^2-weighted Cs^+ EXAFS L_3-edge.

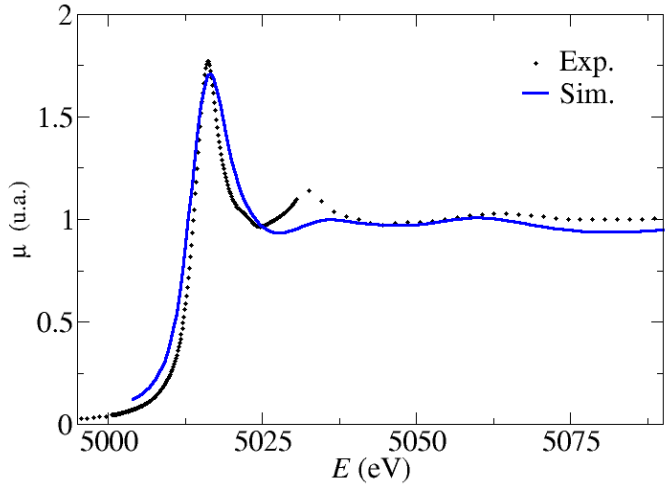

Figure 5.19: Cs^+ XANES L_3-edge.

Table 5.5: Properties of the Cs^+ aqueous solution. Standard deviation in parenthesis.

Property	this work	Literature
$R_{\text{M-O}_\text{I}}$ (Å)	3.12	3.20-3.30,[29] 2.98,[30] 3.07[31] 3.25,[6] 3.01-3.00[32]
CN_I	9.9	7.0-8.2,[32] 7.8-9.1[29] 8.0,[30,31] 10[6]
DW (Å^2)	0.075	
tilt angle$_I$ (°)	122(39)	119,[32] 135-155[29]
$\Delta\mu_I$ (D)	-0.1(0.3)	
$\Delta\mu_{II}$ (D)	0.0(0.3)	
MRT(t*=0) (ps)	6(1)	$\sim$ 100,[44] 1.5-2.2[29]
MRT(t*=2) (ps)	12(1)	
ΔH_{hyd} (kcal/mol)	$-55(9)$	-67.6[45]
D (10^{-5} cm^2/s)	1.5(0.1)	2.1,[45] 1.77,[57] 1.1,[32] 0.83[6]

5.6 Global properties in solution

5.6.1 Radial distribution function

To analyze the evolution of the main structural properties along the group the metal-oxygen Radial Distribution Function (RDF) can be used. Lithium first hydration shell is well defined, showing a depletion between the first and the second shell. Also there is a well defined second shell. Sodium first-shell is located at longer distance, the first minimum does not decay to zero as in the lithium case, meaning more water exchanges in this case. The first peak of the Na-O RDF is wider than that of the Li-O RDF what indicates a less rigid aqua ion. For potassium, rubidium and caesium hydrates the g(r) between the first and second shell is higher, meaning more frequent water exchanges between shells. The second shell is slightly defined for these cations except for the caesium for which a second minimum is lacking and consequently it is not possible to properly assign a second

hydration shell.

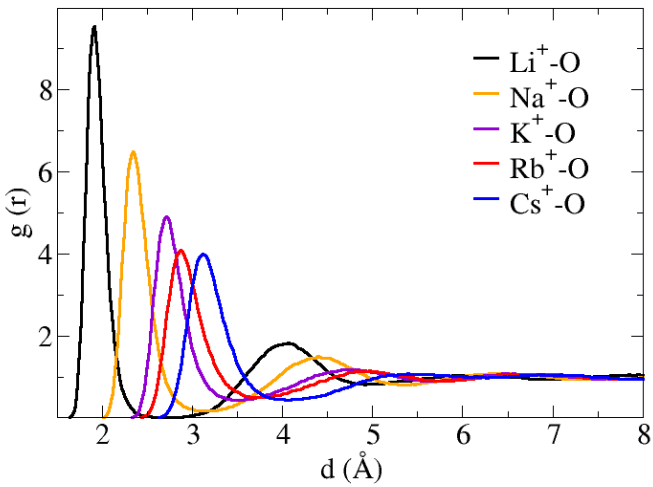

Figure 5.20: Metal-oxygen radial distribution function.

The metal-hydrogen radial distribution function (see Figure 5.21) follows the same trend found M-O RDF, incorporating the effect of the tilt angle in the first maxima location as M-H RDF maxima position depends on the maximum of the M-O RDF and the tilt angle. The average tilt angle of the first-shell molecules decrease along the group, values of 137°, 131°, 126°, 125°, 122°, for lithium, sodium, potassium, rubidium and caesium, were found respectively. The tilt angle runs parallel to the polarizing power, that decreases along the group at the same time that the ionic radii increases.

In Figure 5.22 the RDFs between the first-shell oxygen and hydrogen atoms and the O-H RDF of the MCDHO2 water model are shown. There

Table 5.6: Metal-oxygen radial distribution function data. Distances in Å.

Ion	$R_{\text{M-O}_\text{I}}$(max)	$g(r)_{\text{M-O}_\text{I}}$(max)	$R_{\text{M-O}_\text{I}}$(min)	$g(r)_{\text{M-O}_\text{I}}$(min)
Li^+	1.91	9.5	2.70	0.0
Na^+	2.34	6.5	3.20	0.2
K^+	2.71	4.9	3.49	0.4
Rb^+	2.87	4.1	3.68	0.5
Cs^+	3.12	4.0	4.05	0.5
Ion	$R_{\text{M-O}_\text{II}}$(max)	$g(r)_{\text{M-O}_\text{II}}$(max)	$R_{\text{M-O}_\text{II}}$(min)	$g(r)_{\text{M-O}_\text{II}}$(min)
Li^+	4.06	1.8	4.92	0.8
Na^+	4.02	1.5	5.35	0.8
K^+	4.74	1.2	5.66	0.9
Rb^+	4.9	1.1	5.77	0.9

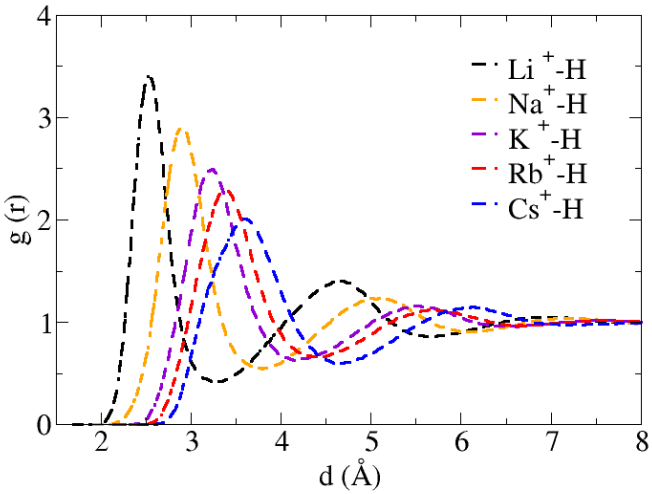

Figure 5.21: Metal-hydrogen radial distribution function.

Table 5.7: Metal-hydrogen radial distribution function data. Distances in Å.

Ion	$R_{\text{M-H}_\text{I}}(\text{max})$	$g(r)_{\text{M-H}_\text{I}}(\text{max})$	$R_{\text{M-H}_\text{I}}(\text{min})$	$g(r)_{\text{M-H}_\text{I}}(\text{min})$
Li^+	2.53	3.4	3.30	0.4
Na^+	2.90	2.9	3.79	0.6
K^+	3.24	2.5	4.14	0.6
Rb^+	3.39	2.3	4.38	0.7
Cs^+	3.60	2.0	4.62	0.6
Ion	$R_{\text{M-H}_\text{II}}(\text{max})$	$g(r)_{\text{M-H}_\text{II}}(\text{max})$	$R_{\text{M-H}_\text{II}}(\text{min})$	$g(r)_{\text{M-H}_\text{II}}(\text{min})$
Li^+	4.67	1.4	5.60	0.9
Na^+	4.40	1.5	5.34	0.8
K^+	5.50	1.2	6.51	1.0
Rb^+	5.67	1.1	6.62	1.0

can be seen how the caesium function is similar to the water one but with a different intensity. Li^+ and Na^+ enviroments exhibit OH RDFs quite different from that of bulk water, while K^+ and Rb^+ are closer to that of Cs^+. This comparison shows how the water bulk structure is recognized in the first shell water molecules of the heavy alkalines.

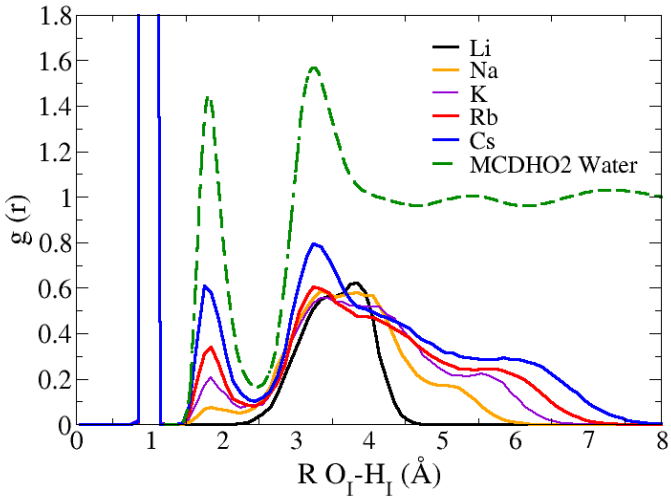

Figure 5.22: RDF between oxygen and hydrogen atoms in the first hydration shell of alkaline cations and OH RDF of the water model.

5.6.2 Energetic properties

The hydration enthalpy from the simulations follows the experimental[45] trend (see Figure 5.23), with an average mean error of x.

The average interaction energy between the ion and a first-shell water molecule have been computed together with the interaction among first-shell water molecules have been computed (see Table 5.8). The ion-water interaction decreases descending in the group as there is a relation between the interaction energy and the ionic radii, which determines how close the two particles can approach each other, as well as the relative water orientation with respect to the ion (tilt angle). For Li^+ the water molecules are oriented by the cation having a high repulsive interaction among them.

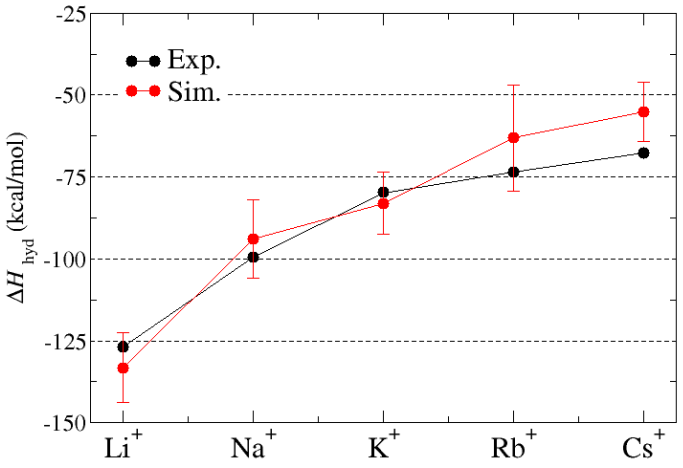

Figure 5.23: Hydration enthalpy (kcal/mol). Red dots experimental values.[45] Black dots calculated values from the simulations with error bars defining its mean error.

This water orientation evolves descending in the group loosing the ion-dipole orientation as the ion becomes larger and less polarizing. In the caesium case the first-shell water molecules are able to interact attractively among them.

5.6.3 Hydrogen bonding

Descending in the alkaline group, the average number of hydrogen bonds formed by the first-shell water molecules increases, because the ion is lossing its ability to orient the water molecules (see Figure 5.24). Then, the water molecules can adopt part by the tetrahedral arrangement of liquid water, appearing hydrogen bonds among first-shell water molecules.

Table 5.8: Average interaction energy between two first-shell particles (kcal/mol). I : Ion. W : water. Standard deviation in parenthesis.

Ion	$\text{Eint}_{I-W_{1st}}$	$\text{Eint}_{W_{1st}-W_{1st}}$
Li^+	-40.6(2.2)	8.2(1.1)
Na^+	-22.5(2.2)	4.5(1.2)
K^+	-17.4(2.0)	2.5(1.6)
Rb^+	-12.9(1.8)	0.7(1.7)
Cs^+	-10.2(1.5)	-1.0(1.8)

Also, it is observed how the type of hydrogen bond changes when descending in the group (see Table 5.10). For the lithium the 77.4% of the hydrogen bonds among first-shell and second shell water molecules are formed by a first-shell water molecule donating the hydrogen to a water molecule of the second shell. For the caesium this percentage goes down to 66%. The relative number of accepted hydrogen bonds by first-shell molecules in the alkaline group is quite similar (23% for Li^+ and 34% for Cs^+). It is interesting to point out that the lithium tetrahydrate adopts a structure where the four water molecules do not form hydrogen bonds among them. On the contrary, the caesium decahydrate adopts a structure where each of the first-shell water molecules is able to form on average one hydrogen bond among them, but less than two hydrogen bonds with second shell water molecules. The hydrogen bond network of the second shell is similar for all the cations, the main difference comes from to the relative number of water molecules in the second shell with respect to the amount of the first-shell solvent molecules.

Table 5.9 and Figure 5.25 collects the hydrogen bond interaction energy (E_{HB}) among first, second and third-shell (bulk) water molecules. As can be seen, E_{HB} 1-1 and E_{HB} 1-2 follow different trend along the group. E_{HB} 1-2 decreases with the polarizing capabilities of the cation and the polarization of first-shell water molecules. Interestingly E_{HB} 1-1 increases due

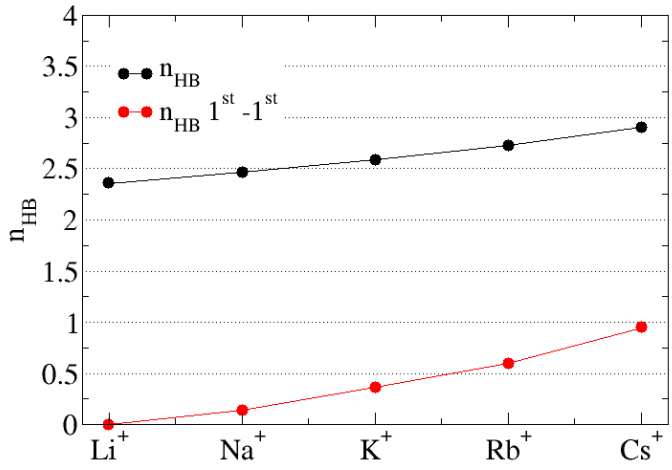

Figure 5.24: Average number of hydrogen bonds for first-shell water molecules. Black dots: average number of hydrogen bonds per molecule. Red dots: average number of hydrogen bonds between first-shell water molecules.

to the same factors. As can be seen in Table 5.8 there is a smooth change between the ion-water and water-water repulsion along the group, whereas the ion-water interaction energy decreases the water-water interaction energy increases together with the hydrogen bond number between first-shell water molecules.

Concerning first-second shell hydrogen bonds, only Li^+, -7.1 kcal/mol, the interaction energy is greater than the pure water value, -6.6 kcal/mol, as it is the only cation that polarizes its first hydration shell strongly. The hydrogen bond interaction energy among water molecules of the first-shell increases along the group, but with values smaller than those corresponding

to bulk, due to the first-shell geometrical constraints. It is observed that the hydrogen bonds among second-shell water molecules and second and third shell (or bulk) converges to the bulk value.

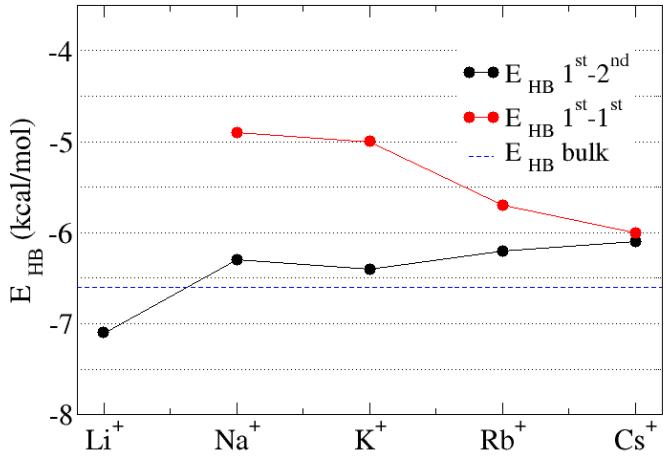

Figure 5.25: Average hydrogen bond interaction energy (kcal/mol). Black dots: average interaction energy per hydrogen bond between a molecule of the first-shell and a molecule of the second shell. Red dots: average interaction energy per hydrogen bonds between first-shell molecules. Blue line: MCDHO2 bulk water value.

Table 5.9: Energy of hydrogen bonds formed by water molecules of different shells (kcal/mol). Standard deviation in parenthesis

Ion	Li^+	Na^+	K^+	Rb^+	Cs^+
E_{HB} 1-1		-4.9(2.7)	-5.0(2.6)	-5.7(2.5)	-6.0(2.5)
E_{HB} 1-2	-7.1(2.7)	-6.3(2.4)	-6.4(2.4)	-6.2(2.3)	-6.1(2.3)
E_{HB} 2-2	-6.6(2.5)	-6.6(2.5)	-6.6(2.4)	-6.6(2.4)	-6.6(2.4)
E_{HB} 2-3	-6.6(2.5)	-6.6(2.4)	-6.6(2.4)	-6.5(2.4)	-6.6(2.4)

Table 5.10: Hydrogen bond statistics: average number of hydrogen bonds per water molecule in 1^{st} and 2^{nd} hydration shells. don/acc means the water molecule acting as donor/acceptor of the hydrogen bond.

Ion	Li^+	Na^+	K^+	Rb^+	Cs^+
n_{HB} 1^{st} shell	**2.4**	**2.5**	**2.7**	**2.7**	**2.8**
n_{HB} 1-1	0	0.1	0.4	0.6	0.9
n_{HB} 1-2	2.4	2.3	2.2	2.2	1.9
n_{HB} 1-2 don.	77%	71%	67%	66%	66%
n_{HB} 1-2 acc.	22%	29%	33%	34%	34%
n_{HB} 2^{nd} shell	**3.6**	**3.6**	**3.7**	**3.7**	**3.7**
n_{HB} 1-2	0.7	0.8	0.9	0.9	0.8
n_{HB} 2-2	1.0	1.0	1.0	1.0	1.1
n_{HB} 2-3	1.9	1.8	1.8	1.8	1.8
n_{HB} 2-3 don.	59%	58%	57%	57%	56%
n_{HB} 2-3 acc.	41%	42%	43%	43%	44%

5.6.4 Dynamic properties

Figure 5.26 shows the mean residence time (MRT) of a water molecule in the first hydration shell. MRT decreases from lithium to potassium, whereas from potassium to caesium similar MRTs appear. Although the experimental trend with higher values for the smaller and polarizing cations has been obtained, the computed values are underestimated in two orders of magnitude with respect to the experimental ones. Thus, in this study the MRT values using t* = 0 are 74 ps, 15 ps, 6 ps, 5 ps and 6 ps for lithium, sodium, potassium, rubidium and caesium respectively, experimental[44] values around 100 ps are found for all them, the longer one for lithium, then decreasing along the group.

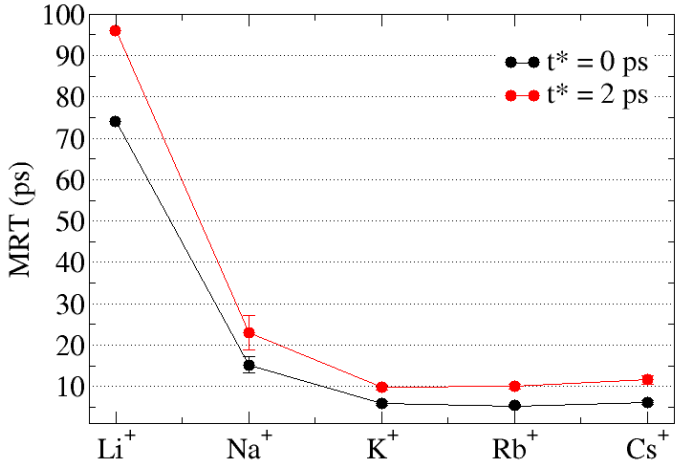

Figure 5.26: Mean residence time of first-shell molecules computed by the Impey method. Black dots: MRT using t* = 0 ps. Red dots: MRT using t* = 2 ps.

Regarding the ion mobility the obtained values for self-translational diffusion coefficients follow the experimental trend,[45] increasing from lithium to potassium and then becoming roughly constant. As the MCDHO2 water model underestimates the water self-diffusion, $1.8{\cdot}10^{-5}$ cm^2/s respect the experimental value of $2.4{\cdot}10^{-5}$ cm^2/s,[58] the ion diffusion has been corrected by the water self-diffusion value. In this way, we present the relative value water-model corrected, D_i/D_w, which is less depending of the water model. Once it is corrected, the relative ion diffusion (see Figure 5.28 bottom) is very similar to what has been obtained experimentally.[45]

To complete the description of the dynamical properties, reorientational motions of the water molecules surronding the alkaline cations have been examined. In a general overview the slowest water dynamics is found for the lithium and the fastest for the caesium (see Table 5.11). As already saif, the Li^+ is the most polarizing alkaline cation being able to trap in its electric field the dipole moment of the first-shell water molecules, fixing their orientation more than the other alkaline cations. This can be observed in all the components, but particularly in the case of the dipole moment vector.

Li^+ and Na^+ first-shell water molecules have correlational times clearly longer than those of bulk ones, while for the rest of alkaline cations similar times are found. Considering that the time uncertainty is 2 ps, these values are undistinguishable to those of the bulk water. In QMMM works[28,29] the reorientational times for the Rb^+ and Cs^+ were calculated. In these works a relative slower dynamics compared to the bulk water dynamics $(\tau/\tau_w) \sim 0.2$ was found, whereas our work τ/τ_w reveals values around 1 (see Table 5.12).

An aspect previously discussed in the literature is the structure-breaking and/or hydrophobic nature of Rb^+ and Cs^+ ions in aqueous solutions. Their structure-breaking nature has been previously involved on the basis of shorter reorientational times than bulk water for first-shell solvent molecules[31] or higher degree of flexibility of ion hydrates together with rel-

atively fast solvent exchange processes.[59] Other authors[60,61] define their hydration as hydrophobic based on the identification of HBs inside the first-hydration shell. It is true that our HB analysis provides a picture in which first-shell solvent molecules define a non-negligible percentage of first-shell first-shell HBs, a typical feature of hydrophobicity and absent in strongly hydrated cations. However, a hydrophobic solute perturbs water in a way that reinforces the hydrogen bond network. This fact causes the water reorientation dynamics to slow down in an isotropic way, that is, OH and dipole vector reorientation should be equally affected.[62] Based on our MRTs for first-shell water molecules, Rb^+ and Cs^+ present longer times than the corresponding values of pure water (2 ps using $t^* = 0$ ps), so no structure-breaking features can be inferred from this property. However, reorientational times do reveal a differential behavior for both ions.

Although the ratio of ion and water reorientational times (τ/τ_w) is close to one in all cases, the tendency for Rb^+ is different from that of Cs^+. Caesium exhibits a clear structure-breaking character with first-shell reorientation dynamics faster than bulk water for both dipole and OH vectors. The rubidium ion shows a slightly longer reorientational time for the dipole water vector and a slightly shorter reorientational time for the OH bond, making it more difficult to define its hydration character from a dynamical perspective (see Figure 5.27). In this sense, our results seem to agree with the recent O K-edge XAS study[61] where the differential behavior found for Cs^+ in the alkaline series is justified on the basis of a larger H-bond network around the ion to compensate to some extent the structure-breaking effect. For an appropriate description of the Rb^+ and Cs^+ behavior in water we have been forced to deal with cation–water aggregates which do not follow the conventional concept of aqua ion usually associated to an ion placed in the center of an ensemble of water molecules. This is due to the fact that heavy alkaline–water interactions are only slightly larger than the water–water interactions. The efficient stabilization of water molecules in stable clusters leads to the QM prediction that gas phase cation hydrates are more stable when a water cluster joins the cation than when a conventional aqua ion is formed (Table 2). This situation is facilitated by the high

degree of polarizability of both ions, a degree of freedom the model here presented takes into account.

Table 5.11: First, $\tau_{1,n}$, and second order, $\tau_{2,n}$, reorientational time of first-shell water molecules (ps).

Ion	$\tau_{1,\mu}$	$\tau_{2,\mu}$	$\tau_{1,HH}$	$\tau_{2,HH}$	$\tau_{1,\perp}$	$\tau_{2,\perp}$	$\tau_{1,OH}$	$\tau_{2,OH}$
Li^+	40	7	9	4	7	3	10	5
Na^+	12	3	6	3	7	2	7	3
K^+	7	3	6	3	5	2	6	2
Rb^+	8	2	5	3	5	2	6	2
Cs^+	7	2	5	2	5	2	6	2
Water	5	2	6	3	4	2	6	3

Table 5.12: Published reorientational times (ps).

Ion	$\tau_{1,\mu}$	$\tau_{2,\mu}$	$\tau_{1,HH}$	$\tau_{2,HH}$	$\tau_{1,\perp}$	$\tau_{2,\perp}$
Rb^+	1.3[28]	0.4[28]	1.2[28]	0.6[28]	1.0[28]	0.4[28]
Cs^+	1.1, 2.3, 1.9[29]	0.5, 1.2, 1.0[29]	0.9, 1.9, 1.6[29]	0.4, 0.9, 0.9[29]	1.4, 2.9, 2.4[29]	0.4, 1.0, 1.0[29]
Water	6.8[28] , 7.5[44]	2.9[28] , 2.5[44]	6.6[28]	3.2[28]	4.7[28]	2.3[28]

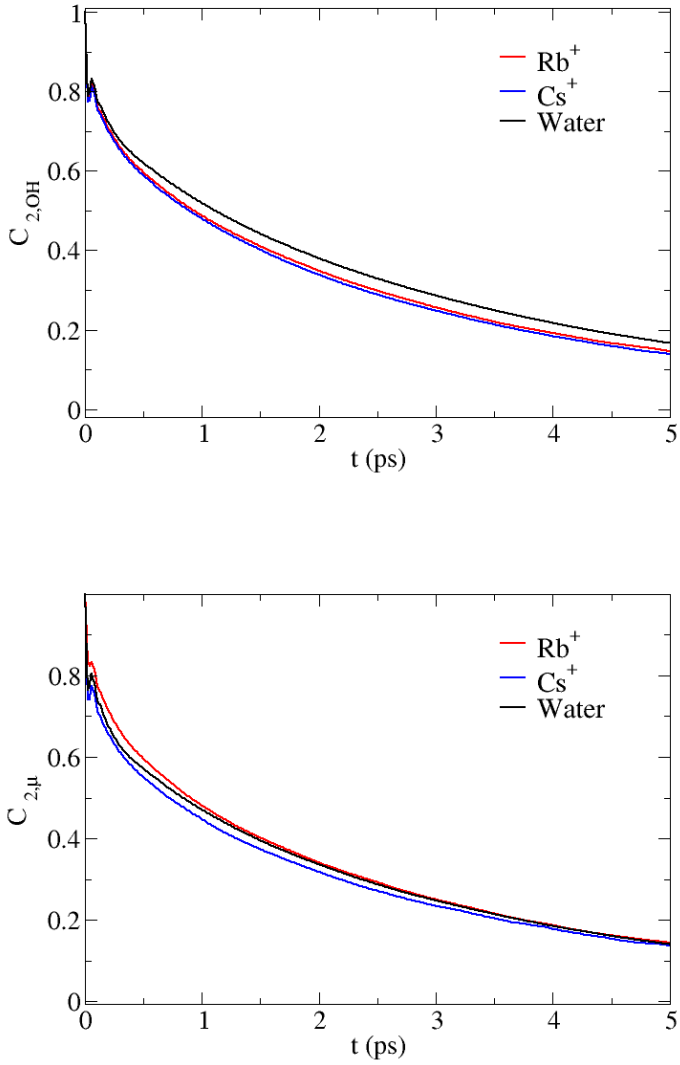

Figure 5.27: $\tau_{2,\mu}$ and $\tau_{2,OH}$ correlational functions.

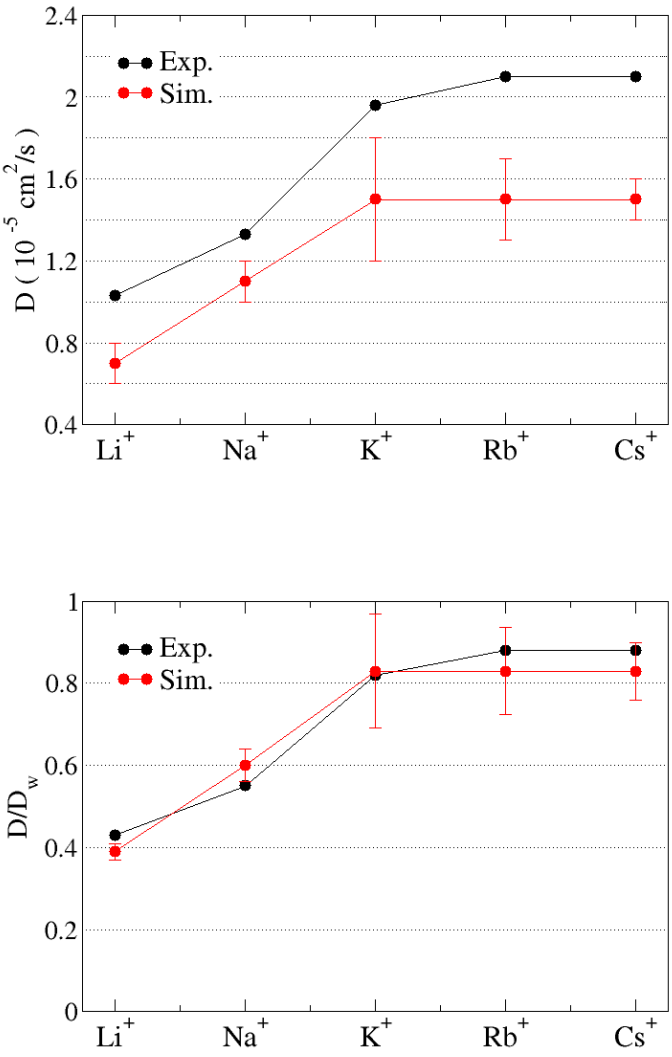

Figure 5.28: Self-diffusion coefficient (top), self-diffusion coefficient relative to the bulk water diffusion coefficient (bottom).

5.6.5 Molecular asymmetry

Another interesting structural feature derived from the results is the degree of radial symmetry retained in the first hydration shell.

The time correlation function of the eccentricity vector increases along the group. When the correlation times are examined it could be said that in the case of lithium the center of mass is defined by the same number of water molecules (that sometimes cross the cutoff of the first-shell) and for the case of the caesium there is also the effect of the continuous exchange of water molecules in the first-shell. This to say that the time for the caesium should be much larger if the water exchanges are reduced.

Table 5.13: Comparison of the M-O peak distance and M-O average distance.

Ion	M-O peak (Å)	$< R_{M-O} >$ (Å)	Δ R (Å)
Li^+	1.91	1.95	0.04
Na^+	2.34	2.42	0.08
K^+	2.72	2.82	0.10
Rb^+	2.87	3.02	0.15
Cs^+	3.12	3.25	0.13

To illustrate how this eccentricity is reflected in the cation cluster structure, Figure 5.30 shows the closest hydration environment of Cs^+ in a representative snapshot taken from the MD simulation. The two views displayed show the presence of regions around the metal cation which are partially de-populated of water molecules (left side of Figure 5.30), whereas in a populated region the water molecules are interacting simultaneously with the cation and forming HBs with other water molecules of the same shell (right side of Figure 5.30).

One might think that this snapshot could not be representative of the

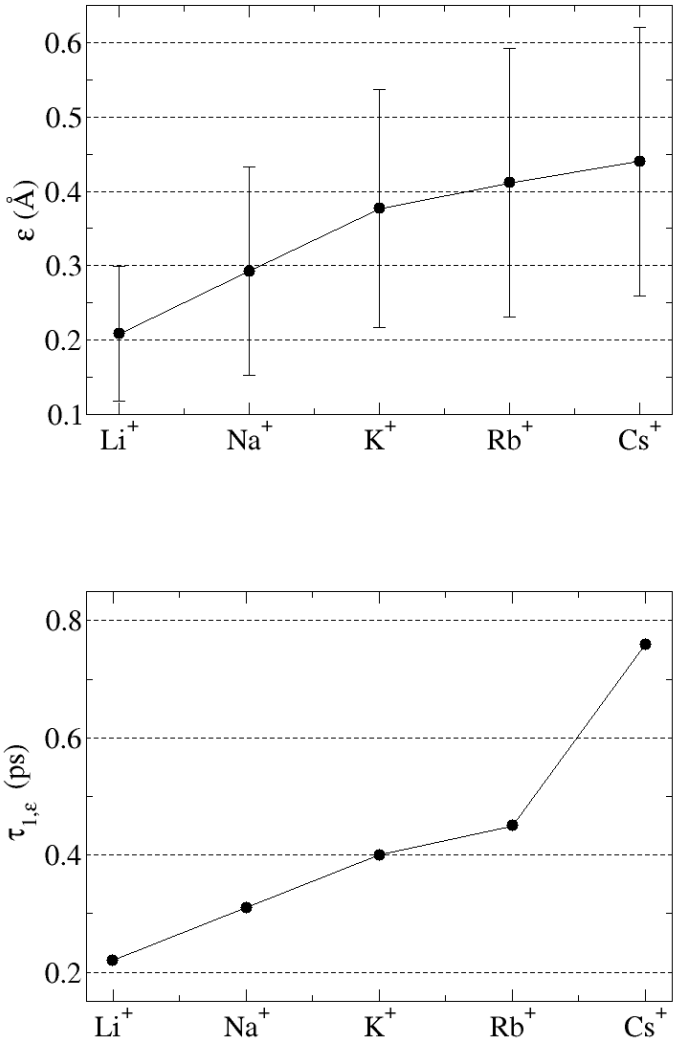

Figure 5.29: Eccentricity, ϵ (Å), and eccentricity reorientational time, $\tau_{1,\epsilon}$ (ps). Standard deviation defined by error bars.

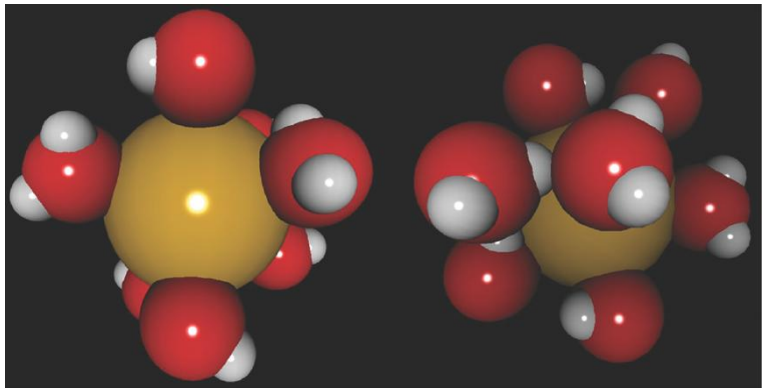

Figure 5.30: Two views of a representative structure and its first hydration shell containing ten solvent molecules taken from the MD simulation.

average hydration shell, but if the Li^+ hydration is considered the result would be very different. The Li^+ tetrahydrate exhibits a first-shell tetrahedral structure and the eccentricity of the first-shell water molecule mass center and the cation is only 0.2 Å. Therefore, the tendency observed in the energetic analysis of the clusters $[M(H_2O)_n]^+$ concerning the preference of surface clusters is translated in some way to aqueous solutions where asymmetric coordination shells are defined for the two ions (see Figure 5.29).

The eccentricity of the first hydration shell also contributes to an asymmetric M–O first peak, which is quantified by the difference between the peak maxima, and the first-shell R_{M-O} average values.

5.7 Global properties in gas phase

In order to test the general character of the developed intermolecular potentials, we have checked the behaviour of them for gas phase clusters.

5.7.1 Average dipole moment

The average dipole moment of the water molecules in alkaline hydrates was calculated in the gas phase, studying cluster with a number of water molecules varying from 1 to 25 at 100 K. In order to take into account the multiple minima problem an iterative procedure of heating was applied until convergence was achieved (50 iterations). In the heating step the cluster is equilibrated at 300 K to favor the rearrangement of the water molecules, inside a sphere that avoids the water evaporation. When increasing the size of the ion and the number of water molecules more configurations are needed to converge the property because the water structure beyond the first-shell becomes a delicate compromise between ion-water and water-water interactions.

When dealing with the monohydrate cation, its polarization depends on the capability of the ion. For the lithium the largest polarization is found and for the caesium the smallest one. When water molecules are added to the cluster the average polarization decreases as a consequence of the apparence of water-water interactions. However, when second hydration shell water molecules are incorporated the average dipole moment slighly increases as a consequence of the first-second hydrogen bonds (see Figure 5.31).

When the first hydration shell does not accept more water molecules those molecules are located in a second shell. If the ion is not able to orient the water molecules following an ion-dipole orientation, the cluster looks like a water cluster with an ion attached to the surface instead of an ion that orders the water molecules in concentric shells (see Figure 5.32). Same tendence was obtained in previous theoretical works.[63]

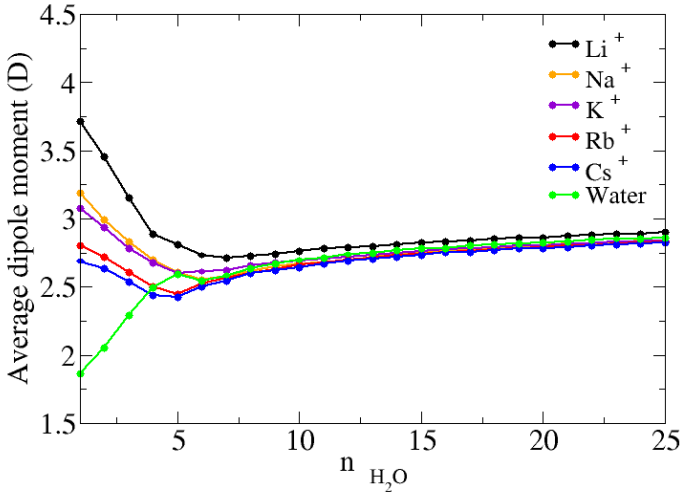

Figure 5.31: Average dipole moment of the water molecules.

Figure 5.32: Lithium (left) and caesium hydrates (right) with 25 water molecules.

5.8 Bibliography

[1] Scrosati, B.; Garche, J. *J. Power Sources* **2010**, *195*, 2419–2430.

[2] *Potassium and Sodium (In Biological Systems). Van Nostrand's Encyclopedia of Chemistry.*; 2005; Vol. g.

[3] Glezaku, V.; Chen, Y.; Fulton, J.; Schenter, G.; Dang, L. *Theor. Chem. Acc.* **2006**, *115*, 86–99.

[4] Vao-Soongnern, V.; Pipatpanukul, C.; Horpibulsuk, S. *J. Mater. Sci.* **2015**, *50*, 7126–7136.

[5] Mancinelli, R.; Boti, A.; Bruni, F.; Ricci, M. A.; Soper, A. K. *J. Phys. Chem. B* **2007**, *11*, 13570–13577.

[6] Lee, S. H.; Rasaiah, J. Y. *J. Phys. Chem.* **1996**, *100*, 1420–1425.

[7] San-Román, M. L.; Carrillo-Tripp, M.; Saint-Martin, H.; Cobos, J. H.; Ortega-Blake, I. *Theor. Chem. Acc.* **2006**, *115*, 177–189.

[8] Loeffler, H. H.; Rode, B. M. *J. Chem. Phys.* **2002**, *117*, 110–116.

[9] Lyubartsev, A. P.; Laasonen, K.; Laaksonen, A. *J. Chem. Phys.* **2001**, *114*, 3120–3126.

[10] Tongraar, A.; Liedl, K. R.; Rode, B. M. *Chem. Phys. Lett.* **1998**, *286*, 56–64.

[11] Sripa, P.; Tongraar, A.; Kerdcharoen, T. *J. Mol. Liq.* **2015**, *208*, 280–285.

[12] Sripa, P.; Tongraar, A.; Kerdcharoen, T. *J. Phys. Chem. A* **2013**, *117*, 1826–1833.

[13] Tongraar, A.; Liedl, K. R.; Rode, B. M. *J. Phys. Chem. A* **1998**, *102*, 10340–10346.

[14] Carrillo-Tripp, M.; Saint-Martin, H.; Ortega-Blake, I. *The J. Chem. Phys.* **2003**, *118*, 7062–7073.

[15] Ma, H. *Int. J. Quantum Chem.* **2014**, *114*, 1006–1011.

[16] Chandrasekhar, J.; Spellmeyer, D.; Jorgensen, W. *J. Am. Chem. Soc.* **1984**, *106*, 903–910.

[17] Gaiduk, A. P.; Zhang, C.; Gygi, F.; Galli, G. *Chem. Phys. Lett.* **2014**, *604*, 89–96.

[18] Bankura, A.; Carnevale, V.; Klein, M. L. *Molecular Physics* **2014**, *112*, 1448–1456.

[19] Faginas-Lago, N.; Lombardi, A.; Albertí, M.; Grossi, G. *J. Mol. Liq.* **2015**, *204*, 192–197.

[20] Ikeda, T.; Boero, M. *J. Chem. Phys.* **2012**, *137*, 041101(1)–041101(4).

[21] D'Angelo, P.; Persson, I. *Inorg. Chem* **2004**, *43*, 3543–3519.

[22] Fulton, J.; Pfund, D.; Wallen, S.; Newville, M.; Stern, E.; Yanjun Ma, *J. Chem. Phys.* **1996**, *105*, 2161–2166.

[23] Kubozono, Y.; Hirano, A.; Kahino, S.; Emura, S.; Ishida, H. *Z. Naturforsch.* **1994**, *49a*, 727–729.

[24] Ohkubo, T.; Konishi, T.; Hattori, Y.; Kanoh, H.; Fujikawa, T.; Kaneko, K. *J. Am. Chem. Soc.* **2002**, *124*, 11860–11861.

[25] Pham, V.; Fulton, J. L. *J Chem. Phys.* **2013**, *138*, 044201.

[26] Lee, S. H.; Rasaiah, J. C. *J. Chem. Phys.* **1994**, *101*, 6964–6974.

[27] San-Román, M. L.; Hernández-Cobos, J.; Saint-Martin, H.; Ortega-Blake, I. *Theor. Chem. Acc.* **2010**, *126*, 197–211.

[28] Hofer, T. S.; Randolf, B. R.; Rode, B. M. *J. Comput. Chem.* **2005**, *26*, 949–956.

[29] Schwenk, C. F.; Hofer, T. S.; Rode, B. M. *J Chem. Phys. A* **2004**, *108*, 1509–1514.

[30] Fan, Q.; Tanaka, M.; Tanaka, K.; Sakaguchi,; Takahashi, Y. *Geochim. Cosmochim. Acta* **2014**, *135*, 49–65.

[31] Mähler, J.; Persson, I. *Inorg. Chem* **2011**, *51*, 425–438.

[32] Ikeda, T.; Boero, M. *J. Chem. Phys.* **2015**, *143*, 194510.

[33] Bouazizi, S.; Nasr, S. *J. Mol. Struct.* **2007**, *837*, 206–213.

[34] Rudolph, W.; Brooker, M. H.; Pye, C. C. *J. Phys. Chem.* **1995**, *99*, 3793–3797.

[35] Mason, E.; Anell, S.; Neilson, G.; Rempe, S. B. *J. Phys. Chem. B* **2015**, *119*, 2003–2009.

[36] Licheri, G.; anf G. Pinna, G. P. *Chem. Phys. Lett.* **1975**, *35*, 119–123.

[37] Palinkas, G.; Radnai, T.; Hajdu, F. *Z. Naturforsch* **1979**, *35a*, 107–114.

[38] Spangberg, D.; Hermansson, K. *J. Phys. Chem.* **2004**, *120*, 4829–4842.

[39] Szasz, G.; Heinzinger, K.; Palinkas, G. *Chem. Phys. Lett.* **1981**, *78*, 194–196.

[40] Larentzos, J. P.; Crescenti, L. J. *J. Phys. Chem.* **2008**, *112*, 14243–14250.

[41] Impey, R.; Madden, P.; McDonald, I. *J. Phys. Chem.* **1983**, *87*, 5071–5083.

[42] Bock, C.; Markham, G.; Katz, A.; Glusker, J. *Theor. Chem. Acc.* **2006**, *115*, 100–112.

[43] Ikeda, T.; Boero, M.; Terakura, K. *J. Chem. Phys.* **2006**, *126*, 034501.

[44] Ohtaki, H.; Radnai, T. *Chem. rev.* **1993**, *83*, 1157–1204.

[45] Marcus, Y. *Ion properties*; Markel Dekker, Inc, 1997.

[46] Galib, M.; Baer, M.; Skinner, L.; Mundy, C.; Huthwelker, T.; Schenter, G.; Benmore, C.; Govind, N.; Fulton, J. *J. Chem. Phys.* **2017**, *146*, 084504.

[47] Azam, S. S.; Hofer, T. S.; Randolf, B. R.; Rode, B. M. *J. Phys. Chem.* **2009**, *113*, 1827–1833.

[48] Liu, Y.; Haigang Lu, Y. W.; Li, Q. *J. Chem. Phys.* **2012**, *132*, 124503.

[49] Helm, L.; Merbach, A. *Coord. Chem. Rev.* **1999**, *187*, 151–181.

[50] Kodre, A.; Arcon, I.; Gomilsek, J. P.; Preseren, R.; Frahm, R. *J. Phys. B* **2002**, *35*, 3497–3513.

[51] Ohta, A.; Kagi, H.; Tsuno, H.; Nomura, M.; Kawabe, I. *Am. Mineralogist* **2008**, *93*, 1384–1392.

[52] Bernieri, E.; Mobilio, S.; Filipponi, A. *Phys. Rev. B* **1988**, *38*, 3298–3304.

[53] Qin, H.; Yokoyama, Y.; Fan, Q.; Iwatani, H.; Tanaka, K.; Sakaguchi, A.; Kanai, Y.; Zhu, J.; Onda, Y.; Takahashi, Y. *Geochem. J.* **2012**, *46*, 297–302.

[54] Ohta, A.; Kagi, H.; Tsuno, H.; Nomura, M.; Kawabe, I. *Am. Mineral.* **2008**, *93*, 1384–1392.

[55] Rossetti, I.; Sordelli, L.; Ghigna, P.; Pin, S.; Scavini, M.; Forni, L. *Inorg. Chem* **2011**, *50*, 3757–3765.

[56] Kodre, A.; Arcon, I.; Hribar, M.; Stuhec, M.; Villain, F.; Parent, P. *J. Phys. IV* **1994**, *4 (C9)*, C9–397–C9–400.

[57] Sato, H.; Yui, M.; Yoshikawa, H. *J. Nucl. Sci. Technol.* **1996**, *33*, 950.

[58] Krynicki, K.; Green, C.; Sawyer, D. *Faraday Discuss Chem. Soc.* **1978**, *66*, 199–208.

[59] Sripa, P.; Tongraar, A.; Kerdcharoen, T. *Chem. Phys.* **2016**, *479*, 72–80.

[60] Dao, H.; Rasaiah, J.; Miller, D. *J. Phys. Chem. B* **2007**, *111*, 209–217.

[61] Waluyo, I.; Nordlund, D.; Bergmann, U.; Schlesinger, D.; Pettersson, L.; Nilsson, A. *J. Chem. Phys.* **2014**, *140*, 244506.

[62] Tielrooji, K.; van der Post, S.; Hunger, J.; Bonn, M.; Bakker, J. *J. Phys. Chem. B* **2011**, *115*, 12638–12647.

[63] Bucher, D.; Kuyucak, S. *J. Phys. Chem. B* **2008**, *112*, 10786–10790.

Chapter 6

Heavy alkaline-earths

The heavy Alkaline Earth cations, Sr^{2+}, Ba^{2+} and Ra^{2+}, have been chosen to be studied in this work. Sr^{2+}, Ba^{2+} and Ra^{2+} have radioactive isotopes. All of them have radioactive isotope, ^{90}Sr, is used as fuel in thermoelectric generators,[1] is found in nuclear waste and due to their environmental interest its separation process from other ions[2–4] is currently being studied. Barium has multitude of applications and although its radioactivity is low it is known that their soluble solutions are poisonous.[5] Radium has medical applications in cancer treatment.[6,7]

6.1 Strontium

There are several works about the structural properties of the strontium aqua ion. By means of EXAFS studies coordination numbers between 7.3 and 10.3[8–14] have been proposed, being 8 the most frequent value.[10,12,15,16] A small range of interatomic distances, between 2.57 and 2.64 Å was found. By means of classical molecular dynamics[15–18] coordinations around 8 have been found with interatomic distances in the range 2.5-2.7 Å. In a QM/MM study[19] a coordination of 9 with peak distance at 2.69 Å was found. Data are collected in Table 6.1.

In this work a first-shell coordination number of 8.0 with a peak distance at 2.57 Å have been found. The second hydration shell at 4.72 Å is formed by 22 water molecules (see Figure 6.10 and 6.11). Although there are several water exchanges changing the coordination number, the lifetime of the enneahydrate and heptahydrate are relatively short with respect to the octahydrate (see Figure 6.1).

The first-shell water molecules are orientated by the cation forming a tilt angle of 141° and are polarized exhibiting an enhanced dipole moment of 0.15 D with respect to bulk water (see Table 6.1). As the experimental EXAFS[10] function presents a MEE at 6.5 A^{-1} (KN_1, $KM_{4,5}$ and $KM_{2,3}$ transitions form the MEE[14]), to improve the comparison with the simulated spectra the Ohta et al methodology[20] has been used, including in the process the spectrum range [0-10] A^{-1} to remove the MEE. As can be seen in Figure 6.3 there is an excellent agreement between the experimental EXAFS function and the simulated one once the MEE has been removed. This is also confirmed by the good agreement observed between the experimental and the simulated XANES spectra[10] (see Figure 6.4).

Table 6.1: Properties of Sr^{2+} aqueous solution. Standard deviation in parenthesis.

Property	this work	Literature
$R_{\text{M-O}_\text{I}}$ (Å)	2.57	2.5,[17] 2.57,[9] 2.55-2.58[21] 2.58,[15,16,22] 2.60,[18] 2.61[10] 2.62,[8] 2.64,[12] 2.643[14] 2.67,[11] 2.69[19]
CN_I	8.1	7.3,[8] 7.3-7.9,[17] 7.6[18] 7.8,[9] 8.0,[10,12,15,16] 8.0-8.1[10] 8.3,[13] 9,[19] 8.2-8.28[21] 8-9,[11] 10.3[14]
DW (Å^2)	0.017	0.0116,[10] 0.0115,[13] 0.021[14]
tilt angle$_\text{I}$ (°)	141(19)	155[19]
$R_{\text{M-O}_\text{II}}$ (Å)	4.72	4.78-4.85,[21] 4.97,[19] 4.9[12]
CN_II	22.4	19.0-22.7,[21] 23.5,[19] 15[12]
tilt angle$_\text{II}$ (°)	110(38)	-
$\Delta\mu_\text{I}$ (D)	0.2(0.3)	
$\Delta\mu_\text{II}$ (D)	0.0(0.3)	
MRT(t*=0) (ps)	65	1000[23]
MRT(t*=2) (ps)	90	
ΔH_{hyd} (kcal/mol)	$-353(15)$	-351.3[23]
D (10^{-5} cm^2/s)	0.6(0.2)	0.72[17]

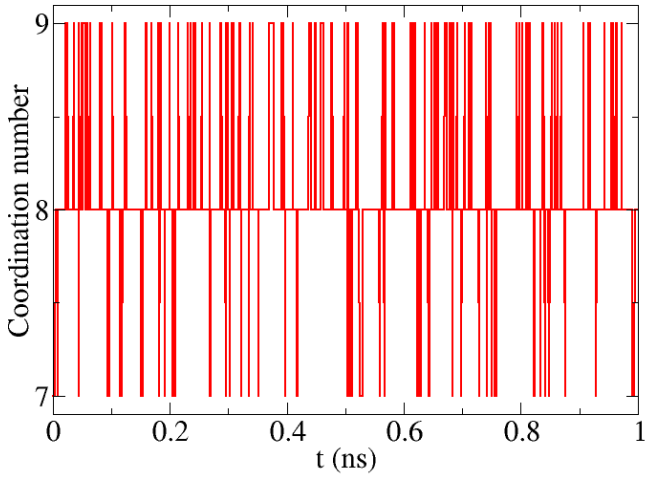

Figure 6.1: Time evolution of Sr^{2+} coordination number in aqueous solution.

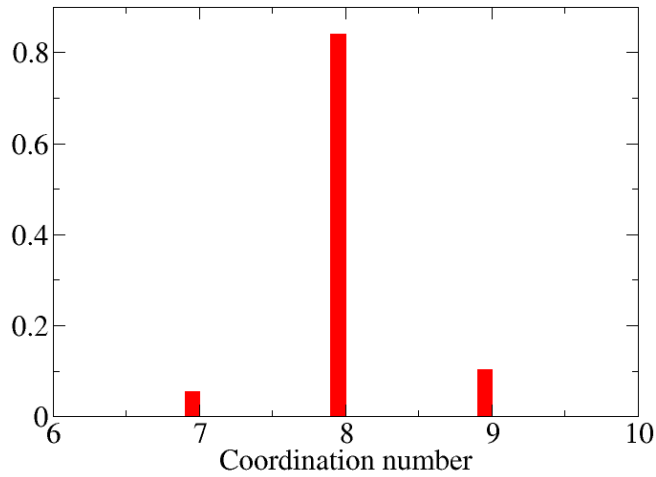

Figure 6.2: Coordination number histogram of Sr^{2+} on aqueous solution.

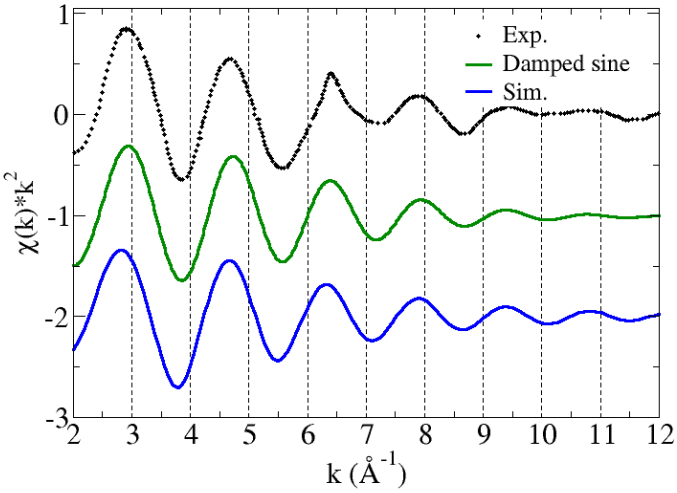

Figure 6.3: k^2-weighted Sr^{2+} K-edge EXAFS.

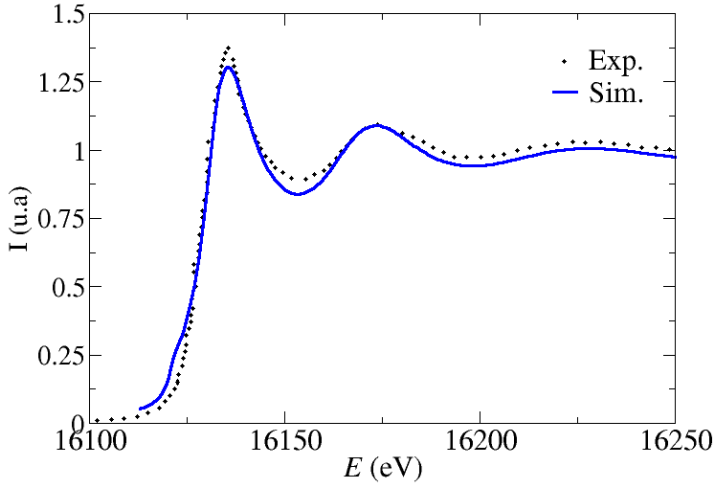

Figure 6.4: Sr^{2+} K-edge XANES.

6.2 Barium

There are not many experimental studies about the barium hydration (see Table 6.2). A LAXS-EXAFS[10] study determined its coordination number around 8 with an interatomic distance of 2.82 Å. MD studies[15,22] using a rigid water model obtained first-shell coordination numbers between 8.6 and 8.8 with peak distances of 2.75 and 2.78 Å. A QM/MM study[24] obtained a first-shell coordination number of 9.3 with a peak distance at 2.86 Å and a second shell coordination number of 23.5. In an AIMD study[25] a first-shell coordination number of 8 was found at 2.8 Å. Data are collected in Table 6.2.

In this work a first-shell coordination number of 9.4 with an interatomic distance of 2.81 Å has been found. The coordination number is changing between 9 and 10 with high frequency as is shown in Figure 6.5. The second shell is formed by ∼20 water molecules centered at 4.9 Å (see Figures 6.10 and 6.11). First and second shell water molecules are slightly polarized, showing a dipole moment increase compared to bulk water of 0.05 D and 0.02 D, respectively. The EXAFS function[10] presents a MEE at 5.5 A^{-1} that has been removed using the Ohta's methodology.[20] The simulated EXAFS function has a similar frequency and intensity, although at high k we find a more damped simulated function that may indicate a slightly less robust aqua ion (see Figure 6.7). In fact, the simulated DW is three times greater than the experimental one reported by Persson et al.[10]

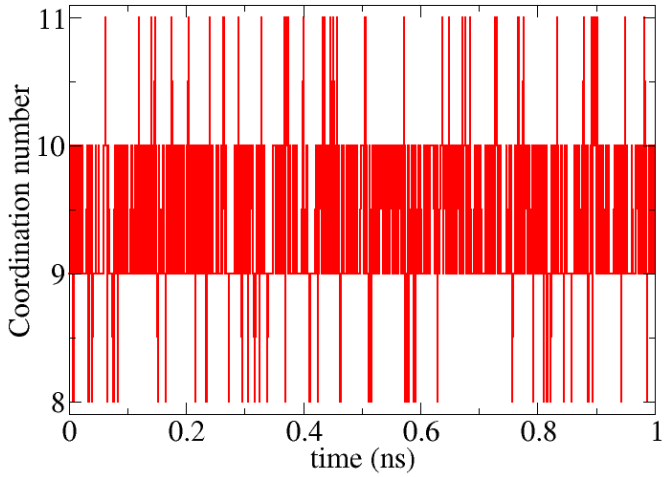

Figure 6.5: Time evolution of Ba^{2+} coordination number in aqueous solution.

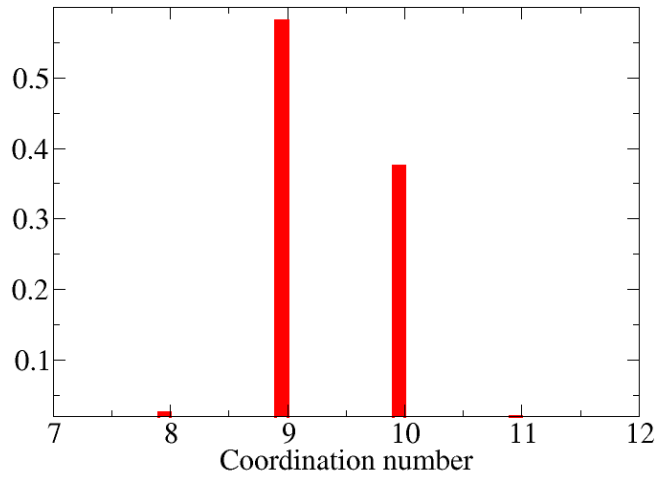

Figure 6.6: Coordination number histogram of Ba^{2+} in aqueous solution.

Table 6.2: Properties of Ba^{2+} aqueous solution. Standard deviation in parenthesis.

Property	this work	Literature
$R_{\text{M-O}_\text{I}}$ (Å)	2.81	2.6[15] , 2.75[22] , 2.78[26] 2.8,[25] 2.82,[10] 2.86[24]
CN_I	9.4	7.8[26] , 8[25] , 8.1[10] 8.3-8.4,[15] 8.6,[22] 9.3[24]
DW (Å^2)	0.034	0.0112,[10] 0.012[26]
tilt angle$_\text{I}$ (°)	138(38)	155[24]
$R_{\text{M-O}_\text{II}}$ (Å)	4.92	5[24]
CN_II	20.2	23.5[24]
tilt angle$_\text{II}$ (°)	111(20)	
$\Delta\mu_\text{I}$ (D)	0.1(0.3)	
$\Delta\mu_\text{II}$ (D)	0.0(0.3)	
MRT(t*=0) (ps)	38	130[22]
MRT(t*=2) (ps)	53	
ΔH_hyd (kcal/mol)	$-322(12)$	-318.4[23] , -300[22]
D (10^{-5} cm^2/s)	0.8(0.1)	0.847,[23] 0.9[15]

6.3 Radium

There are few theoretical works about the hydration of the divalent radium cation,[27,28] and only one theoretical work devoted to study its hydration in aqueous solution[29] by means of a Frament Molecular Orbital (FMO-MD). A first-shell coordination number of 8.1 was obtained with a peak distance of 2.85 Å. Although longer distances are expected when descending in the group, this is not the case due to the relativistisc contraction of the inner orbitals.[30] Data are collected in Table 6.3.

In this work a first hydration shell number of 9.8 with peak distance at 2.93 Å have been found. The coordination number changes between 8

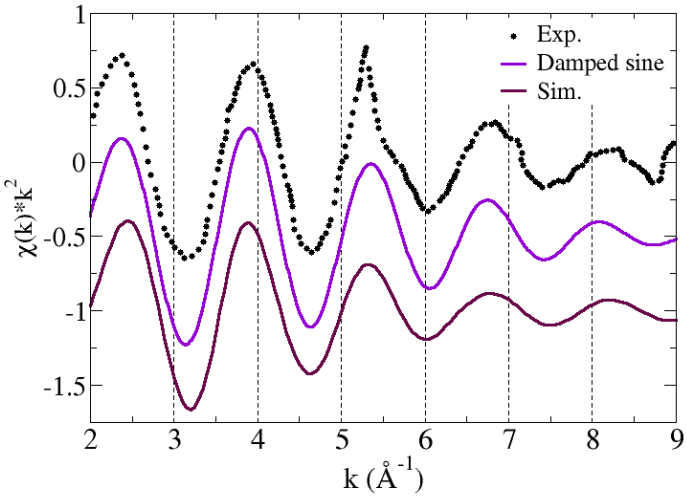

Figure 6.7: k^2-weighted Ba^{2+} K-edge EXAFS.

and 11 along the simulation 9 and 10 being the more frequent coordinations (See Figures 6.8 and 6.9). The second hydration shell is formed by 21 water molecules with a peak distance of 5.02 Å.

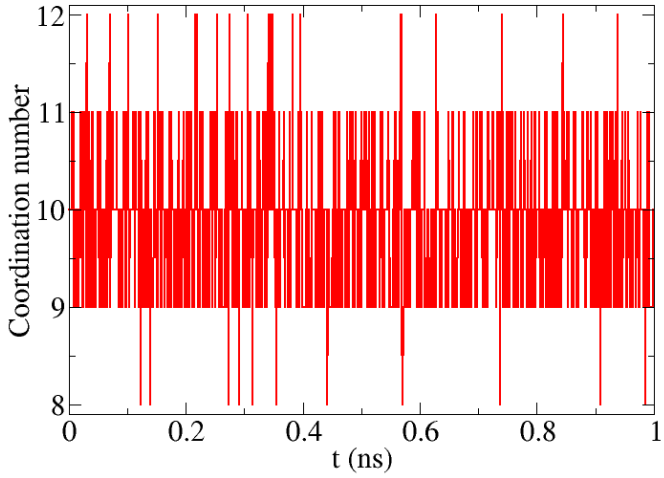

Figure 6.8: Time evolution of Ra^{2+} coordination number aqueous solution.

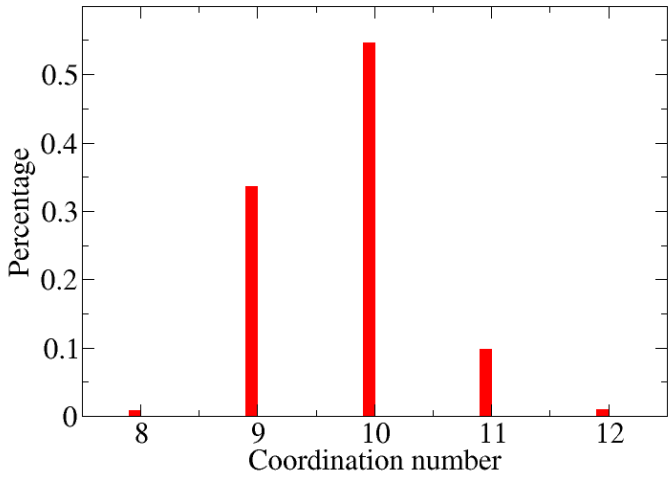

Figure 6.9: Coordination number histogram of Ra^{2+} in aqueous solution.

Table 6.3: Properties of Ra^{2+} aqueous solution. Standard deviation in parenthesis.

Property	this work	Literature
$R_{\text{M-O}_\text{I}}$ (Å)	2.93	2.85[29]
CN_I	9.8	8.1[29]
DW (Å^2)	0.034	
tilt angle$_\text{I}$ (°)	135(22)	
$R_{\text{M-O}_\text{II}}$ (Å)	5.02	
CN_II	20.9	
tilt angle$_\text{II}$ (°)	109(38)	
$\Delta\mu_\text{I}$ (D)	0.0(0.3)	
$\Delta\mu_\text{II}$ (D)	0.0(0.3)	
MRT(t*=0) (ps)	20(4)	
MRT(t*=2) (ps)	29(4)	
ΔH_{hyd} (kcal/mol)	-302(21)	-315.7[23]
D (10^{-5} cm^2/s)	0.9(0.1)	0.889[23]

6.4 Global properties in solution

6.4.1 Radial distribution Function

Figures 6.10 and 6.11 plot the M-O and M-H RDFs of the three heavy alkaline-earth divalent cations in water. The first and second hydration shells are well defined with a depletion zone between these two shells. Barium and radium first and second-shell are found at a similar distance and with a similar disorder. Although for radium aqua ion it may be expected a longer M-O distance than for barium one due to a longer ionic radii, the relativistic effects over its inner orbitals causes a decrease in the bond length (See hydrates in gas phase, Table 3.5). This fact justifies that Ba^{2+} and Ra^{2+} have similar radii, although slightly smaller for the barium (1.42 Å and 1.48 Å are the experimentally determined ionic radii[31] for barium and radium, both in octa-coordinated compounds). Same conclusions can

be extracted from the M-H RDF, as the function is similar for both cations. Tilt angle is very similar in the three cases, although decreases smoothly from 141° for strontium to 138° for barium and 135° for radium.

Table 6.4: Metal-oxygen radial distribution function data. Distances in Å.

Ion	$R_{\text{M-O}_\text{I}}(\text{max})$	$g(r)_{\text{M-O}_\text{I}}(\text{max})$	$R_{\text{M-O}_\text{I}}(\text{min})$	$g(r)_{\text{M-O}_\text{I}}(\text{min})$
Sr^{2+}	2.57	10.0	3.34	0.0
Ba^{2+}	2.81	7.0	3.65	0.1
Ra^{2+}	2.93	6.9	3.77	0.2
Ion	$R_{\text{M-O}_\text{II}}(\text{max})$	$g(r)_{\text{M-O}_\text{II}}(\text{max})$	$R_{\text{M-O}_\text{II}}(\text{min})$	$g(r)_{\text{M-O}_\text{II}}(\text{min})$
Sr^{2+}	4.73	1.8	5.55	0.8
Ba^{2+}	4.92	1.6	5.80	0.8
Ra^{2+}	5.03	1.5	5.96	0.8

Table 6.5: Metal-hydrogen radial distribution function data. Distances in Å.

Ion	$R_{\text{M-H}_\text{I}}(\text{max})$	$g(r)_{\text{M-H}_\text{I}}(\text{max})$	$R_{\text{M-H}_\text{I}}(\text{min})$	$g(r)_{\text{M-H}_\text{I}}(\text{min})$
Sr^{2+}	3.16	4.0	3.97	0.3
Ba^{2+}	3.35	3.5	4.27	0.4
Ra^{2+}	3.48	3.3	4.40	0.5
Ion	$R_{\text{M-H}_\text{II}}(\text{max})$	$g(r)_{\text{M-H}_\text{II}}(\text{max})$	$R_{\text{M-H}_\text{II}}(\text{min})$	$g(r)_{\text{M-H}_\text{II}}(\text{min})$
Sr^{2+}	5.32	1.5	6.25	0.8
Ba^{2+}	5.52	1.3	6.55	0.9
Ra^{2+}	5.67	1.3	6.71	0.9

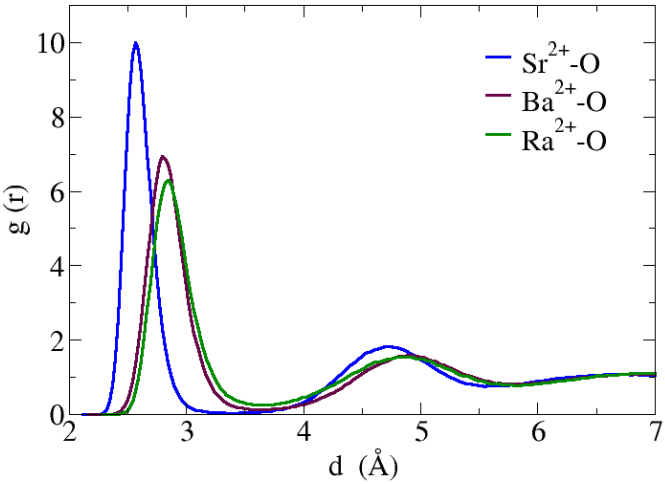

Figure 6.10: Metal-oxygen radial distribution function.

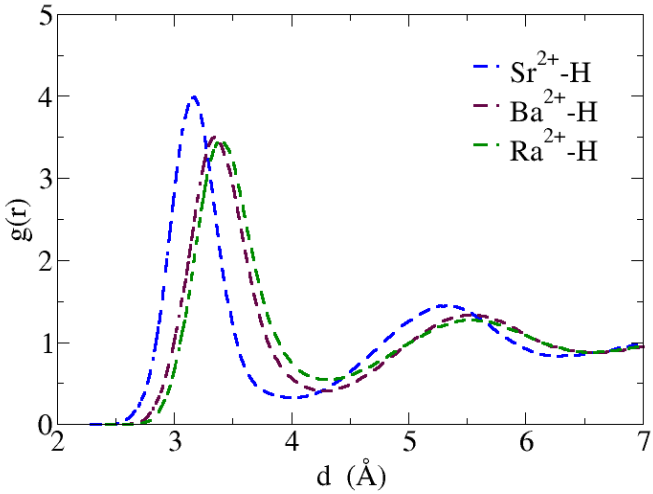

Figure 6.11: Metal-hydrogen radial distribution function for the heavy alkaline-earths cations.

6.4.2 Energetic properties

The calculated hydration enthalpy follows the experimental trend, with an error smaller than 2% (see Figure 6.12) the largest deviation appears in the Ra^{2+} case where the experimental uncertainty is larger.

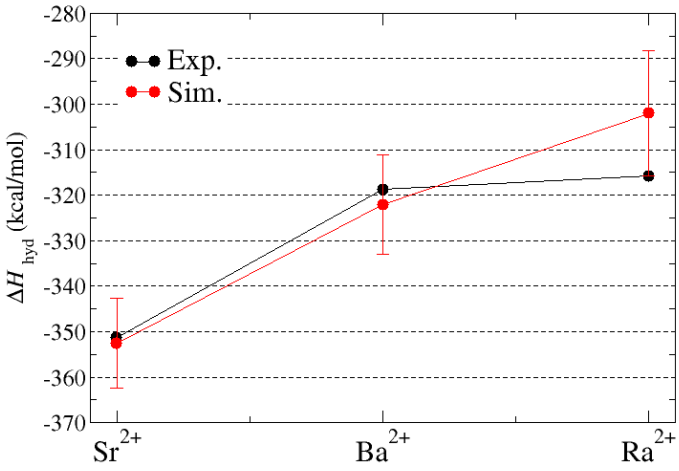

Figure 6.12: Hydration enthalpy (kcal/mol). Red dots: experimental values.[23] Black dots calculated values from simulations with error bars defining its mean error.

6.4.3 Hydrogen bonding

Table 6.6 collects the number of HBs formed by water molecules in each hydration shell and its distribution among shells. Strontium first-shell water molecules have an average of 2 HBs with second-shell water molecules. Although first-shell water molecules mainly donates hydrogen bonds to second-shell molecules, a 16% of HBs are formed by first-shell molecules

accepting it. The average number of HBs for first-shell water molecules around Ba^{2+} and Ra^{2+} increases to ~ 2.3, and also the tendency to form more HBs between first-shell molecules. Regarding water molecules in the second shell, the bulk water HBs number is almost recovered. Interestingly, almost one HB is formed between water molecules belonging to the second shell. This suggest particular compactness of the first-shell. A similar distribution of the HBs in the second-shell is found for the three cations.

For the Sr^{2+} the HBs between first and second shell water molecules are slightly more energetic than the hydrogen bonds in bulk water, -6.6 kcal/mol (see Table 6.7). In the barium and radium cases the opposite situation is found. For all the cations less energetic HBs among second-shell water molecules is found. HBs between second shell molecules and bulk molecules converge to the HBs bulk energy.

Table 6.6: Hydrogen bond statistics: average number of hydrogen bonds per water molecule in 1^{st} and 2^{nd} hydration shells. don/acc means the water molecule acting as donor/acceptor of the hydrogen bond.

Ion	Sr^{2+}	Ba^{2+}	Ra^{2+}
n_{HB} 1st shell	**2.1**	**2.2**	**2.3**
n_{HB} 1-1	0.1	0.2	0.3
n_{HB} 1-2	2.0	2.0	2.0
n_{HB} 1-2 don.	84%	79%	78%
n_{HB} 1-2 acc.	16%	21%	22%
n_{HB} 2nd shell	**3.6**	**3.6**	**3.6**
n_{HB} 1-2	0.9	1.0	0.9
n_{HB} 2-2	0.8	0.8	1.0
n_{HB} 2-3	1.9	1.8	1.8
n_{HB} 2-3 don.	64%	63%	63%
n_{HB} 2-3 acc.	36%	37%	37%

Table 6.7: Hydrogen bond energetics (kcal/mol). Standard deviation in parenthesis.

Ion	Sr^{2+}	Ba^{2+}	Ra^{2+}
E_{HB} 1-1	-2.6(2.5)	-4.1(2.6)	-4.3(2.6)
E_{HB} 1-2	-6.7(2.6)	-6.4(2.5)	-6.3(2.5)
E_{HB} 2-2	-6.4(2.5)	-6.4(2.5)	-6.4(2.5)
E_{HB} 2-3	-6.6(2.5)	-6.6(2.5)	-6.5(3.7)

6.4.4 Dynamic properties

MRT values decrease from strontium to radium (See Figure 6.13), for t*=0 65 ps, 38 ps and 18 ps have been found for strontium, barium and radium, respectively. Experimentally values around 1 ns for strontium and barium have been proposed by Helm and Merbach.[32]

The cation self-difussion coefficient (Figure 6.14) follows the experimental[23] trend, increasing along the group. But there is an underestimation of around 20-40 % when is compared the relative diffusion coefficient (D/D_w), except for the Ra^{2+} that there is overestimated in $\sim$ 20% .

The reorientational dynamics of first-shell water molecules is similar for barium and radium aqua ions, and is longer for those molecules around the strontium ion (see Table 6.8). But for all the ions the dynamics of the first-shell water molecules is longer than in bulk water (water values are in Table 5.11). In a QM/MM study[24] faster dynamics (see Table 6.9) for the barium first-shell molecules respect the bulk water molecules has been found, in contrast to what is found in this work.

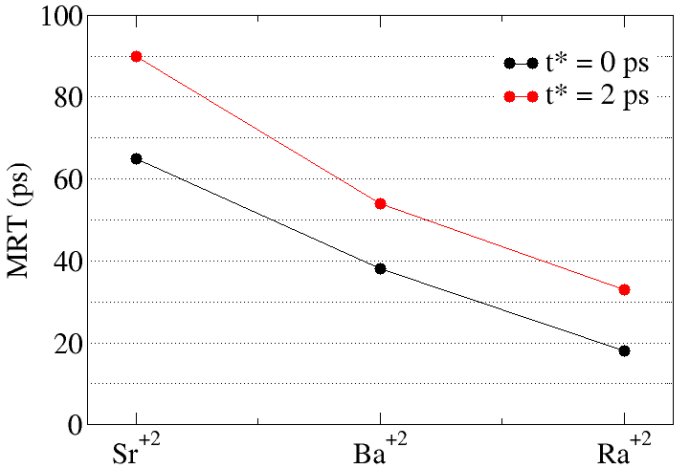

Figure 6.13: Mean residence times of first-shell molecules computed by the Impey method. Black dots: MRT using t* = 0 ps. Red dots: MRT using t* = 2.

Table 6.8: Reorientational time temporal correlation (ps).

Ion	$\tau_{1,\mu}$	$\tau_{2,\mu}$	$\tau_{1,HH}$	$\tau_{2,HH}$	$\tau_{1,\perp}$	$\tau_{2,\perp}$	$\tau_{1,OH}$	$\tau_{2,OH}$
Sr^{2+}	44	8	7	5	5	2	16	4
Ba^{2+}	26	4	6	4	5	2	10	3
Ra^{2+}	23	4	5	4	4	2	11	3
Water	5	2	6	3	4	2	6	3

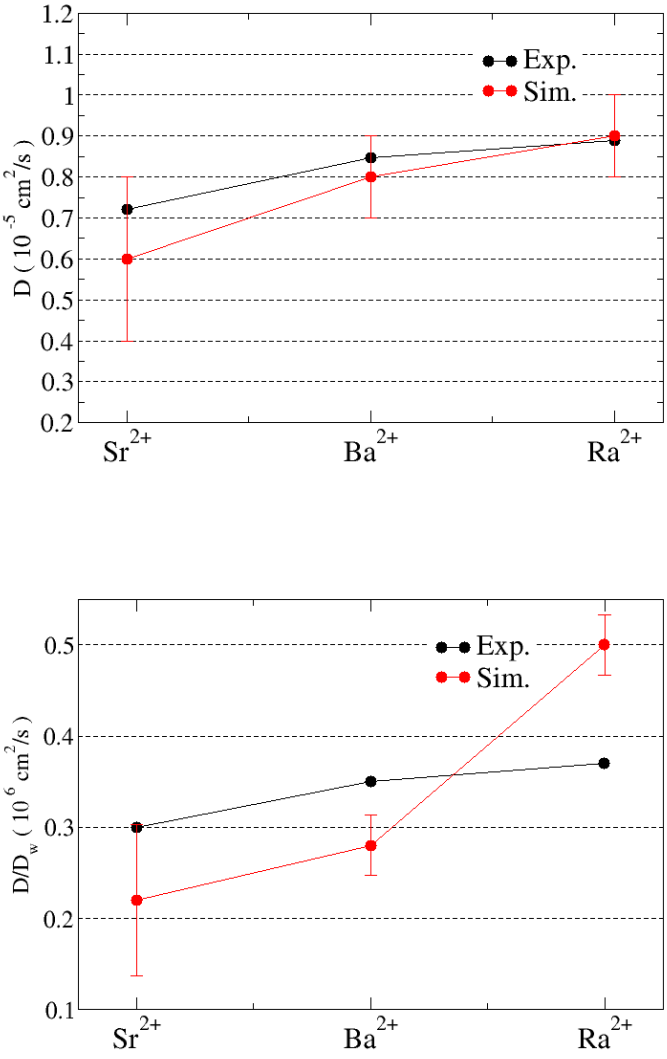

Figure 6.14: Self-diffusion coefficients (top), self-diffusion coefficient relative to bulk water (down).

Table 6.9: Published reorientational times (ps).

Ion	$\tau_{1,\mu}$	$\tau_{2,\mu}$	$\tau_{1,HH}$	$\tau_{2,HH}$	$\tau_{1,\perp}$	$\tau_{2,\perp}$
Ba^{2+}	8.8[24]	3.1[24]	4.0[24]	2.3[24]	3.5[24]	1.6[24]
Water	7.7[24] , 7.5[33]	3.1[24] , 2.5[33]	7.2[24]	3.1[24]	4.9[24]	2.3[24]

6.4.5 Molecular asymmetry

The first-shell assymetry and its correlational time has been calculated as was explained in a previous section (5.6.5). Values are shown in Table 6.10. The eccentricity slightly increases from strontium to radium, being coherent with the increase of the ionic radii. Its correlational time increases as well, the values for the heavy alkaline-earth being similar to those of the light alkalines, the correlational time of Li^+, Na^+ and K^+ are 0.2, 0.3 and 0.4 Å, respectively.

Table 6.10: Eccentricity, ϵ (Å), and eccentricity reorientational time, $\tau_{1,\epsilon}$ (ps). Standard deviation in parenthesis

Ion	ϵ (Å)	$\tau_{1,\epsilon}$ (ps)
Sr^{2+}	0.17(0.08)	0.2
Ba^{2+}	0.22(0.10)	0.3
Ra^{2+}	0.24(0.10)	0.4

6.5 Bibliography

[1] Golsmid, H. J. *Introduction to Thermoelectricity*; Springer, 2016.

[2] Horwitz, E.; Dietz, M.; Fisher, D. *Anal. Chem.* **1991**, *63*, 522–525.

[3] Potera, C. *Environ. Health Perspec.* **2011**, *116*, A244–A247.

[4] Sylvester, P. *Encyclopedia of Separation Science* **2000**, *9*, 4261–4267.

[5] Kresse, R.; Baudis, U.; Jäger, P.; Riechers, H.; Wagner, H.; Winkler, J.; Wolf, H. *Ullmann's Encyclopedia of Industrial Chemistry,* **2012**, *4*, 621–640.

[6] Wenter, V.; Herlermann, A.; Fendler, W.; Ilhan, H.; Tirichter, N.; Bartenstein, P.; Stief, C.; Fougere, C.; Albert, N.; Rominger, A.; Gratzke, C. *Oncotarget* **2017**, *8*, 44131–44140.

[7] Dronsfield, A.; Ellis, P. *Education in chemistry* **2011**, *45*, 56–59.

[8] Pfund, D. M.; Darab, J. G.; Fulton, J. L.; M, Y. *J. Phys. Chem.* **1994**, *98*, 13102–13107.

[9] Seward, T.; Henderson, C.; Charnock, J.; Driesner, T. *Geochim. Cosmochim. Acta* **1999**, *63*, 2409–2418.

[10] Persson, I.; Sandstrom, M.; Yokoyama, H.; Chaudhry, M. *Z. Naturforsch* **1995**, *50a*, 21–37.

[11] Ramos, S.; Neilson, G.; Barnes, A.; Capitán, M. *J. Chem. Phys.* **2003**, *118*, 5542–5546.

[12] Caminiti, R.; Misinu, A.; Paschina, G.; Pinna, G. *J. Appl. Cryst.* **1982**, *15*, 482–487.

[13] Parkman, R. H.; Charnock, J. M.; Livens, F.; Vaughan, D. J. *Geochim. Cosmochim. Acta* **1998**, *62*, 1481–1492.

[14] D'Angelo, P.; Nolting, H.; Pavela, N. *Phys. Rev. A* **1996**, *53*, 798–805.

[15] Larentzos, J. P.; Crescenti, L. J. *J. Phys. Chem.* **2008**, *112*, 14243–14250.

[16] Tofteberg, T.; Öhrn, A.; Karlström, G. *Chem Phys. Lett.* **2006**, *429*, 436–439.

[17] Deublein, S.; Reisser, S.; Vrabec, J.; Hasse, H. *J. Phys. Chem. B* **2012**, *116*, 5448–5457.

[18] Harris, D. J.; Brodholt, J. P.; Sherman, D. M. *J. Chem. Phys. B* **2003**, *107*, 9056–9058.

[19] Hofer, T.; Randolf, B.; Rode, B. *J. Phys. Chem. B* **2006**, *110*, 20409–20417.

[20] Ohta, A.; Kagi, H.; Tsuno, H.; Nomura, M.; Kawabe, I. *Am. Mineralogist* **2008**, *93*, 1384–1392.

[21] Boda, A.; De, S.; Musharaf, S.; Tulishetti, S.; Khan, S.; Singh, J. *J. Mol. Liq.* **2012**, *172*, 110–118.

[22] Raieri, P.; Demichelis, R.; Gale, J. D. *J. Phys. Chem. C* **2015**, *119*, 24447–24458.

[23] Marcus, Y. *Ion properties*; Markel Dekker, Inc, 1997.

[24] Hofer, T. S.; Rode, B. M.; Randolf, B. R. *Chem. Phys.* **2004**, *312*, 81–88.

[25] Chaudhari, M. I.; Soniat, M.; Rempe, S. B. *J. Phys. Chem. B* **2015**, *119*, 8746–8753.

[26] D'Angelo, P.; Pavel, N. V.; Roccatano, D. *Phys. Rev. B* **1996**, *54*, 12129–12138.

[27] Matsuda, A.; Mori, H. *J. Comput. Chem. Jpn.* **2014**, *13*, 105–113.

[28] Glendening, E.; Feller, D. *J. Phys. Chem.* **1996**, *100*, 4790–4797.

[29] Matsuda, A.; Mori, H. *J. Solution Chem.* **2014**, *43*, 1669–1675.

[30] Holleman, A.; Wiberg, E. En *Inorganic Chemistry*; of Munchen, U., Ed.; Walter de Gruyter, 2001.

[31] Atomistic Simulation Group, I. C. L. 1999; `http://abulafia.mt.ic.ac.uk/shannon/ptable.php`.

[32] Helm, L.; Merbach, A. *Coord. Chem. Rev.* **1999**, *187*, 151–181.

[33] Ohtaki, H.; Radnai, T. *Chem. rev.* **1993**, *83*, 1157–1204.

Chapter 7

Transition metals and rare earths

7.1 Transition metals

The hydration of scandium, cobalt and cadmium cations has been studied, all of them metals with multitude of industrial applications as catalysis or its inclusion in metal alloys.[1,2] Scandium and cadmium hydration are not well stablished, being good examples to test the power of combining theoretical and experimental tools to shed light on their hydration structures. Cobalt seawater speciation is of particular interest due to radioactive cobalt leaking to the sea.[3]

7.2 Scandium

At a first sight, the scandium case could be considered as a trivial case, where a small trivalent cation is surrounded by a few water molecules forming a well defined hydration shell. But this its not the case, as there is a great dispersion of hydration number values, probably due to a historical misinterpretation of the results as explained below.

The first characterization of the scandium hydrate in solution was done by means of Raman spectroscopy by Kanno et al[4] in 1989. In that work the scandium Raman spectrum using a non-complexing counterion was compared with the Raman spectrum of an Aluminum hexahydrate. They did not find a band at ~ 330 cm^{-1} in the $ScCl_3$ sample where was stated that no chloro-complex is formed. The same happened for the $Sc(ClO_4)_3$ sample. However that band is present in the case of the Al^{3+} spectrum. These authors concluded that the different number of bands, and particularly the no appearance of the band at 330 cm^{-1}, is related to a different coordination number, different from 6, for the scandium cation in solution. Another fact to consider a coordination number different from 6 is the ionic radius. Which is in between the aluminum and the yttrium ions that defined in solution a hexahydrate and octahydrate aqua ion, respectively.[4] Few years later in 1997, some of the same authors performed an EXAFS analysis[5] where a coordination of 7 was fixed, obtaining a first-shell peak distance at 2.18 Å. Likewise, they carried out an XRD study[6] where a heptahydrate was obtained with a first shell distance of 2.15 Å.

More recently in 2000, with the improved performance of the Raman difference spectroscopy, the hepta-coordination was discarded.[7] This new study found that the hexa-coordination is the preferred one. In this case the corresponding number of bands for a MX_6 skeleton for a non-complexing scandium solution was found, and was confirmed that scandium forms chloro-complexes.

Persson et al. performed in 2001 and 2005 a series of EXAFS and LAXS studies, where initially considered a coordination 8[8,9] but further analysis led to a coordination 6 with the possibility of one or two apical water molecules[10] between the first and the second-shell. When the XANES spectra were compared,[10] the no splitting of the pre-edge in the solution sample was considered another argument to discard the pure hexahydrated structure. Very recently D'Angelo[11] et al. built an ab-initio intermolecular potential to run MD simulations where 8 water molecules in the first hydration shell and one apical molecule were found. Apparently, a good

agreement between the experimental and the simulated EXAFS spectrum was presented. Data are collected in Table 7.1.

Due to technical difficulties in the generation of the potentials for highly polarizing cations explained in section 2.4.2 of this work, the potential was performed including only structures belonging to a given coordination number. Here we have included the potentials generated with structures containing 6 water molecules (Pot6) and 7 water molecules (Pot7). Results obtained are essentially the same. In addition, we generated potentials with 4 and 8 water molecules obtaining the same results. For sake of simplicity, only the potentials included in the work[12] *Theor. Chem. Acc. 136, 47 (2017)* are presented in the main text. In the appendix it may be examined the results for coordinations 4 and 8.

In this work, an hexahydrate was obtained with a peak 1^{st} shell peak distance at 2.15 Å. 13 water at 4.3 Å form the second shell (see Figure 7.12 and 7.13). No water exchanges, between first and second shells has been observed. Same distance, 2.15 Å was obtained for the quantum-mechanically optimized hexahydrate in a cavity model (PCM) at the MP2//aug-cc-PVTZ level. First-shell molecules are highly polarized, their dipole increases up to 4.6 D. There is a $\sim$ 5 % error in the ΔH_{hyd} for Pot 6 and $\sim$ 2 % error for Pot7. This energy gap is already observed in the energetic reproduction of the hexahydrated cluster.

The aqua ion structure was validated comparing XAS simulations with the experimental XAS spectra published by Lindqvist-Reis et al. in 2006.[10] There is an excellent agreement between the experimental EXAFS function and the simulated one as can be seen in Figure 7.1. In the XANES simulation the main features of the experimental spectra have been also obtained, as the hump following the edge and the global shape of the peak (see in Figure 7.2). Figure 7.3 displays the XANES spectra simulated from the QM optimized geometries corresponding to the $[Sc(H_2O)_n]^{3+}$ for n=6, 7 and 8. Although without statistical average these simulated spectra give an idea about the features in the spectrum when changing the coordina-

tion number and his related Sc-O distances. In the hexahydrate simulation similar features to those found in the experimental spectrum are observed, whereas in the heptahydrate and octahydrate cases more intense, narrower and white lines are observed.

The Fourier transform of the velocity autocorrelation function (FT-VAC) has been computed for the aqua ion in solution and the hexahydrate in gas phase (Figure 7.4). The hexahydrate power spectrum in gas phase presents two peaks at low frequency, 115 and 180 cm^{-1} that can be associated to bending modes, whereas at higher frequencies three bands appear at 350–385, 460 and 510 cm^{-1}, which can be associated to the ScO stretching modes region. Thus, the 370 cm^{-1} broad band can be associated to *Eg* stretching mode, whereas the 460 cm^{-1} peak is an *Ag* symmetric stretching mode. A final stretching mode, mixed with some bending moves, is centered at 510 cm^{-1}. The other two bands come from the convolution of the stretching and bending modes, whose peak center is around 50 cm^{-1} blue-shifted with respect that of gas phase.

When the aqua ion is immersed in solution, the power spectrum changes:
(i) a general broadening of the narrow bands observed in gas phase.
(ii) the appearance of bands due to new intermolecular bulk water interactions these new bands appear in the 30–100 cm^{-1} region.

Rudolph and Pye[7] studied the vibrational spectrum of a 1.65 M aqueous solution of $Sc(ClO4)_3$ containing a perchloric acid excess to prevent hydrolysis of Sc^{3+} aqua ion. Raman spectrum presents two bands, one of them depolarized (*Eg*) at 410 cm^{-1}, and the other one, polarized (*A1g*) at 442 cm^{-1}, which corresponds to the stretching modes. A third vibrational IR active band (*F1u*) is centered at 460 cm^{-1}, which may also by assigned to an Sc-O asymmetric stretching mode. Bearing in mind the 50–60 cm^{-1} blue shifting of our power spectra, these three bands are well recognized in the gas-phase spectra. Aqua ion solution leads to convolution of the three bands in only one broad band containing all of them. It must be pointed out that the computed power spectrum does nottake into account the IR

and Raman intensities.

Table 7.1: Properties of Sc^{3+} aqueous solution. Standard deviation in parenthesis.

Property	Pot6	Pot7	Literature
$R_{\text{M-O}_\text{I}}$ (Å)	2.15	2.14	2.10-2.27,[13] 2.158,[10] 2.18[5] 2.16-2.19[11]
NC_I	6.0	6.0	6,[7,10] 7,[4–6] 8,[8,9,11] 7-9[13]
DW (Å^2)	0.0039	0.0037	0.0082,[11] 0.0039[10]
tilt angle$_\text{I}$ (^{o})	159(12)	158(11)	169-170[13]
$R_{\text{M-O}_\text{II}}$ (Å)	4.32	4.30	4.10,[6] 4.27[10]
NC_II	13.5	13.7	13[6]
tilt angle$_\text{II}$ (^{o})	128(27)	128(27)	
$\Delta\mu_\text{I}$ (D)	1.7(0.4)	1.7(0.4)	
$\Delta\mu_\text{II}$ (D)	0.3(0.3)	0.3(0.3)	
MRT (ps)	-	-	
ΔH_hyd (kcal/mol)	-909(18)	-925(14)	-948[14]
D (10^{-5} cm^2/s)	0.5(0.1)	0.5(0.1)	0.574[14]

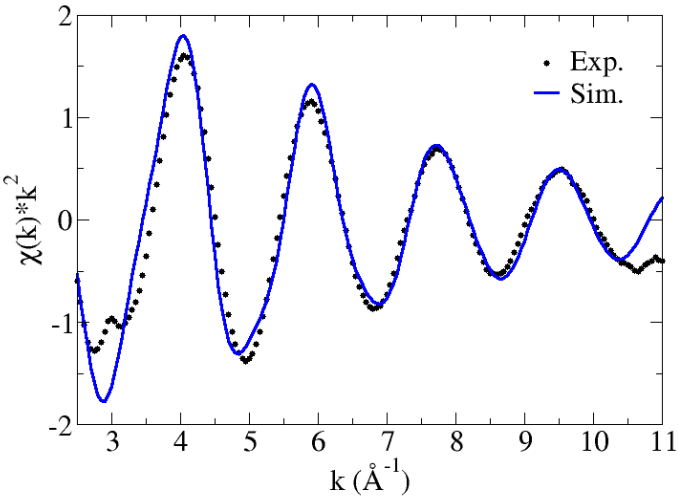

Figure 7.1: k^2-weighted Sc^{3+} K-edge EXAFS.

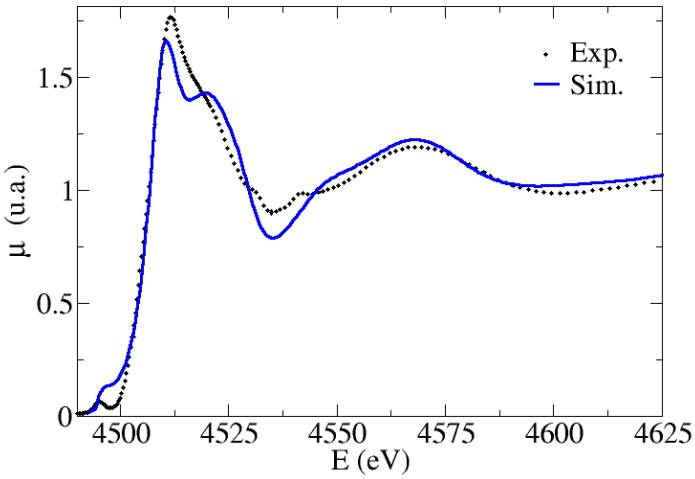

Figure 7.2: Sc^{3+} K-edge XANES.

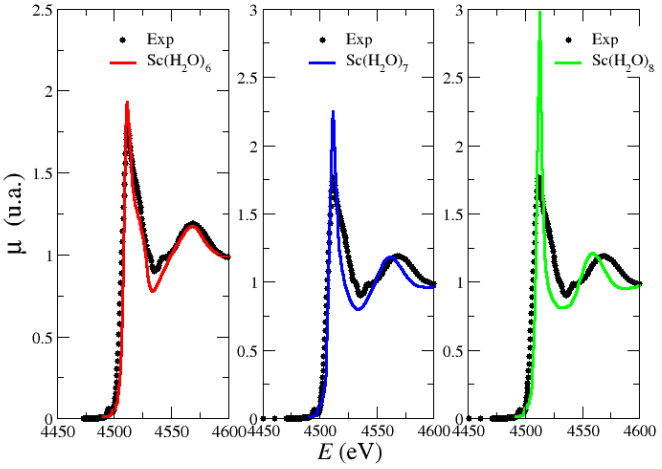

Figure 7.3: Sc^{3+} K-edge XANES of QM clusters of $[Sc(H_2O)_n]^{3+}$.

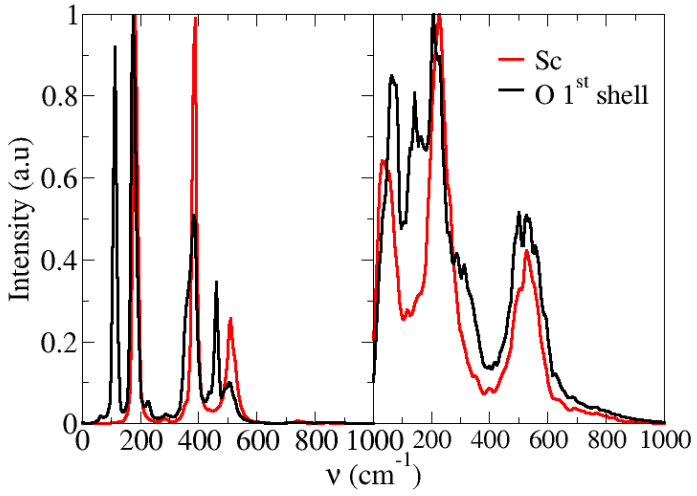

Figure 7.4: FT-VAC of Sc^{3+} aqua ion in the gas phase (left) and solution (right).

7.3 Cobalt

Cobalt as a subproduct of the nuclear technology has a great environmental interest. Due to the recent Fukushima accident (2011) the nuclear central leaked a high amount of radioactive materials to the sea, among them the cobalt isotope ^{60}Co. It is not surprising the growing interest on the study of the cobalt speciation on seawater.

On December 2016 this PhD student participated in an X-ray absorption experiment at the SOLEIL synchrotron in the beamline MARS with the members of the *Human and Environmental Radiochemistry group* of the University of Nize Sophia Antipolis. Among the experiments carried out, the XAS spectra of a $CoCl_2$ 0.05M aqueous solution was collected. The K-edge XAS spectrum of the aqueous cobalt(II) was recorded in fluorescence mode. Measurements were done at room temperature with a Si [111] monochromator. The storage ring was running at an energy of 2.5 GeV with a top up electron current of 200 mA. The sample was kept in a vial with a kapton window. Three scans were performed and the signal averaged. EXAFS and XANES spectra are plotted in Figures 7.5 and 7.6.

Previous EXAFS studies[15–17] about the cobalt(II) hydration obtained always a coordination of 6 and a first-shell position between 2.06 and 2.09 Å. A set of CPMD simulations[16] also obtained a coordination number of 6 with a peak distance between 2.10 and 2.14 Å. Due to the low number of water molecules in the simulation box (64 water molecules) the second shell is not well defined, coordination values between 5.7 and 14.8 with peak distance between 4.20 and 4.28 Å were found. In the same work classical MD simulations were also carried out obtaining an hexahydrate with a first-shell distance of 2.07 Å and a second shell formed by 11.5 water molecules with a maximum in the RDF at 4.3 Å.

In this work an stable hexahydrate with first-shell peak distance at 2.10 Å has been obtained and a well defined second shell formed by 14.4 water molecules at 4.27 Å. No water exchange between first and second shells was

Table 7.2: Properties of Co^{2+} aqueous solution. Standard deviation in parenthesis.

Property	this work	Literature
$R_{\text{M-O}_\text{I}}$ (Å)	2.09	2.06-2.092[15] , 2.10-2.14[16] 2.08[17]
CN_I	6.0	6.0[15–17]
DW (Å^2)	0.0080	0.012-0.015[16]
tilt angle$_I$ (°)	146(16)	
$R_{\text{M-O}_\text{II}}$ (Å)	4.24	4.10-4.28[16]
CN_{II}	15.0	12.48-13.18[16]
tilt angle$_{II}$ (°)	116(36)	
$\Delta\mu_I$ (D)	0.7(0.3)	
$\Delta\mu_{II}$ (D)	0.1(0.3)	
MRT (ps)	inf	$\sim 1{\cdot}10^6$
ΔH_{hyd}	-479(18)	-487[14]
D (10^{-5} cm^2/s)	0.6(0.1)	0.732[14]

observed. First and second shell water molecules are polarized by 0.7 D and 0.1 D, repectively. The simulated EXAFS one matches the intensity and frequency of the experimental spectrum (Figure 7.5). The main features of the XANES have been also reproduced in the simulation (Figure 7.6).

The Fourier transform of the velocity autocorrelation function of the aqua ion in gas phase and in solution are presented in Figure 7.7. The hexahydrate power spectra in gas phase present two peaks at low frequency, 105 and 160 cm^{-1} that can be associated to intermolecular bending modes, whereas at higher frequencies three bands appear at 265-285, 397 and 510 cm^{-1}, which can be associated to the Co-O stretching mode region. When the hexahydrate in solution is analyzed, as explained in the case of Sc^{3+} there is a broadening of the bands together a shift $\sim$ 50 cm^{-1} to lower frequencies.

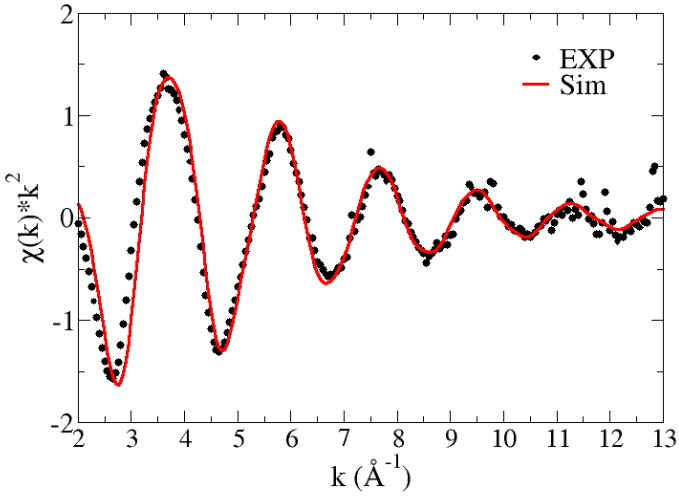

Figure 7.5: k^2-weighted Co^{2+} K-edge EXAFS.

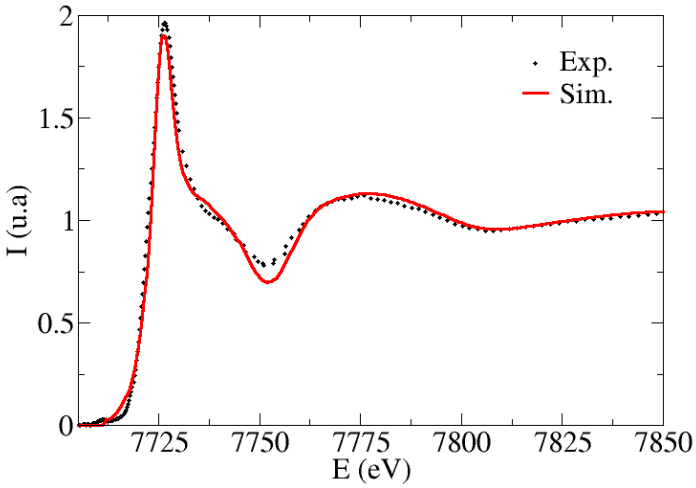

Figure 7.6: Co^{2+} K-edge XANES.

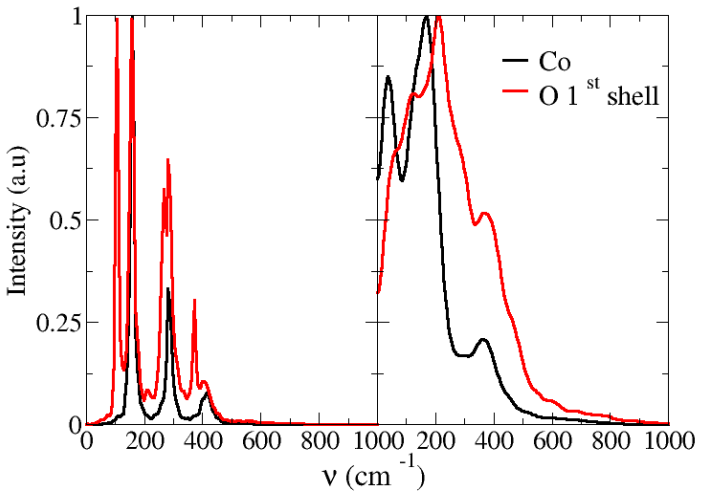

Figure 7.7: FT-VAC of Co^{2+} aqua ion in gas phase (left) and in solution (right).

7.4 Cadmium

There are few works about the cadmium hydration. XRD studies[18–20] fixing the coordination to 6 obtained distances between 2.29 and 2.31 Å. A Raman[21] study observed the bands corresponding to a hexahydrate. D'Angelo et. al performed a series of studies[22–24] including EXAFS, XANES and LAXS analysis together MD simulations. Through the EXAFS[22] analysis a coordination number of 6 with a peak distance at 2.302 Å were found. Computer simulations[24] found coordination numbers for the first and second hydration shells between 6.3 and 8 and between 12.5 and 16.8, respectively, with their corresponding distances between 2.22 Å and 2.33 Å and between 4.55 Å and 4.66 Å. In the XANES[23] study the inclusion of a 70% of heptacoordinated structures and a 30 % of hexacoordinated structures

were needed in order to reproduce the experimental XANES features. Data are collected in Table 7.3.

In this work an aqua ion with an average first-shell coordination number of 6.5 with peak distance at 2.29 Å and second shell composed by 17 water molecules with peak distance at 4.42 Å were found. The coordination number is changing mostly between 6 and 7 along the simulation (see Figure 7.8). Main properties are collected in Tables 7.3.

Figure 7.10 compares the simulated and experimental[22] EXAFS functions. The simulated and experimental XANES[23] spectra are compared in Figure 7.11. In both cases a good agreement is found.

Table 7.3: Properties of Cd^{2+} aqueous solution. Standard deviation in parenthesis.

Property	this work	Literature
$R_{\text{M-O}_\text{I}}$ (Å)	2.29	2.27,[17] 2.29,[18] 2.31[19,20] 2.22-2.35[23]
CN_I	6.53	6[17,19–21] , 6.3-8.0[23]
DW (Å^2)	0.012	
tilt angle$_\text{I}$ (°)	144(18)	
$R_{\text{M-O}_\text{II}}$ (Å)	4.42	4.2,[20] 4.55-4.66[23]
CN_II	17.1	12[20]
tilt angle$_\text{II}$ (°)	111(36)	
$\Delta\mu_\text{I}$ (D)	0.5(0.3)	
$\Delta\mu_\text{II}$ (D)	0.1(0.3)	
MRT(t*=0) (ps)	85	
MRT(t*=2) (ps)	337	
ΔH_hyd (kcal/mol)	-420(14)	-438[14]
D (10^{-5} cm^2/s)	0.6(0.1)	0.719,[14] 0.68-0.73[23]

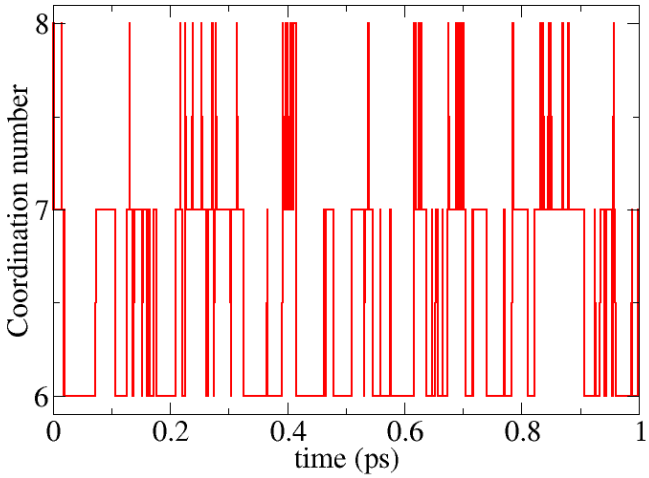

Figure 7.8: Time evolution of Cd^{2+} coordination number.

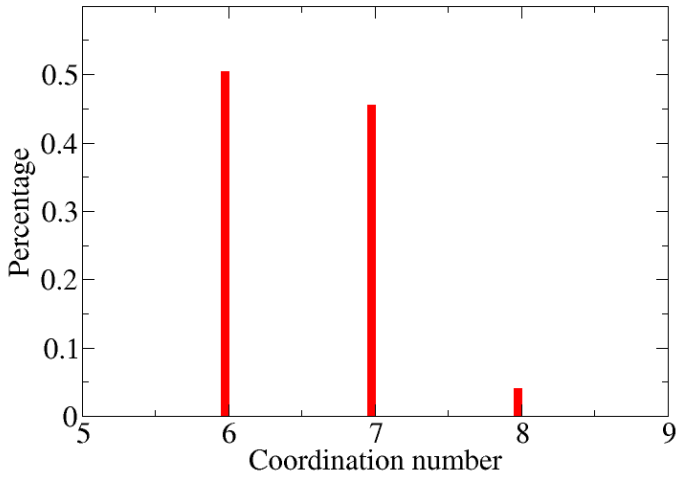

Figure 7.9: Coordination number histogram of Cd^{2+} in aqueous solution.

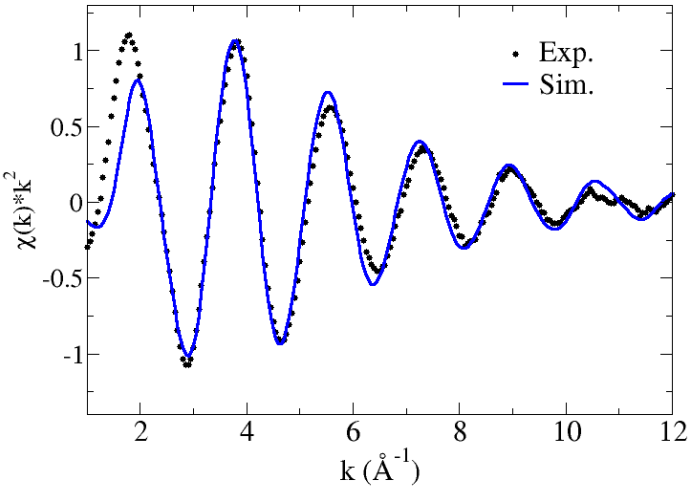

Figure 7.10: k^2-weighted Cd^{2+} K-edge EXAFS.

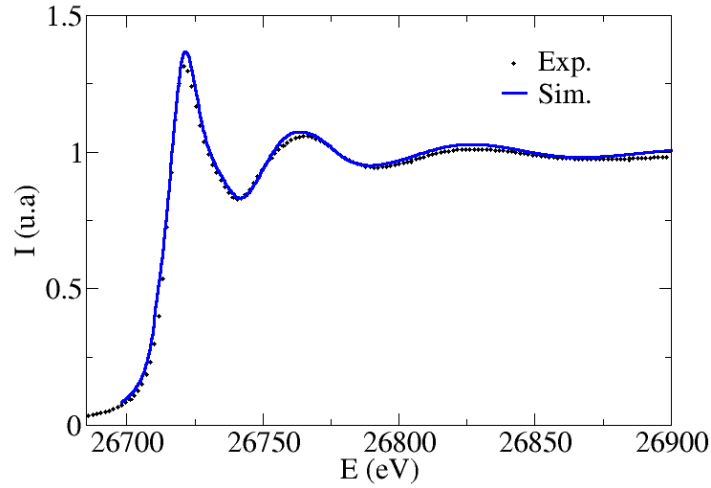

Figure 7.11: Cd^{2+} K-edge XANES.

7.5 Global properties in solution

7.5.1 Radial distribution function

M-O and M-H RDFs are shown in Figure 7.12 and 7.13 and maxima and minima data collected in Tables 7.4 and 7.5. The transition metal cations studied present several differences among them, as expected from their different electronic structure and oxidation states. Scandium is the most polarizing cation, for this reason the first-shell is the most ordered. Although Co^{2+} has the same ionic radius of scandium in hexacoordinated compounds,[25] 0.745 Å, and a lower oxidation state, it has a shorter M-O distance, 2.09 Å, than the scandium, 2.15 Å. This is due to the increase in covalent character in the metal-oxygen bond, but with more disorder in the first hydration shell. As the Cd^{2+} is the less polarizing cation, its hydration shells are the most disordered.

The second shell follows the same trend found in the first-shell concerning position and structural order. Sc-O RDF has a depletion zone between first and second shells as there are no water molecules exchanges. Similar depletion zones are found for the cobalt and cadmium cases. The tilt angle is high for all the cations meaning that there is a favored ion-dipole arrangeament of the first-shell water molecules. Average tilt angle is 159°, 147°and 144° for Sc^{3+}, Co^{2+} and Cd^{2+}, respectively.

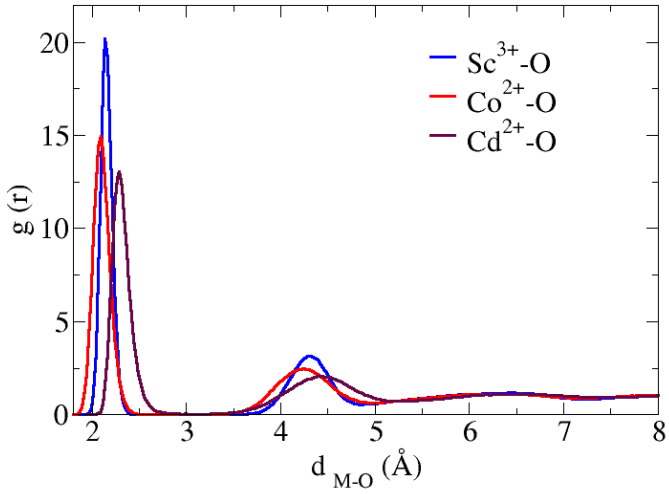

Figure 7.12: Metal-oxygen radial distribution function. Distances in Å.

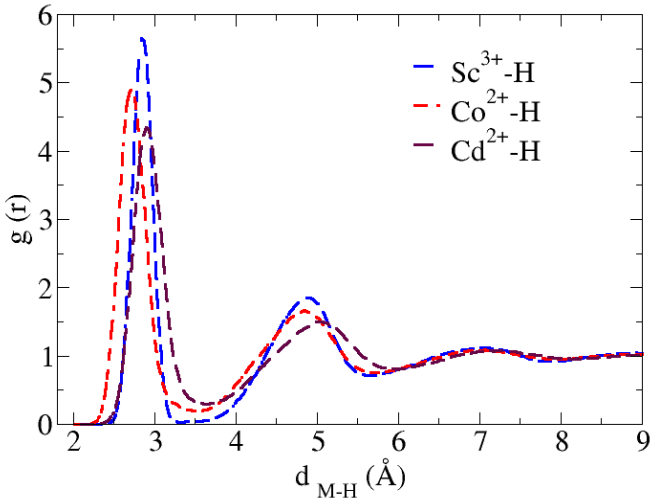

Figure 7.13: Metal-hydrogen radial distribution function. Distances in Å.

Table 7.4: Metal-oxygen radial distribution function data. Distances in Å.

Ion	$R_{\text{M-O}_\text{I}}(\text{max})$	$g(r)_{\text{M-O}_\text{I}}(\text{max})$	$R_{\text{M-O}_\text{I}}(\text{min})$	$g(r)_{\text{M-O}_\text{I}}(\text{min})$
Sc^{3+}	2.15	20.3	3.00	0.0
Co^{2+}	2.09	15.0	3.00	0.0
Cd^{2+}	2.29	13.1	3.07	0.0
Ion	$R_{\text{M-O}_\text{II}}(\text{max})$	$g(r)_{\text{M-O}_\text{II}}(\text{max})$	$R_{\text{M-O}_\text{II}}(\text{min})$	$g(r)_{\text{M-O}_\text{II}}(\text{min})$
Sc^{3+}	4.32	3.2	4.85	0.6
Co^{2+}	4.24	2.5	4.95	0.7
Cd^{2+}	4.20	2.1	5.17	0.7

Table 7.5: Metal-hydrogen radial distribution function data. Distances in Å.

Ion	$R_{\text{M-H}_\text{I}}(\text{max})$	$g(r)_{\text{M-H}_\text{I}}(\text{max})$	$R_{\text{M-H}_\text{I}}(\text{min})$	$g(r)_{\text{M-H}_\text{I}}(\text{min})$
Sc^{3+}	2.85	5.7	3.32	0.0
Co^{2+}	2.72	4.9	3.52	0.2
Cd^{2+}	2.90	4.4	3.64	0.3
Ion	$R_{\text{M-H}_\text{II}}(\text{max})$	$g(r)_{\text{M-H}_\text{II}}(\text{max})$	$R_{\text{M-H}_\text{II}}(\text{min})$	$g(r)_{\text{M-H}_\text{II}}(\text{min})$
Sc^{3+}	4.90	1.9	5.65	0.7
Co^{2+}	4.85	1.7	5.68	0.8
Cd^{2+}	5.03	1.5	6.00	0.8

7.5.2 Energetic properties

The hydration enthalpies obtained from the simulations agree well with the experimental[14] values, being underestimated in a 2-4%.

7.5.3 Hydrogen bonding

In the scandium aqueous solution, there is an average of two HBs on its first-shell water molecules, all their hydrogen bonds are stablished as HB

donors from the first-shell molecules to the second shell molecules (see Table 7.6). The corresponding HB energies are higher than those of the bulk ones (-6.6 kcal/mol) due to the high polarization of the first-shell water molecules and also the polarization of the second shell water molecules. This is particularly significant for the Sc^{3+} ion. A slight enhancement of the HB energy formed by the second shell and the bulk (see Table 7.7) is also observed for Sc^{3+}.

For the divalent cations, most of the HBs of first-shell water molecules act as donors, but there is a non-negligible contribution, 10-15 % of HBs where first-shell water molecules play the acceptor role. For the cobalt and cadmium, energy of HBs formed by the first and second shell is higher than that of the bulk. Contrary HB energy for bonds formed between second and bulk molecules are such those of bulk. This is due to the fact the electric field of these cations is not able to polarize enough the second shell molecules (their dipole enhancement is less than 0.1 D).

For all cations it is found an energy interaction between molecules at the second shell smaller than the corresponding to bulk because the ion-dipole orientation by the polarized first-shell water molecules is favored. Given that charge transfer in the first-shell water molecules is not included the dipole moment might be enhanced to compensate it, meaning that polarization could to be overestimated.

7.5.4 Dynamic properties

Water exchanges between first and second shell have not been observed in the scandium and cobalt. Comparison between simulated diffusion coefficient and experimental values[14] are shown in Figure 7.14. The diffusion coefficient has also been normalized by the bulk water value to show the relative difussion coefficient. When the coefficients are corrected by the water self-diffusion there is a good agreement between theoretical and ex-

Table 7.6: Hydrogen bond statistics: average number of hydrogen bonds per water molecule in 1^{st} and 2^{nd} hydration shells. don/acc means the water molecule acting as donor/acceptor of the hydrogen bond.

Ion	Sc^{2+}	Co^{2+}	Cd^{2+}
n_{HB} 1st shell	**2.0**	**2.2**	**2.1**
n_{HB} 1-1	0.0	0.0	0.0
n_{HB} 1-2	2.0	2.2	2.1
n_{HB} 1-2 don.	99%	88%	86%
n_{HB} 1-2 acc.	1%	12%	14%
n_{HB} 2nd shell	**3.5**	**3.6**	**3.6**
n_{HB} 1-2	0.9	0.9	0.9
n_{HB} 2-2	0.4	0.7	0.8
n_{HB} 2-3	2.2	2.0	2.0
n_{HB} 2-3 don.	75%	67%	66%
n_{HB} 2-3 acc.	26%	33%	34%

Table 7.7: Hydrogen bond energetics (kcal/mol). Standard deviation in parenthesis.

Ion	Sc^{3+}	Co^{2+}	Cd^{2+}
E_{HB} 1-2	-13.7(4.2)	-8.7(3.2)	-7.7(3.0)
E_{HB} 2-2	-6.1(2.8)	-6.3(2.6)	-6.4(2.5)
E_{HB} 2-3	-7.1(2.8)	-6.7(2.5)	-6.6(2.5)

perimental values, being a difference of 10-20%.

The reorientational dynamics of the first-shell water molecules has been computed and reorientational times have been collected in Table 7.8. The rotational dynamics of the first-shell water molecules is considerably longer for the scandium cation than for cobalt and cadmium, mainly in the rotation involving the dipole moment component. This reflects the strong effect that presence of a trivalent charge at short distance causes on the water dyanmics. For the divalent, the rotational behaviour also out a dynamics slower than that corresponding to bulk water. As already observed HB energy and other structural parameters, Co^{2+} hydration shell is more compact and rigid than that of Cd^{2+}.

Table 7.8: Reorientational times (ps).

Ion	$\tau_{1,\mu}$	$\tau_{2,\mu}$	$\tau_{1,HH}$	$\tau_{2,HH}$	$\tau_{1,\perp}$	$\tau_{2,\perp}$	$\tau_{1,OH}$	$\tau_{1,OH}$
Sc^{3+}	1435	114	29	24	26	14	51	18
Co^{2+}	74	25	16	10	12	4	23	8
Cd^{2+}	65	14	10	6	8	3	24	5
Water	5.0	2	6	3	4	2	6	3

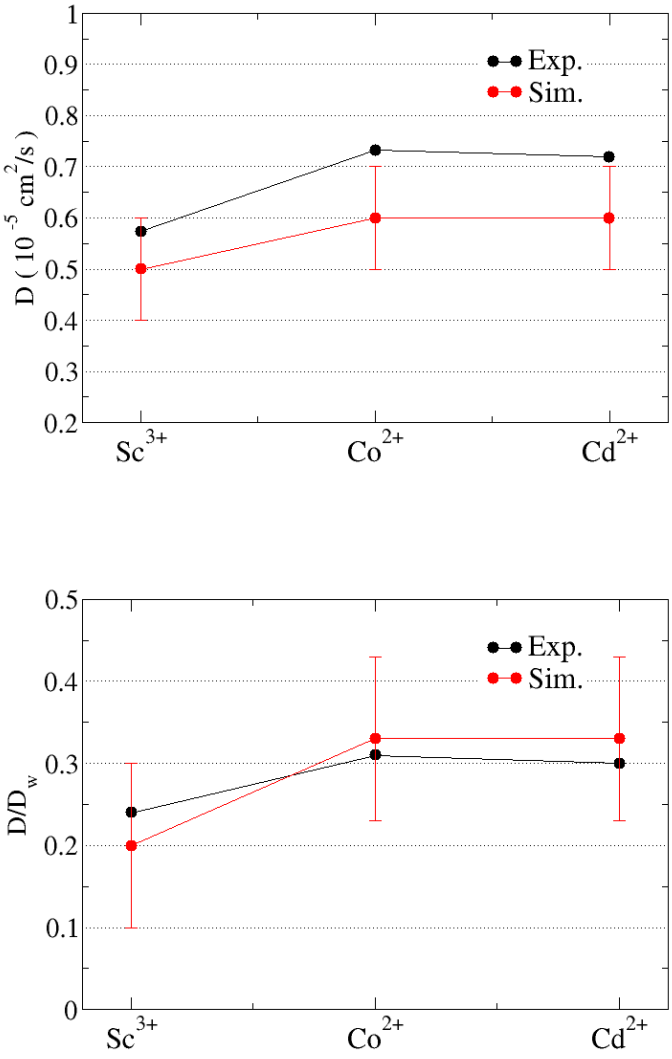

Figure 7.14: Self-diffusion coefficient (top), self-diffusion coefficient relative to the bulk water diffusion coefficient (bottom).

7.5.5 Molecular assymetry

The molecular eccentricity and its correlation functions have been computed. As can be observed in the Table 7.9. The first-shell assymetry is small and increases from scandium to cadmium, but its dynamics is similar in all cases.

Table 7.9: Eccentricity, ϵ (Å), and eccentricity reorientational time, $\tau_{1,\epsilon}$ (ps). Standard deviation in parenthesis.

Ion	ϵ (Å)	$\tau_{1,\epsilon}$ (ps)
Sc^{3+}	0.10(0.04)	0.2
Co^{2+}	0.11(0.05)	0.2
Cd^{2+}	0.14(0.06)	0.2

7.6 Lanthanoids

Lanthanum, neodymium and thulium cations in aqueous solution have been studied. These cations cover the lanthanide radii range going from the lightest lanthanoid to one of the heaviest one. As it is well known there is an orbital contraction when progressing in the series which causes a decreasing of atomic radii and then the shortening of the Ln^{3+}-ligand distances and a smooth change in the coordination number. Lanthanoids cations have many applications,[26–28] among them the investigation of the parallelism of their chemistry with that of actinoids. The Ln(III) oxidation state is the most stable for all the lanthanoid cations, being that the oxidation state studied in this work.[29]

7.7 Lanthanum

The lanthanum is the largest and lightest lanthanoid cation. Several experimental studies about its hydration structure have been performed. By

means of EXAFS spectroscopy, coordination numbers around 9 with peak distances between 2.54 and 2.58 Å[30–35] have been reported. In a Raman study[36] the bands corresponding to an ennea-coordination were observed. In QM/MM studies[37,38] the variation of the coordination between 9 and 10 in the first-shell, and around 23-25 water molecules forming a second hydration shell were obtained. Classical MD simulations[39,40] gave a coordination number of ∼9 with peak distances between 2.52 and 2.56 Å. In QMMM studies[37,38] the second hydration shell is located between 4.7 and 5.0 Å and in classical MD simulations[39,40] is around 4.7 Å. Data are collected in Table 7.10.

In this work it was obtained an aqua ion formed by 9 water molecules with peak distance at 2.58 Å. The second shell peak is centered at 4.77 Å and contains ∼ 19 water molecules. Both first and second shell water molecules are polarized by the cation, by 0.6 and 0.1 D, respectively. Main results are shown in Table 7.10. The comparison between the simulated and experimental EXAFS function[35] is shown in Figure 7.15. Experimental EXAFS spectra contains a MEE around 5 $Å^{-1}$ associated to the channel $LN_{4,5}$.[41]

Table 7.10: Properties of La^{3+} aqueous solution. Standard deviation in parenthesis.

Property	this work	Literature
$R_{\text{M-O}_\text{I}}$ (Å)	2.58	2.52,[39] 2.54,[30] 2.56[31–33,40] 2.56-2.58,[34] 2.545,[42] 2.552-2.560[35] 2.59,[42] 2.61,[38] 2.65[37]
CN_I	9.0	8.3,[42] 8.9,[40] 9.0[31–33,36,42] 9.02,[39] 9.2,[30] 9.5,[38] 9.6,[37] 12[34]
DW (Å^2)	0.012	0.0085,[35] 0.009,[30,42] 0.0086-0.0107[32]
tilt angle$_\text{I}$ (°)	147(16)	180[37]
$R_{\text{M-O}_\text{II}}$ (Å)	4.77	4.68,[40] 4.65,[39] 4.70,[38] 5.0[37]
CN_II	19.4	15.9,[40] 18.8,[39] 23,[37] 25.6[38]
tilt angle$_\text{II}$ (°)	122(32)	
$\Delta\mu_\text{I}$ (D)	0.6(0.3)	0.5[43]
$\Delta\mu_\text{II}$ (D)	0.1(0.3)	
MRT(t*=0) (ps)	345	980,[40] 1082,[39] 40[37]
MRT(t*=2) (ps)	423	
ΔH_hyd (kcal/mol)	-760(9)	-792[14]
D (10^{-5} cm^2/s)	0.6(0.1)	0.619[14]

7.8 Neodymium

A coordination number of 8.6 with a first-shell distance at 2.48 Å was obtained by means of Neutron Diffraction.[44] There are several EXAFS studies[31–35] which obtained a Nd-O_I distance range of 2.49-2.53 Å. The hydration number of the Nd^{3+} has been considered 9 in most cases,[31,32,34] although coordinations between 9 and 10.2[30,35] have been also reported and a study[33] considers a coordination 12, being the last result out of range. Data are collected in Table 7.11.

The publication where the MCDHO2 water model[45] was tested, used

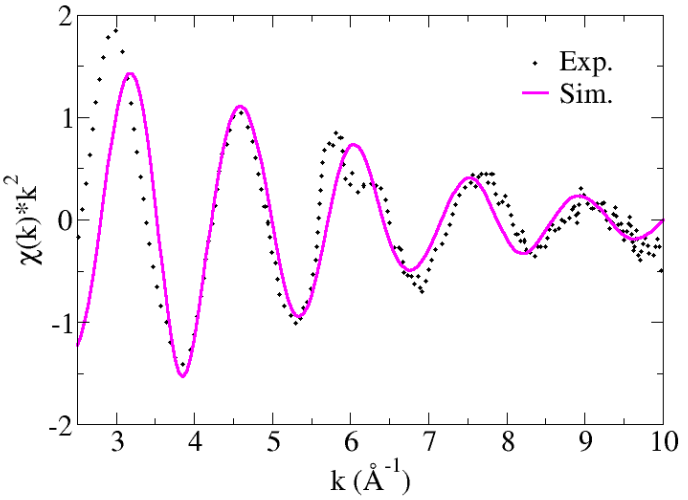

Figure 7.15: k^2-weighted La L_3-edge EXAFS.

some lanthanoid cations among them the neodymium, to check the behaviour of the proposed water model. A coordination number of 8.9 with a peak distance of 2.63 Å was obtained. In other MD studies,[39,46] a coordination number of 9.0 and peak distances between 2.43 and 2.48 Å were obtained. The same coordnation with peak distance of 2.48 Å with an average of 20.2 water moleculesin the 2ndhydration shell was obtained in a QMCF-MD study.[47] When the aqua ion geometry was analyzed it was observed that the structure evolves dynamically between a square antiprism, a bicapped prism and a tricapped prism.[47]

This work has found a first-shell coordination number of 8.7 with a first Nd-O RDF maximum located at 2.50 Å and a second shell formed by 18 water molecules with a peak distance of 4.70 Å. The first-shell coordination number varies between 8 and 9 along the simulation (see Figure 7.16). The

first-shell water molecules are strongly polarized with respect to the bulk ones, by increasing their dipole moment by 0.67 D, whereas the second shell molecules are only slightly polarized, $\Delta\mu_{II}$ is 0.06 D.

Previous to this work, the L_3 XAS spectrum of a 0.1 M solution of neodymium triflate was recorded by our group in transmission mode at the European Synchrotron ERSF (Grenoble, France). The measurements were performed at room temperature with a Si [311] monochromator. The storage ring was running at 6 GeV with an electron current of 200 mA. Four scans were recorded and the signal averaged. As can be seen in Figure 7.18, there is a good agreement between the experimental and simulated EXAFS spectra in the frequency. The observed difference in intensity can be assigned to a more disordered aqua ion in the simulation. The obtained Debye-Waller factor, 0.012 $Å^2$, is in the upper limit of the range of published Debye-Waller values for this cation 0.0069-0.01 $Å^2$.[30–35] Although a MEE is present in the experimental spectra associated to the channel $LN_{4,5}$,[41]it does not affect much the comparison with the simulated spectra.

The results obtained in this work differ from those obtained with the same water model in the work presented by Villa et al.[45] In this work a shorter intermolecular distance, 2.50 Å vs 2.63 Å, and a slightly minor coordination number, 8.65 vs 9.0, have been found. This difference can be related to the water model limitation explained at section 2.4, and a good example of the good reproduction of the interaction energy on the basis of longer distances or the compromise of reasonable reproduction of structural and energy properties simultaneously.

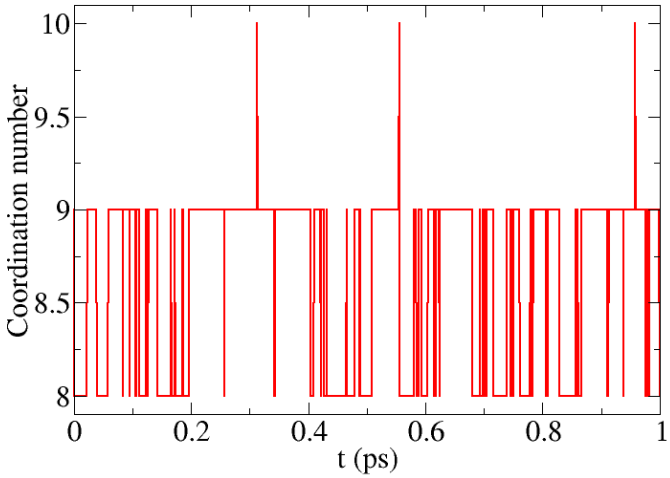

Figure 7.16: Time evolution of Nd^{3+} coordination number in aqueous solution.

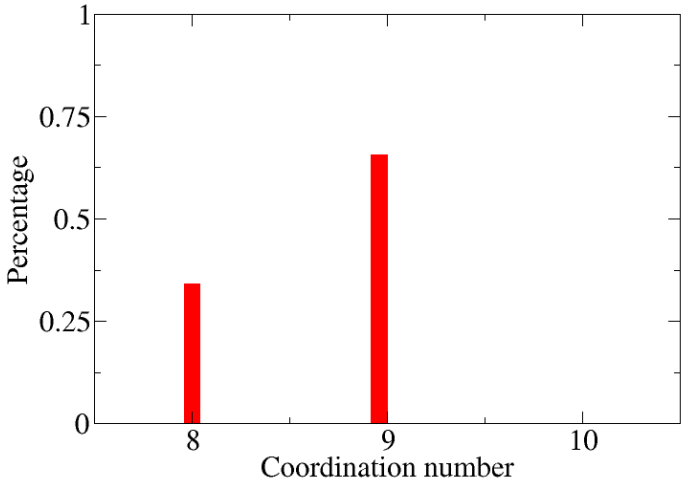

Figure 7.17: Coordination number histogram of Nd^{3+} in aqueous solution.

Table 7.11: Properties of Nd^{3+} aqueous solution. Standard deviation in parenthesis.

Property	this work	Literature
$R_{\text{M-O}_\text{I}}$ (Å)	2.50	2.43[46] , 2.48[39] , 2.48-2.49[34] 2.488-2.490[35] , 2.48[44] , 2.49[30] 2.524-2.527[31–33] , 2.56[47] , 2.63[45]
CN_I	8.7	8.6[44] , 8.9[45] , 8.96[47] 9.0[31–33,39,46] , 9.5[30] 9.9-10.2[35] , 12[34]
DW	0.012	0.0069-0.010[31–33] , 0.0067-0.0082[34] 0.0083-0.0086[35] , 0.009[30]
tilt angle$_\text{I}$ (°)	150(16)	148[45]
$R_{\text{M-O}_\text{II}}$ (Å)	4.70	4.63[39]
CN_II	18.3	19.3[39] , 20.2[47]
tilt angle$_\text{II}$ (°)	122(31)	
$\Delta\mu_\text{I}$ (D)	0.7(0.3)	
$\Delta\mu_\text{II}$ (D)	0.1(0.3)	
MRT(t*=0) (ps)	232	1818-1205,[45] 1482[39]
MRT(t*=2) (ps)	288	
ΔH_hyd (kcal/mol)	-798(16)	-824,[14] -877,[46] -842[45]
D (10^{-5} cm^2/s)	0.6(0.1)	0.616[14]

7.9 Thulium

Coordination numbers between 7.9 and 8.8 and interatomic distances between 2.33 Å and 2.35Å have been obtained by means of EXAFS[31–33,35] spectroscopy. A coordination number of 8.1 with an interatomic distance of 2.33 Å was obtained in classical MD study.[39] From a QMCF-MD study[48] a coordination number of 8.3 with an interatomic distance of 2.44 Å and a second shell coordination number of 20 were obtained. Data are collected in Table 7.12.

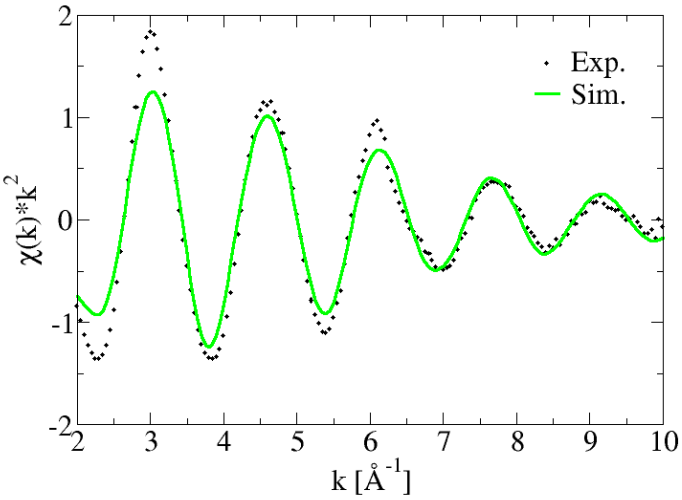

Figure 7.18: k^2-weighted Nd^{3+} L_3-edge EXAFS.

In this work a first-shell coordination number of 7.7 with peak distance at 2.33 Å and a second shell coordination number of 16.8 with peak distance at 4.55 Å were obtained. The first-shell coordination number changes between 7 and 8 along the simulation, being 8 the most repeated coordination (see Figures 7.19 and 7.20). First and second shell water molecules increase their polarization with 0.95 D and 0.12 D, respectively. Main results are shown in Tables 7.12.

Previous to this work, the L3 XAS spectrum of a 0.1 M solution of thulium triflate was recorded by our group in transmission mode at the European Synchrotron ERSF (Grenoble, France). The measurements were performed at room temperature with a Si [311] monochromator. The storage ring was running at 6 GeV with an electron current of 200 mA. Four

scans were recorded and the signal averaged. The comparison of the simulated and experimental EXAFS spectra is shown in Figure 7.21. There is a good agreement in the frequency and there is a lack of intensity on the simulated spectra that may be in part due to high disorder in the first-shell in the simulation than in the experimental solution, and/or a lower coordination number number in the MD simulation than the experimental sample.

Table 7.12: Properties of Tm^{3+} aqueous solution. Standard deviation in parenthesis.

Property	this work	Literature
$R_{\text{M-O}_\text{I}}$ (Å)	2.33	2.33-2.34,[35] 2.33,[39] 2.35,[31–33] 2.44[48]
CN_I	7.7	7.9,[35] 8.06[39] , 8.3,[48] 8.80[31–33]
DW (Å^2)	0.012	0.0059-0.0062,[35] 0.0059[31–33]
tilt angle$_\text{I}$ (°)	150(15)	
$R_{\text{M-O}_\text{II}}$ (Å)	4.55	4.50[39]
CN_II	16.8	18.3,[39] 20.1[48]
tilt angle$_\text{II}$ (°)	121(30)	
$\Delta\mu_\text{I}$ (D)	1.0(0.4)	
$\Delta\mu_\text{II}$ (D)	0.1(0.4)	
MRT(t*=0) (ps)	248	$1{\cdot}10^5$,[49] 527[39]
MRT(t*=2) (ps)	339	
ΔH_hyd (kcal/mol)	-856(11)	-883[14]
D (10^{-5} cm^2/s)	0.6(0.1)	0.581[14]

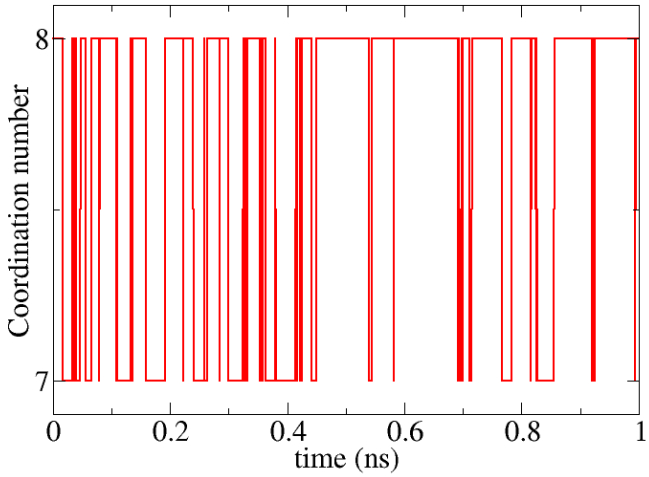

Figure 7.19: Coordination number evolution of Tm^{3+} aqueous solution.

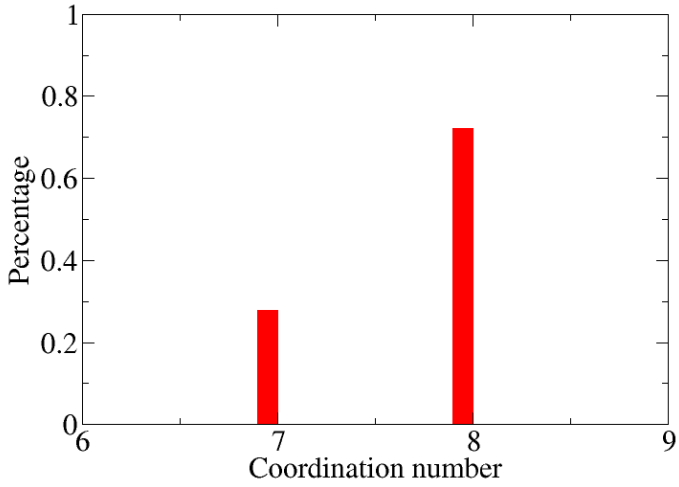

Figure 7.20: Coordination number histogram of Tm^{3+} aqueous solution.

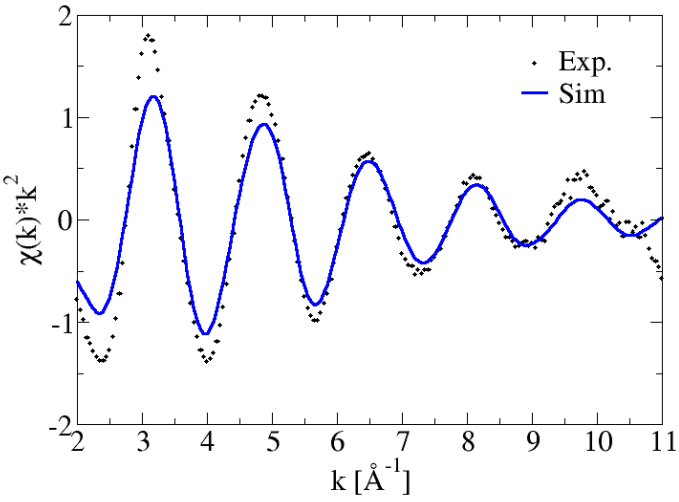

Figure 7.21: k^2-weighted Tm^{3+} L_3-edge EXAFS.

7.10 Global properties in solution

7.10.1 Radial distribution function

Ln-O and Ln-H RDFs for the lanthanoids cations studied have been plotted in Figure 7.22 and 7.14. As the ionic radius decreases along the lanthanide series, we obtain shorter intermolecular distances when we progress in the series (see Figure 7.22). The intensity of the first peak in the Ln^{3+}-O RDF doesn't follow an intuitive trend. It's expected that as the ionic radius decreases shorter Ln^{3+}-O distances must be found, as well as less disorder in the first hydration shell. This reasoning line is broken by thulium which has a less intense first peak than neodymium.

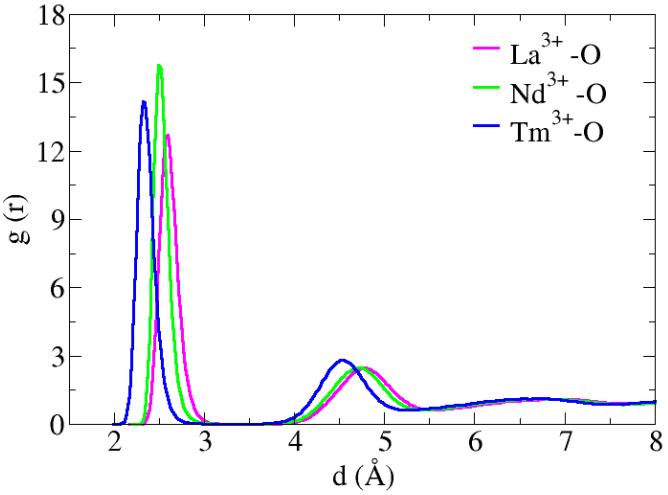

Figure 7.22: Metal-oxygen radial distribution function.

Table 7.13: Metal-oxygen radial distribution function data. Distances in Å.

Ion	$R_{\text{M-O}_\text{I}}$(max)	$g(r)_{\text{M-O}_\text{I}}$(max)	$R_{\text{M-O}_\text{I}}$(min)	$g(r)_{\text{M-O}_\text{I}}$(min)
La^{3+}	2.58	12.7	3.45	0.0
Nd^{3+}	2.50	15.9	3.40	0.1
Tm^{3+}	2.33	14.3	3.30	0.0
Ion	$R_{\text{M-O}_\text{II}}$(max)	$g(r)_{\text{M-O}_\text{II}}$(max)	$R_{\text{M-O}_\text{II}}$(min)	$g(r)_{\text{M-O}_\text{II}}$(min)
La^{3+}	4.76	2.5	5.53	0.6
Nd^{3+}	4.74	2.5	5.42	0.6
Tm^{3+}	4.54	2.3	5.27	0.6

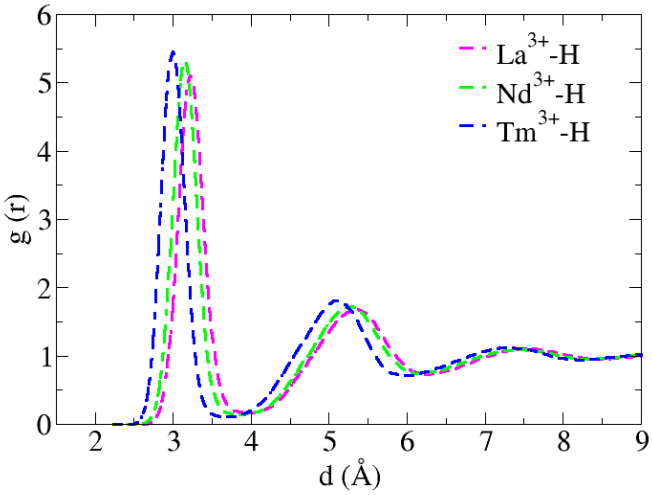

Figure 7.23: Metal-hydrogen radial distribution function.

Table 7.14: Metal-hydrogen radial distribution function data. Distances in Å.

Ion	$R_{\text{M-H}_\text{I}}(\text{max})$	$g(r)_{\text{M-H}_\text{I}}(\text{max})$	$R_{\text{M-H}_\text{I}}(\text{min})$	$g(r)_{\text{M-H}_\text{I}}(\text{min})$
La^{3+}	3.22	5.1	3.97	0.2
Nd^{3+}	3.15	5.3	3.84	0.2
Tm^{3+}	2.99	5.5	3.69	0.1
Ion	$R_{\text{M-H}_\text{II}}(\text{max})$	$g(r)_{\text{M-H}_\text{II}}(\text{max})$	$R_{\text{M-H}_\text{II}}(\text{min})$	$g(r)_{\text{M-H}_\text{II}}(\text{min})$
La^{3+}	5.36	1.7	6.25	0.7
Nd^{3+}	5.27	1.7	6.17	0.7
Tm^{3+}	5.10	1.8	5.95	0.7

7.10.2 Energetic properties

The simulated hydration enthalpy follows the experimental trend, being underestimated in less than 5 %. The hydration enthalpy grows along the lanthanide series as the intermolecular distance shrinks, being visible in the interaction energies of the hydrated clusters. For the studied cations, the interaction energies of the enneahydrates are -493.2 kcal/mol, -529.0 kcal/mol and -583.2 kcal/mol for lanthanum, neodymium and thulium, respectively, whereas the intermolecular distances are 2.62 Å, 2.55 Å and 2.43 Å.

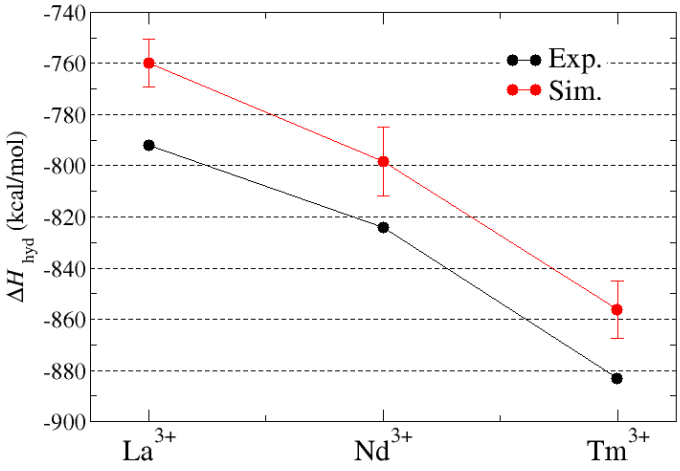

Figure 7.24: Hydration enthalpy.

7.10.3 Hydrogen bonding

The HB network of the first two hydration shells for the three cations have similar description. As in the case of other highly charged cations, the first-

shell water molecules are donating 2 HBs to second shell water molecules. Second shell water molecules accept one hydrogen bond from first-shell water molecules and are donating almost 2 to the third shell water molecules (see Table 7.15).

The high orientational order imposed by the central trivalent cation is reflected in the absence of HBs among first-shell water molecules. Ion-water interactions are much stronger than the water-water ones due to the polarization of the first-shell water molecules and the high cation charge. In the analysis of the second shell water molecules, it is observed a non-negligible number of HBs formed by molecules of the same shell (0.6-0.8). HBs between second and bulk molecules evidence the smooth transition to bulk value. Data are collected in Table 7.16.

Table 7.15: Hydrogen bond statistics: average number of hydrogen bonds per water molecule in 1^{st} and 2^{nd} hydration shells. don/acc means the water molecule acting as donor/acceptor of the hydrogen bond.

Ion	La^{3+}	Nd^{3+}	Tm^{3+}
n_{HB} 1^{st} shell	**2.0**	**2.0**	**2.0**
n_{HB} 1-1	0.0	0.0	0.0
n_{HB} 1-2	2.0	2.0	2.0
n_{HB} 1-2 acc.	94%	95%	97%
n_{HB} 1-2 don.	6%	5%	3%
n_{HB} 2^{nd} shell	**3.6**	**3.6**	**3.6**
n_{HB} 1-2	0.9	0.9	0.9
n_{HB} 2-2	0.8	0.7	0.6
n_{HB} 2-3	1.9	2.0	2.0
n_{HB} 2-3 acc.	70%	71%	72%
n_{HB} 2-3 don.	30%	29%	28%

Table 7.16: Hydrogen bond energetics (kcal/mol). Standard deviation in parenthesis.

Ion	La^{3+}	Nd^{3+}	Tm^{3+}
E_{HB} 1-2	-8.2(3.1)	-8.5(3.2)	-9.9(3.6)
E_{HB} 2-2	-6.1(2.6)	-6.1(2.6)	-6.1(2.7)
E_{HB} 2-3	-6.6(2.5)	-6.7(2.6)	-6.8(6.8)

7.10.4 Dynamic properties

The computed ion diffusion values are similar to the experimental ones. This difference increases when are compared the relative to the water difussion coefficcients, being the difference $\sim 20\%$ (see Figures 7.25).

The reorientational dynamics of the first-shell water molecules for these aqua ions is slower than the dynamics of bulk water, being slower for thulium, and faster for the less polarizing lanthanoid, lanthanum. This is reflected in the stronger HB energy between first and second water molecules for the Tm^{3+} aqua ion compared to for the La^{3+} one. In a QM/MM study[37] about the La^{3+} hydration, the reorientational dynamics of the first hydration shell molecules was calculated, finding a relative faster dynamics than what is found in this work (see Table 7.18). The correlational times of the different components are shown in the Table 7.17.

Table 7.17: Reorientational time (ps).

Ion	$\tau_{1,\mu}$	$\tau_{2,\mu}$	$\tau_{1,HH}$	$\tau_{2,HH}$	$\tau_{1,\perp}$	$\tau_{2,\perp}$	$\tau_{1,OH}$	$\tau_{1,OH}$
La^{3+}	108	27	11	10	9	4	34	6
Nd^{3+}	122	28	10	8	9	3	38	6
Tm^{3+}	173	34	74	15	17	6	62	10
Water	5	2	6	3	4	2	6	3

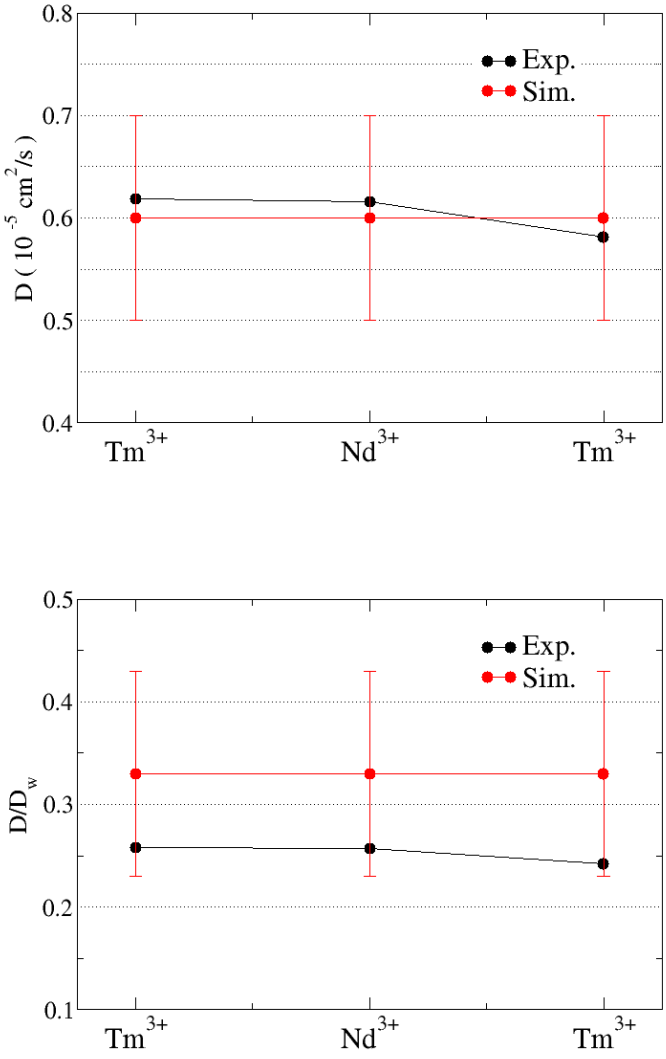

Figure 7.25: Self-diffusion coefficient (top), self-diffusion coefficient relative to the bulk water diffusion coefficient (bottom).

Table 7.18: Published reorientational times (ps).

Ion	$\tau_{1,\mu}$	$\tau_{2,\mu}$	$\tau_{1,HH}$	$\tau_{2,HH}$	$\tau_{1,\perp}$	$\tau_{2,\perp}$
La^{3+}	55.4[37]	21.0[37]	12.6[37]	7.8[37]	11.9[37]	6.8[37]
Water	12.6,[37] 7.5[49]	7.8[37] , 2.5[49]	55.4[37]	21.0[37]	5.4[37]	2.9[37]

7.10.5 Molecular assymetry.

The first-shell assymetry, given by the excentricity value, is shown in Table 7.19. As expected for highly-charged aqua ions, the mean distance between the metal cation and the mas center of the first-shell water molecules is small, 0.12-0.13 Å, reflecting a small decoupling due to thermal motion and water release between the first and the second shell. No differences between the cations can be inferred from the results.

Table 7.19: Eccentricity, ϵ (Å), and eccentricity reorientational time, $\tau_{1,\epsilon}$ (ps). Standard deviation in parenthesis.

Ion	ϵ (Å)	$\tau_{1,\epsilon}$ (ps)
La^{2+}	0.13(0.06)	0.3
Nd^{2+}	0.12(0.06)	0.3
Tm^{2+}	0.12(0.06)	0.3

7.10.6 Second shell effects on XANES spectrum.

For the three lanthanides XANES spectra above the white line present is a hump assigned to a second shell contribution, observed in previous studies of other ions as Ir^{3+},[50] Ni^{2+},[51] La^{3+}[52] or Lu^{3+}.[52] This feature is found on the experimental lanthanide XANES spectra and it appears in the simulated spectrum in the computations performed in this work. However a

drawback comes out when the signal broadening is tuned, creating an artifact in the hump region. For this reason the optical broadening in the XANES simulation has not been modified.

In Figures 7.26, 7.27 and 7.28 are shown the comparison between the simulated XANES including first hydration shell in the calculations and including first and second shell, and the comparison between the experimental XANES spectra and the simulated spectra incluyding first and second shell in the calculation.

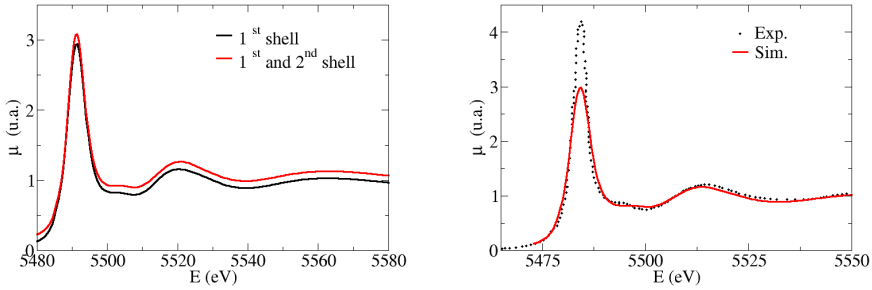

Figure 7.26: La^{3+} L_3-edge XANES.

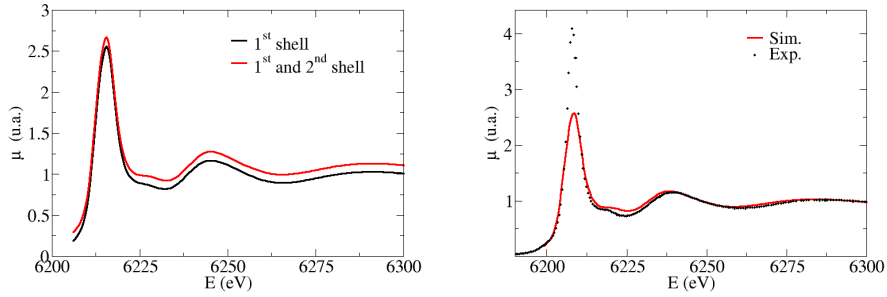

Figure 7.27: Nd^{3+} L_3-edge XANES.

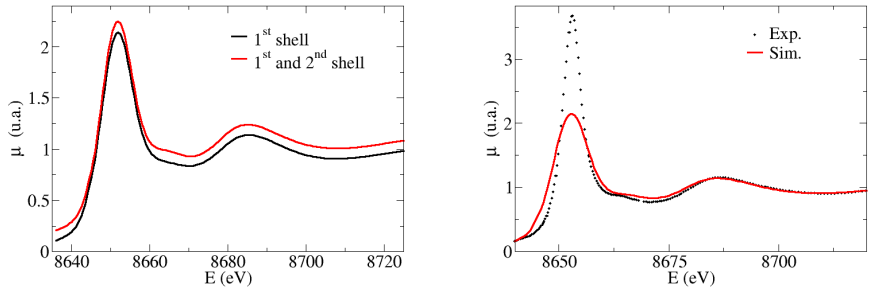

Figure 7.28: Tm^{3+} L_3-edge XANES.

7.11 An actinide case: Th^{4+}

The tetravalent thorium cation has been studied in aqueous solution. All thorium isotopes are radioactive and are used as fuel in nuclear power plants. They have long life-time, this being the reason to be the most abundant actinoid in earth.

Several studies have dealt with Th^{4+} hydration. A coordination number of 8.1 was obtained by RMN.[53] By means of XRD[54] an aqua ion with a coordination number of 10 at 2.46 Å was obtained. A coordination number of 8 with peak distance at 2.48 Å was obtained by a LAXS study.[55] In a more recent and combined LAXS and EXAFS study by Torapava[56] et al., a hydration number of 9 with peak distance at 2.46 Å and a second shell formed by 18 water molecules at 4.66 Å and a coordination of 9 with peak distance at 2.45 Å was obtained by means of LAXS and EXAFS, respectively. Another EXAFS study[57] obtained a much larger coordination number, ∼12, with a peak distance of 2.45 Å.

In a classical MD study,[58] a first-shell coordination number of 8.5 with peak distance at 2.45 Å and ∼18 water molecules at 4.75 Å forming the second shell were obtained. In another MD study[59] where a polarizable water model is used, a first-shell coordination number of 9 at 2.4 Å was obtained. A third MD study[60] defines the hydrated ion with 9 water molecules, the second shell is formed by 19 water molecules a distance of 4.75 Å. Spezia et al. performed a set of CPMD simulations[61] obtaining a first-shell coordination number around 9 with peak distance at 2.45-2.48 Å in the first-shell and 16-21 water molecules at 4.5-4.6 Å forming the second hydration-shell. Data are collected in Table 7.20.

This work finds an aqua ion with a first-shell formed by 9 water molecules at an average distance of 2.47 Å, and a second shell at 4.65 Å formed by ∼ 19 water molecules. First-shell water molecules are strongly polarized, 4.3 D, due to the tetravalent charge of the cation and to the no inclusion of charge transfer in our model. First-shell water molecules are in ion-dipole orientation, forming an average tilt angle of 157° as obtained for other

highly charged aqua ions.[62] Second shell water molecules are also polarized forming on average one hydrogen bond with first-shell water molecules and two hydrogen bonds with third-shell water molecules. During the simulation no water exchange between first and second shells was observed. Main properties are collected in Tables 7.20.

As can be seen in the Figure 7.29, the simulated EXAFS function agrees quite well with the experimental spectrum obtained by Rother et al[57] on intensity, frequency and signal decayment. This indicates an excellent structural description of the developed model. The data analysis of the experimental EXAFS spectrum carried out by the authors[57] led them to a really high coordination number, ~ 13 with a Debye-Waller factor for the Th-O_I paths of 0.0072 Å^2. The high similarity between the simulated spectrum of this work and the experimental spectrum lead us to conclude that the structural parameters reported by the analysis of the experimental spectrum (CN_I and DW_{Th-O_I}) are unrealistic, because a higher coordination number together with a lower DW factor should produce a more intense signal. In addition, a longer Th-O distance than that found in this work seems to be unrealistic as well. The really good agreement reached for the Th^{4+} aqueous solution XANES (see Figure 7.30), that must be pointed out, was obtained obtained with the same set of snapshots employed in the EXAFS calculation, reinforces the consistency of structural results obtained from MD simulations.

Table 7.20: Properties of Th^{4+} aqueous solution. Standard deviation in parenthesis.

Property	this work	Literature
$R_{\text{M-O}_\text{I}}$ (Å)	2.47	2.4,[59] 2.45,[61] 2.46[54] 2.465,[63] 2.48,[55] 2.451-2.462[56] 2.54,[64] 2.54-2.55,[60] 2.45-2.49[61]
CN_I	9.0	8.0[55] , 8.1[53] , 8.25[58] 9.0[56,59,60,64] , 8-9[61] , 9.2[63] 10[54] , 12.4-12.7[57]
DW (Å^2)	0.0090	0.0067[56] , 0.0072[57]
tilt angle$_\text{I}$ (°)	157(13)	160[59]
$R_{\text{M-O}_\text{II}}$ (Å)	4.65	4.59[59] , 4.5-4.6[64] , 4.5-4.6[61] 4.75[58,60]
CN_II	18.6	18[59] , 16-21[61] , 17.5[58] 18.9[60] , 19.8[64]
tilt angle$_\text{II}$ (°)	129(26)	155[59]
$\Delta\mu_\text{I}$ (D)	1.3(0.4)	
$\Delta\mu_\text{II}$ (D)	0.2(0.3)	
MRT(t*=0) (ps)	inf	
MRT(t*=2) (ps)	inf	
ΔH_hyd (kcal/mol)	-1414(10)	-1448[14]
D (10^{-5} cm^2/s)	0.5(0.1)	1.53,[65] 1.7[63]

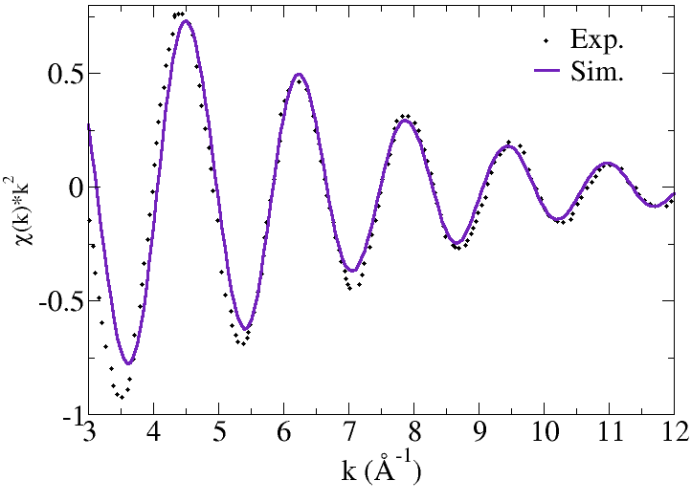

Figure 7.29: k^2-weighted Th L_3-edge EXAFS.

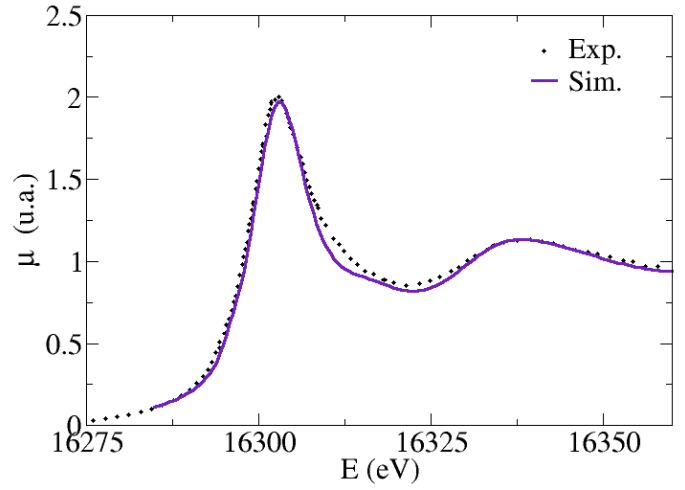

Figure 7.30: Th L_3-edge XANES.

Th-O RDF shows a well defined first and second hydration shells (see Figure 7.31). RDF Data are collected in Table 7.21. The first-shell water molecules are forming on average 2 hydrogen bonds with the second shell water molecules. As expected for a highly charged and polarizing cation, all the first-shell water molecules are highly polarized, oriented following an ion-dipole patternonly define HBs whith the second shell waters.

The second shell water molecules are mainly accepting one hydrogen bond from the first-shell water molecules and acting as donors in two HBs with the third shell water molecules. There is a small amount of hydrogen bonds among second shell water molecules which are energetically less favorable than those of the pure water. As there is not charge transfer included in the model the molecule polarization increases to compensate it, causing the overestimation of the E_{HB} terms.

The first-shell dynamics is considerably lower than that of bulk, the dipole moment component being the most affected one (see Table 7.24).

Table 7.21: Thorium-oxygen and thorium-hydrogen distribution function data. Distances in Å.

$R_{\mathrm{M\text{-}O_I}}(\mathrm{max})$	$g(r)_{\mathrm{M\text{-}O_I}}(\mathrm{max})$	$R_{\mathrm{M\text{-}O_I}}(\mathrm{min})$	$g(r)_{\mathrm{M\text{-}O_I}}(\mathrm{min})$
2.47	15.8	3.40	0.0
$R_{\mathrm{M\text{-}O_{II}}}(\mathrm{max})$	$g(r)_{\mathrm{M\text{-}O_{II}}}(\mathrm{max})$	$R_{\mathrm{M\text{-}O_{II}}}(\mathrm{min})$	$g(r)_{\mathrm{M\text{-}O_{II}}}(\mathrm{min})$
4.64	3.4	5.30	0.48
$R_{\mathrm{M\text{-}H_I}}(\mathrm{max})$	$g(r)_{\mathrm{M\text{-}H_I}}(\mathrm{max})$	$R_{\mathrm{M\text{-}H_I}}(\mathrm{min})$	$g(r)_{\mathrm{M\text{-}H_I}}(\mathrm{min})$
3.15	6.3	3.74	0.033
$R_{\mathrm{M\text{-}H_{II}}}(\mathrm{max})$	$g(r)_{\mathrm{M\text{-}H_{II}}}(\mathrm{max})$	$R_{\mathrm{M\text{-}H_{II}}}(\mathrm{min})$	$g(r)_{\mathrm{M\text{-}H_{II}}}(\mathrm{min})$
5.20	2.0	6.05	0.063

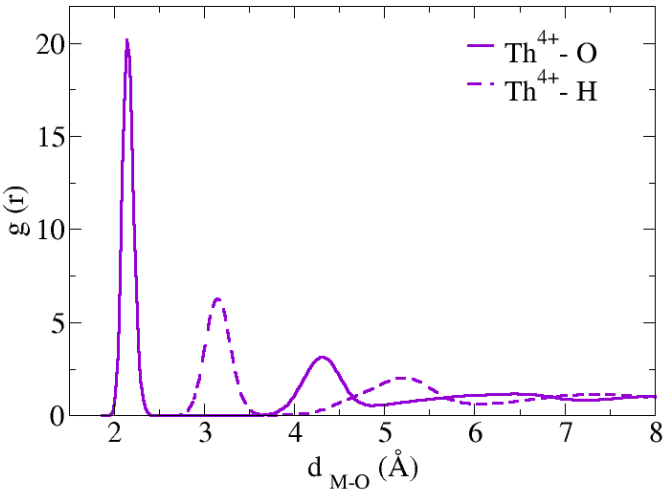

Figure 7.31: Thorium-oxygen and thorium-hydrogen radial distribution function.

Table 7.22: Hydrogen bond energetics (kcal/mol). Standard deviation in parenthesis.

Ion	Th^{4+}
E_{HB} 1-2	-10.8(4)
E_{HB} 2-2	-5.7(3)
E_{HB} 2-3	-7.0(3)

Table 7.23: Hydrogen bond statistics: average number of hydrogen bonds per water molecule in 1^{st} and 2^{nd} hydration shells. don/acc means the water molecule acting as donor/acceptor of the hydrogen bond.

Ion	Th^{4+}
n_{HB} 1^{st} shell	**2.0**
n_{HB} 1-1	0
n_{HB} 1-2	2.0
n_{HB} 1-2 don.	99%
n_{HB} 1-2 acc.	1%
n_{HB} 2^{nd} shell	**3.5**
n_{HB} 1-2	1.0
n_{HB} 2-2	0.5
n_{HB} 2-3	2.0
n_{HB} 2-3 don.	77%
n_{HB} 2-3 acc.	23%

Table 7.24: Reorientational time. (ps)

Ion	$\tau_{1,\mu}$	$\tau_{2,\mu}$	$\tau_{1,HH}$	$\tau_{2,HH}$	$\tau_{1,\perp}$	$\tau_{2,\perp}$	$\tau_{1,OH}$	$\tau_{2,OH}$
Th^{4+}	1084	78	30	21	26	13	61	17
Water	5	2	6	3	4	2	6	3

7.12 Bibliography

[1] Crawley, M.; Trost, B. *Applications of transition metal catalysis in drug discovery and development. An industrial perspective.*; Wiley, 2012.

[2] Royset, J.; Ryum, N. *International materials reviews* **2005**, *50*, 19–44.

[3] Yu, W.; He, J.; Lin, W.; Li, Y.; Men, W.; Wang, F.; Huang, J. *J.*

Environ. Radioact. **2015**, *142*, 54–61.

[4] Kanno, H.; Yamaguchi, T.; Ohtaki, H. *J. Phys. Chem.* **1989**,

[5] Yamaguchi, T.; Niihara, M.; Takamuku, T.; Wakita, H.; Kanno, H. *Chem. Phys. Lett.* **1997**, *274*, 485–490.

[6] Smirnov, P.; Wakita, H.; Yamaguchi, T. *J. Phys. Chem. B* **1998**, *102*, 4802–4808.

[7] Rudolph, W. W.; Pye, C. C. *J. Phys. Chem.* **2000**, *104*, 1627–1639.

[8] Sandström, M.; Persson, I.; Jalilehvand, F.; Lindqvist-Reis, P.; Spanberg, D.; Hermansson, K. *J. Synch* **2001**, *8*, 657–659.

[9] Abbasi, A.; Lindqvist-Reis, P.; Eriksson, L.; Sandström, D.; Lidin, S.; Persson, I.; Sandström, M. *Chem. Eur. J* **2005**, *11*, 4065–4077.

[10] Lindqvist-Reis, P.; Persson, I.; Sandström, M. *Dalton Trans.* **2006**, *28*, 3868–3878.

[11] Migliorati, V.; D'Angel, P. *Inorg. Chem.* **2016**, *55*, 6703–6711.

[12] Caralampio, D.; Martinez, J.; Pappalardo, R.; Marcos, E. S. *Theor. Chem. Acc.* **2017**, *136*, 47.

[13] Vchirawongkwin, V.; Kritayakornupong, C.; Tongraar, A.; Rode, B. *Dalton Trans.* **2012**, *41*, 11889–11897.

[14] Marcus, Y. *Ion properties*; Markel Dekker, Inc, 1997.

[15] D'Angelo, P.; Benfatto, M.; Longa, S. D.; Pavel, N. *Phys. Rev. B* **2002**, *66*, 064209.

[16] Spezia, R.; Duvail, M.; Vitorge, P.; Cartailler,; Tortajada, J.; Chillemi, G.; D'Angelo, P.; Gaigeot., M. *J. Phys. Chem. A* **2006**, *110*, 13081–13088.

[17] Inada, Y.; Hayashi, H.; Sugimoto, K.; Funahashi, S. *J. Phys. Chem. A* **1999**, *103*, 1401–1406.

[18] Caminiti, R.; Johansson, G. *Acta Chem. Scand.* **1981**, *35A*, 373–381.

[19] Ohtaki, H.; Maeda, M.; Iro, S. *Bull. Chem. Jpn.* **1974**, *47*, 2217–2221.

[20] Bol, W.; Gerrits, G.; Panthaleon, C. *J. Appl. Cryst.* **1970**, *3*, 486–492.

[21] Pye, C.; M.-Tomney,; Rudolph, W. *Can. J. Anal. Sci. Spectrosc.* **2006**, *51*, 140–146.

[22] D'Angelo, P.; Chillemi, G.; Barone, V.; Mancini, G.; Sanna, N.; Persson, I. *J. Phys. Chem. B* **2005**, *109*, 9178–9185.

[23] Chillemi, G.; Barone, V.; D'Angelo, P.; Mancini, G.; Persson, I.; Sanna, N. *J. Phys.Chem. B* **2005**, *109*, 9186–9193.

[24] D'Angelo, P.; Migliorati, V.; Mancini, G.; Chillemi, G. *J. Phys. Chem. A* **2008**, *112*, 11833–11841.

[25] Atomistic Simulation Group, I. C. L. 1999; `http://abulafia.mt.ic.ac.uk/shannon/ptable.php`.

[26] Ganjali, M.; Gupta, V.; Faridbod, F.; Norouzi, P. *Lanthanides series determination by various analytical methods.*; Elsevier, 2016.

[27] Teo, R.; Termini, J.; Gray, H. *J. Med. Chem.* **2016**, *59*, 6012–6024.

[28] Maestro, P.; Huguenin, D. *J. Alloys and Compounds* **1995**, *225*, 520–528.

[29] Richens, D. T. *The Chemistry of Aqua Ions*; John Wiley: Chichester, 1997.

[30] Allen, P.; Bucher, J.; Shuh, D.; anf I. Craig, N. E. *Inorg. Chem.* **2000**, *39*, 595–601.

[31] D'Angelo, P.; Panfilis, S.; Filipponi, A.; Persson, I. *Chem. Eur. J.* **2008**, *14*, 3045–3055.

[32] Persson, I.; anf S. Panfilis, P. D.; Sanström, M.; Eriksson, L. *Chem. Eur. J* **2008**, *14*, 3056–3066.

[33] D'Angelo, P.; Zitolo, A.; Migliorati, V.; Persson, I. *Chem. Eur. J* **2010**, *16*, 684–692.

[34] Solera, J.; García, J.; Proietti, M. *Phys. Rev. B* **1995**, *51*, 2678–2686.

[35] Ohta, A.; Kagi, H.; Tsuno, H.; Nomura, M.; Kawabe, I. *Am. Mineral.* **2008**, *93*, 1384–1392.

[36] Rudolph, W.; Irmer, G. *Dalton Trans.* **2014**, *44*, 295–305.

[37] Hofer, T.; Scharnagl, H.; Randolf, B.; Rode, B. *Chem. Phys.* **2006**, *327*, 31–42.

[38] Luts, O.; Hofer, T.; Randolf, B.; Rode, B. *Chem. Phys. Lett.* **2012**, *536*, 50–54.

[39] Duvail, M.; Vitorge, P.; Spezia, R. *J. Chem. Phys.* **2009**, *130*, 104501.

[40] Clavaguera, C.; Pollet, R.; Soudan, J.; Brenner, V.; Dognon, J. *J. Phys. Chem. B* **2005**, *109*, 7614–7616.

[41] Kodre, A.; Arcon, I.; Hribar, M.; Stuhec, M.; Villain, F.; Parent, P. *J. Phys. IV* **1994**, *4 (C9)*, C9–397–C9–400.

[42] Ishiguro, S.; Umebayashi, Y.; Komiya, M. *Coordination Chemistry Reviews* **2002**, *226*, 103–111.

[43] Petit, L.; Vuilleumier, R.; anf C. Adamo, P. M. *J. Phys. Chem. B* **2008**, *112*, 10603.

[44] Narten, A.; Hahn, L. *J. Phys. Chem.* **1983**, *87*, 3193–3197.

[45] Villa, A.; Hess, B.; Saint-Martin, H. *J. Phys. Chem. B* **2009**, *113*, 7270–7281.

[46] Kowall, T.; Foglia, F.; Helm, L.; Merbach, A. *J. Am. Chem. Soc.* **1995**, *117*, 3790–3799.

[47] Passler, P.; Rode, B. *Chem. Phys. Lett.* **2015**, *642*, 12–16.

[48] Passler, P.; Rode, B. *Chem. Phys. Lett.* **2015**, *638*, 128–132.

[49] Ohtaki, H.; Radnai, T. *Chem. rev.* **1993**, *83*, 1157–1204.

[50] Carrera, F.; Torrico, F.; Richens, T.; Muñoz-Paes, A.; Martinez, J.; Pappalardo, R.; Marcos, E. S. *J. Phys. Chem. B* **2007**, *111*, 8223–8233.

[51] D'Angelo, P.; Roscioni, O. M.; Chillemi, G.; Longa, S. D.; Benfatto, M. *J. Am. Chem. Soc.* **2006**, *128*, 1853–1858.

[52] Morales, N. Estudio teórico de propiedades fisicoquímicas de cationes metálicos en disolución: Evolución en el grupo de los alcalinos y en la serie de los lantánidos. bilio, Universidad de Sevilla, 2015.

[53] Fratiello, A.; Lee, R.; Schuster, R. *Inorg. Chem.* **1970**, *9*, 391–392.

[54] Wilson, R.; Skanthakumar, S.; Burns, P.; Soderholm, L. *Angew. Chem. Int. Ed* **2007**, 8043–8045.

[55] Johansson, G.; Magini, M.; Ohtaki, H. *J. Sol. Chem.* **1991**, *20*, 775–792.

[56] Torapava, N.; Persson, I.; Eriksson, L.; Lundberg, D. *Inorg. Chem.* **2009**, *48*, 11712–11723.

[57] Rothe, J.; Denecke, M.; Neck, V.; Muller, R.; Kim, J. *Inorg. Chem.* **2002**, *41*, 249–258.

[58] Réal, F.; Trumm, M.; Vallet, V.; Schimmelpfenning, B.; Masella, M.; Flament., J. *J. Phys. Chem. B* **2010**, *114*, 15913–15924.

[59] Marjolin, A.; Gourlaouen, C.; Clavaguéra, C.; Ren, P.; Wu, J.; Gresh, N.; Dognon, J.; Piquemal, J. *Theor. Che, Acc.* **2012**, *131*, 1198.

[60] Yang, T.; Tsushima, S.; Suzuki, A. *J. Phys. Chem. A* **2001**, *105*, 10439–10445.

[61] Spezia, R.; Beuchat, C.; Vuileumier, R.; D'Angelo, P.; Gagliardi, L. *J. Phys. Chem. B* **2012**, *116*, 6465–6475.

[62] Martínez, J. M.; Pappalardo, R. R.; Sánchez Marcos, E. *J. Chem. Phys.* **1998**, *109*, 1445–1455.

[63] Montagna, M.; Spezia, R.; Bodo, E. *Inorg. Chem.* **2017**, *56*, 11929–11937.

[64] Carnaval, L.; Weiss, A.; Rode, B. *Comput. Chem.* **2013**, *1022*, 94–102.

[65] Sato, H.; Yui, M.; Yoshikawa, H. *J. Nucl. Sci. Technol.* **1996**, *33*, 950.

Chapter 8

Born model

Sometimes models can predict in a simple way a property. This is the case of the Born model,[1] in which the hydration enthalpy is predicted considering the solvation energy as the difference of the electrostatic work to charge an sphere in vacuum and in solution. Being defined the hydration enthalpy as:

$$\Delta H_{hyd} = -\frac{e^2 Z^2 N_A}{8\pi\epsilon_0 a}\left(1 - \frac{1}{\epsilon} - \frac{T}{\epsilon^2}\frac{d\epsilon}{dT}\right) \tag{8.1}$$

where e is the elemental coulomb charge, Z the ion charge, N_A the avogadro number, a the sphere radii and ϵ the solvent dielectric constant. In order to fit the experimental hydration enthalpies of cations the sphere radii needs to be corrected by 0.85 Å.

In Figure 8.1 is represented the hydration enthalpy of the studied cations in front the cocient between the square of the oxidation state and the ionic radii, employing experimental and theoretical values. The experimental representation employs the hydration enthalpy calculated by Marcus et al.[2] and the ionic radii from a database of the Imperial College of London.[3] Whereas the theoretical values contains the hydration enthalpy from

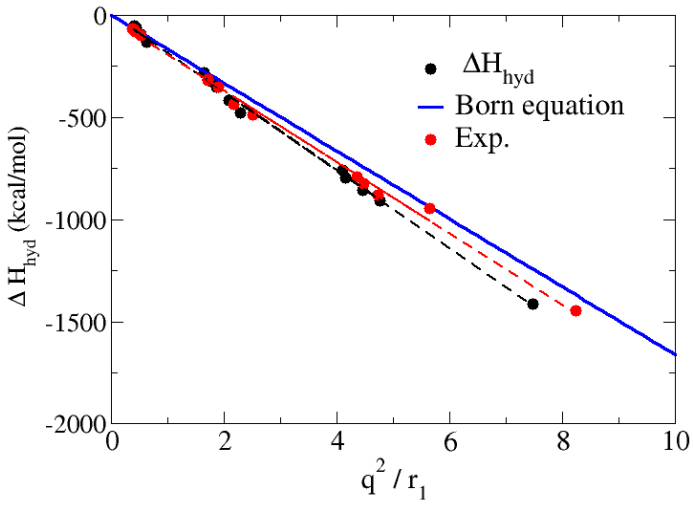

Figure 8.1: Hydration enthalpy versus the effective ionic radii. Dashed lines are the fits of the experimental and theoretical values.

the MD simulations and the ionic radii estimated from the M-O RDF, considering as effective ionic radii the distance where the g(r) has its depletion zone or a minima.

As can be seen in Figure 8.1 both experimental and theoretical representations have similar values to those predicted by the Born model. In the case of the simulated values is found a higher slope (Δ H_{hyd}=-166.1$\cdot\frac{q^2}{r}$ in kcal/mol) than in the case of experimental values (Δ H_{hyd}=-191$\cdot\frac{q^2}{r}$ in kcal/mol). This can be attributed to a higher ϵ of the water model (110)[4] in comparison with the experimental value (78).[1]

In Figure 8.2 a similar plot but considering the hydration enthalpy of

the hydrated ion. Being the $\Delta H_{HIW-hyd}$ calculated as the difference of the configurational energy derived from the MD simulation of the ion and 1000 water molecules and the energy of the hydrated ion together with the energy of a box of pure water with (1000-n) water molecules, "n" being the number of water molecules forming the hydrated ion:

$$\Delta H_{hyd-HIW} = \text{Econf}_{M+1000w} - \text{Econf}_{HIW(M+nw)} - \text{Econf}_{(1000-n)w} \quad (8.2)$$

The energy of the hydrated ion has been calculated from a 300K gas phase MD simulation with the same number of water molecules found in the first-shell of the condensed phase simulation. For low polarizing ions the simulated cluster did not keep all the water molecules in the first-shell, for this reason Na^+, K^+, Rb^+, Cs^+ and Ra^{2+} hydrates are not included in the data.

As can be seen in Figure 8.2 the Born model gives a good prediction of the hydration enthalpy of the hydrated ion. If we compare the slope of the theoretical straight lines one can see that for the hydrated is found a lower slope (ΔH_{hyd}=-136$\cdot\frac{q^2}{r}$ in kcal/mol) than when the bare ion is considered. Being this not intuitive as the ion provoques a dielectric saturation in its near surrounding when orientating the dipole of the nearest water molecules, being possible to consider a smaller dielectric constant near an ion than near a hydrated ion.

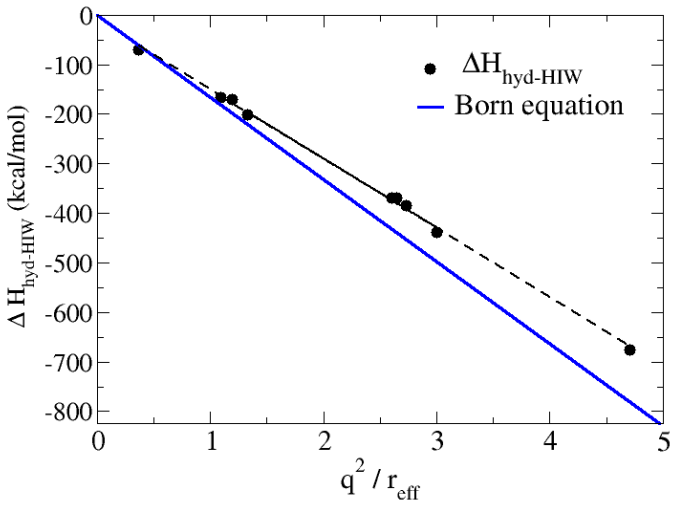

Figure 8.2: Hydration enthalpy of the hydrated ion. Dashed line is the fit of theoretical values.

8.1 Bibliography

[1] Richens, D. T. *The Chemistry of Aqua Ions*; John Wiley: Chichester, 1997.

[2] Marcus, Y. *Ion properties*; Markel Dekker, Inc, 1997.

[3] Atomistic Simulation Group, I. C. L. 1999; `http://abulafia.mt.ic.ac.uk/shannon/ptable.php`.

[4] Villa, A.; Hess, B.; Saint-Martin, H. *J. Phys. Chem. B* **2009**, *113*, 7270–7281.

Chapter 9

Conclusions

In this work several metal cations in aqueous solution have been studied employing ab initio potentials specifically developed to be used in molecular dynamics simulations. To get insight into the hydration of the different metal cations a wide set of physicochemical properties has been calculated. Among all of them, EXAFS spectra define likely the most important test the potentials here presented have undergone. EXAFS spectra is the most suitable experiemntal technique to shed light on structural features (coordination numbers, first-shell distances and localc disorder).

The hydration number of Li^+ and Na^+ was found to be 4 and between 5 and 6, respectively. The first experimental XAS spectrum of Na^+ in aqueous solution[1] was employed to compare with the simulated spectra derived from snapshots of the corresponding MD, finding a good agreement in the distances but overestimating the structural disorder.

For the heavy alkalines (K^+, Rb^+ and Cs^+) for which a wider range of results about their hydration number has been published.[2–25] For our case, the inclusion of surface clusters in the generation of the intermolecular potentials improved the structural description of the near surronding of these cations in aqueous solution. Reorientational properties of first-shell

water molecules were computed, finding values similar to those of the bulk water. From a qualitative point of view, the reorientational motions of OH and μ axis for caesium are slightly faster than for rubidium, but quantitatively both cations have undistigishable values respect to bulk values.[26] The eccentricity parameter has been defined to take into account the shell assymetry.

The water average dipole moment of gas phase clusters for the alkaline cations has been calculated with different number of water molecules, finding an initial dependence of the magnitude to the polarizing capabilities of the cation. When the first-shell is completed and the molecules are placed in a second shell a smooth increase in the property occurs due to the hydrogen bond interactions between water molecules of the cluster, converging the water average dipole moment for all of them for clusters containing more than 8 water molecules.

The Sr^{2+} aqua ion is an octahydrate in solution. For Ba^{2+} a coordination number of 9.4 was found. Several authors found by means of differ approaches lower coordinations.[27–30] However, the comparison between the experimental EXAFS spectrum with our simulated one shows a good agreement, with a slightly overestimation of the structural disorder in the simulation. The good agreement provides a strong support to consider a coordination higher than 8 in the barium hydration. In the radium study a slightly larger aqua ion than barium was found.

For that of the Sc^{3+} hydration, where coordination numbers between 6 and 8 were published,[31–38] our methodology finds a coordination number of 6.[39] Were developed potentials using structures with one coordination number, employing coordinations 4, 6, 7 or 8, obtaining in all simulations a constant hexacoordination. A cobalt-water potential was performed with the final aim of study the cobalt speciation in seawater. For that purpose element its XAS spectra at the SOLEIL synchrotron were measured. The built potential gave excellent structural results when comparing with the experimental EXAFS data. VAC functions has been computed for both

scandium and cobalt, in solution and in gas phase, finding the expected bands of hexahydrates with a blue-shifting in the frequencies when comparing with experimental data. In the Cd^{2+} study a coordination number between 6 and 7 was found, obtaining a good agreement by means of the spectroscopies used in this work.

A few lanthanoids have also been studied in this work. For the La^{3+}, Nd^{3+} and Tm^{3+} coordination numbers of 9.0, 8.7 and 7.7 have been found, respectively. It is also observed the expected smooth decrease in the Ln-O bond length and in the coordination number along the series. Through the XAS analysis a good agreement in the distances with an overestimation of the structural disorder have been found.

The tetravalent thorium in solution has been found to be an enneahydrate. Although fitting error is high, 7.7 kcal/mol, if Table 7.20 is examined, one can state that this error causes an overestimation of the interaction energy in the octahydrate, an underestimation of the decahydrate but a good reproduction of the M-O distances. The simulated cation has been found to be an enneahydrate in solution, and the set of structures used to simulate the EXAFS spectrum leads to a good agreement when comparing with experimental EXAFS spectra.

The hydrogen bond network of the different cations has been characterized to get insight into the aqua ion structure and its interaction with the bulk. In the alkalines, from the comparison of the relative intensity of the first two peaks for the O_I-H_I RDF one can extract a picture of their HB network defined by the first two hydration shells. The energy per hydrogen bond has been calculated by keeping the polarization from the simulation. A good reproduction of the hydration enthalpy allows the analysis of the different energetic contributions. Diffusion coefficients corrected by the PBC effect, are similar to the experimental values.

A MEE removal procedure[40] has been employed in the experimental EXAFS spectra cointainning intense MEE. In the case of the Rb^+ and Cs^+

this removal procedure allowed us to increase the effective k-range of the experimental EXAFS spectra to compare with the simulated one.

As explained in section 3.3 a limitation in the generation of the intermolecular potentials was observed. An energetic difference between the water model and the quantum level used to parametrizate the ion-water interactions for water clusters in ion-dipole configuration has been found. This energetic difference has been found to have effect the PES fitting is more than one coordination number is employed for highly polarizant cations. This energetic difference can be atributed to the different quantum level used in the parametrization of the water model, together with BSSE corrections, and the quantum levels used for the ion-water parametrizations in this work. In order to minimize energy differences it could be interesting to use the same quantum level on the parametrization of the water-water and ion-water interactions, and include in the parametrization of the water model structures from hydration shells to confirm the good reproduction of these situations.

9.1 Bibliography

[1] Galib, M.; Baer, M.; Skinner, L.; Mundy, C.; Huthwelker, T.; Schenter, G.; Benmore, C.; Govind, N.; Fulton, J. *J. Chem. Phys.* **2017**, *146*, 084504.

[2] Glezaku, V.; Chen, Y.; Fulton, J.; Schenter, G.; Dang, L. *Theor. Chem. Acc.* **2006**, *115*, 86–99.

[3] Vao-Soongnern, V.; Pipatpanukul, C.; Horpibulsuk, S. *J. Mater. Sci.* **2015**, *50*, 7126–7136.

[4] Mancinelli, R.; Boti, A.; Bruni, F.; Ricci, M. A.; Soper, A. K. *J. Phys. Chem. B* **2007**, *11*, 13570–13577.

[5] Ma, H. *Int. J. Quantum Chem.* **2014**, *114*, 1006–1011.

[6] Ikeda, T.; Boero, M. *J. Chem. Phys.* **2015**, *143*, 194510.

[7] Liu, Y.; Haigang Lu, Y. W.; Li, Q. *J. Chem. Phys.* **2012**, *132*, 124503.

[8] Ikeda, T.; Boero, M.; Terakura, K. *J. Chem. Phys.* **2006**, *126*, 034501.

[9] Bankura, A.; Carnevale, V.; Klein, M. L. *Molecular Physics* **2014**, *112*, 1448–1456.

[10] Carrillo-Tripp, M.; Saint-Martin, H.; Ortega-Blake, I. *The J. Chem. Phys.* **2003**, *118*, 7062–7073.

[11] Lee, S. H.; Rasaiah, J. Y. *J. Phys. Chem.* **1996**, *100*, 1420–1425.

[12] Azam, S. S.; Hofer, T. S.; Randolf, B. R.; Rode, B. M. *J. Phys. Chem.* **2009**, *113*, 1827–1833.

[13] Faginas-Lago, N.; Lombardi, A.; Albertí, M.; Grossi, G. *J. Mol. Liq.* **2015**, *204*, 192–197.

[14] Tongraar, A.; Liedl, K. R.; Rode, B. M. *J. Phys. Chem. A* **1998**, *102*, 10340–10346.

[15] Ikeda, T.; Boero, M. *J. Chem. Phys.* **2012**, *137*, 041101(1)–041101(4).

[16] Pham, V.; Fulton, J. L. *J Chem. Phys.* **2013**, *138*, 044201.

[17] D'Angelo, P.; Persson, I. *Inorg. Chem* **2004**, *43*, 3543–3519.

[18] Fulton, J.; Pfund, D.; Wallen, S.; Newville, M.; Stern, E.; Yanjun Ma, *J. Chem. Phys.* **1996**, *105*, 2161–2166.

[19] San-Román, M. L.; Hernández-Cobos, J.; Saint-Martin, H.; Ortega-Blake, I. *Theor. Chem. Acc.* **2010**, *126*, 197–211.

[20] Ohkubo, T.; Konishi, T.; Hattori, Y.; Kanoh, H.; Fujikawa, T.; Kaneko, K. *J. Am. Chem. Soc.* **2002**, *124*, 11860–11861.

[21] Kubozono, Y.; Hirano, A.; Kahino, S.; Emura, S.; Ishida, H. *Z. Naturforsch.* **1994**, *49a*, 727–729.

[22] Hofer, T. S.; Randolf, B. R.; Rode, B. M. *J. Comput. Chem.* **2005**, *26*, 949–956.

[23] Schwenk, C. F.; Hofer, T. S.; Rode, B. M. *J Chem. Phys. A* **2004**, *108*, 1509–1514.

[24] Fan, Q.; Tanaka, M.; Tanaka, K.; Sakaguchi,; Takahashi, Y. *Geochim. Cosmochim. Acta* **2014**, *135*, 49–65.

[25] Mähler, J.; Persson, I. *Inorg. Chem* **2011**, *51*, 425–438.

[26] Caralampio, D.; Martínez, J. M.; Pappalardo, R. R.; Marcos, E. S. *Phys. Chem. Chem. Phys.* **2017**, *19*, 28993–29004.

[27] Persson, I.; Sandstrom, M.; Yokoyama, H.; Chaudhry, M. *Z. Naturforsch* **1995**, *50a*, 21–37.

[28] D'Angelo, P.; Pavel, N. V.; Roccatano, D. *Phys. Rev. B* **1996**, *54*, 12129–12138.

[29] Raieri, P.; Demichelis, R.; Gale, J. D. *J. Phys. Chem. C* **2015**, *119*, 24447–24458.

[30] Larentzos, J. P.; Crescenti, L. J. *J. Phys. Chem.* **2008**, *112*, 14243–14250.

[31] Vchirawongkwin, V.; Kritayakornupong, C.; Tongraar, A.; Rode, B. *Dalton Trans.* **2012**, *41*, 11889–11897.

[32] Lindqvist-Reis, P.; Persson, I.; Sandström, M. *Dalton Trans.* **2006**, *28*, 3868–3878.

[33] Yamaguchi, T.; Niihara, M.; Takamuku, T.; Wakita, H.; Kanno, H. *Chem. Phys. Lett.* **1997**, *274*, 485–490.

[34] Migliorati, V.; D'Angel, P. *Inorg. Chem.* **2016**, *55*, 6703–6711.

[35] Kanno, H.; Yamaguchi, T.; Ohtaki, H. *J. Phys. Chem.* **1989**,

[36] Abbasi, A.; Lindqvist-Reis, P.; Eriksson, L.; Sandström, D.; Lidin, S.; Persson, I.; Sandström, M. *Chem. Eur. J* **2005**, *11*, 4065–4077.

[37] Sandström, M.; Persson, I.; Jalilehvand, F.; Lindqvist-Reis, P.; Spanberg, D.; Hermansson, K. *J. Synch* **2001**, *8*, 657–659.

[38] Smirnov, P.; Wakita, H.; Yamaguchi, T. *J. Phys. Chem. B* **1998**, *102*, 4802–4808.

[39] Caralampio, D.; Martinez, J.; Pappalardo, R.; Marcos, E. S. *Theor. Chem. Acc.* **2017**, *136*, 47.

[40] Ohta, A.; Kagi, H.; Tsuno, H.; Nomura, M.; Kawabe, I. *Am. Mineral.* **2008**, *93*, 1384–1392.

Chapter 10

Appendix

10.1 Scandium

Table 10.1: Properties of Sc^{3+} aqueous solution. Mean error between parenthesis.

Property	Pot4	Pot8
$R_{\text{M-O}_\text{I}}$ (Å)	2.15	2.11
NC_I	6.0	6.0
DW (Å^2)	0.00402	0.00388
tilt angle$_\text{I}$ ($^\text{o}$)	158(12)	159(12)
$R_{\text{M-O}_\text{II}}$ (Å)	4.32	4.30
NC_II	13.2	13.5
tilt angle$_\text{II}$ ($^\text{o}$)	128(27)	128(27)
$\Delta\mu_\text{I}$ (D)	1.7(0.4)	1.7(0.4)
$\Delta\mu_\text{II}$ (D)	0.3(0.3)	0.3(0.3)
MRT (ps)	-	-
ΔH_hyd (kcal/mol)	-909(18)	-925(14)
Diffusion (10^{-5} cm^2/s)	0.5(0.1)	0.5(0.1)

10.2 XAS simulation.

The XAS simulation has been performed using 2 differ inputs. In the first input are included all the atoms, in this step is calculated the backscattering potential. In the second step are not included the hydrogen atoms, and the calculation is completed. Here are presented an EXAFS and a XANES example.

EXAFS example:

```
TITLE_Rb_structure_snapshot_NVT_PARTI
EDGE K
S02 1.0
CONTROL 1 0 0 0 0 0
PRINT 0 0 0 3 0 0
COREHOLE RPA
EXAFS 16.0
CRITERIA 4.0 2.5
RPATH 6.0
NLEG 4
RPATH 6.0
TDLDA 1
SCF 6.0
EXCHANGE 0 -5.0 0.
POTENTIALS
0 37 Rb 3 3
1 8 O 3 3
2 1 H 2 2
ATOMS
 0.0000000  0.0000000  0.0000000 0 Rb 0.0000000
 2.5040010 -1.0831000 -0.4564000 1 O  2.7661214
 2.6410000 -1.8961000 -0.9654000 2 H  3.3914707
 3.2770000 -1.2231000  0.1245000 2 H  3.5000290
```

```
-1.4640000 -0.1747000 -2.4274000 1 O  2.8400857
.
.
.
END



TITLE_Rb_structure_snapshot_NVT_PARTII
EDGE K
S02 1.0
CONTROL 0 1 1 1 1 1
PRINT 0 0 0 3 0 0
COREHOLE RPA
EXAFS 16.0
CRITERIA 4.0 2.5
RPATH 6.0
NLEG 4
RPATH 6.0
TDLDA 1
SCF 6.0
EXCHANGE 0 -5.0 0.
POTENTIALS
0 37 Rb 3 3
1 8 O 3 3
ATOMS
 0.0000000  0.0000000  0.0000000 0 Rb 0.0000000
 2.5040010 -1.0831000 -0.4564000 1 O 2.7661214
-1.4640000 -0.1747000 -2.4274000 1 O 2.8400857
.
.
.
END
```

XANES example:

```
TITLE_Rb_structure_snapshot_NVT_PARTI
EDGE K
CONTROL 1 0 0 0 0 0
PRINT 2 2 0 0 0 0
XANES
FMS 6.0 1
AFOLP
OPCONS
MPSE 2
COREHOLE RPA
TDLDA 1
SCF 6.0 0
EXCHANGE 0 0.0 -2.0 2
POTENTIAL
0 37 Rb 3 3
1 8 O 3 3
2 1 H 2 2
ATOMS
 0.0000000  0.0000000  0.0000000 0 Rb 0.0000000
 2.5040010 -1.0831000 -0.4564000 1 O  2.7661214
 2.6410000 -1.8961000 -0.9654000 2 H  3.3914707
 3.2770000 -1.2231000  0.1245000 2 H  3.5000290
-1.4640000 -0.1747000 -2.4274000 1 O  2.8400857
.
.
.
END


TITLE_Rb_structure_snapshot_NVT_PARTII
EDGE K
```

```
CONTROL 0 1 1 1 1 1
PRINT 2 2 0 0 0 0
XANES
FMS 6.0 1
AFOLP
OPCONS
MPSE 2
COREHOLE RPA
TDLDA 1
SCF 6.0 0
EXCHANGE 0 0.0 -2.0 2
POTENTIALS
0 37 Rb 3 3
1 8 O 3 3
ATOMS
 0.0000000  0.0000000  0.0000000 0 Rb 0.0000000
 2.5040010 -1.0831000 -0.4564000 1 O  2.7661214
-1.4640000 -0.1747000 -2.4274000 1 O  2.8400857
.
.
.
END
```